**Short-term operation of the power system and the natural gas system considering uncertainties**

by

**Dan Hu**

A thesis submitted to the graduate faculty

in partial fulfillment of the requirements for the degree of

Doctor of Philosophy

Major: Industrial Engineering

Program of Study Committee:
Sarah M. Ryan, Major Professor
Lizhi Wang
Cameron A. MacKenzie
James D. McCalley
Dan J. Nordman

Iowa State University

Ames, Iowa

2019

# TABLE OF CONTENTS

# LIST OF TABLES

**Page**

# LIST OF FIGURES

**Page**

# ACKNOWLEDGEMENTS

I would like to take this opportunity to express my thanks to those who helped me with this dissertation. First and foremost, I would like to thank my advisor, Dr. Sarah M. Ryan for her guidance, patience, and support throughout my Ph.D. study. Her insights and words of encouragement have often inspired me and renewed my hopes for completing my graduate education.

Many thanks to my committee members, Dr. Lizhi Wang, Dr. Cameron A. Mackenzie, Dr. James D. McCalley, and Dr. Daniel J. Nordman for their great efforts and valuable feedback on my research. I would also like to thank Dr. Zhi Zhou at Argonne National Laboratory for his support and guidance in my research internship project. His valuable time, insightful comments on my Ph.D. study and research, and his sharing of life experiences and thoughts gave me lots of encouragement and help during both my internship and my most stressful time.

I would also like to thank my colleagues, my instructors, department faculty, and staff from the Departments of IMSE and Statistics for keeping me motivated and enjoying my time at Iowa State University. Many thanks to all my friends, including my college classmates, my graduate school friends, and all the friends I met during my two internships. All of our discussions about study and life are the most precious memories to me. In the end, I would like to send my deepest gratitude and love to my parents. Their unconditional love, care, and understanding encouraged me to finish this six-year Ph.D. program.

# ABSTRACT

Electricity generation increasingly relies on natural gas for fuel. The competing demands for gas by natural gas-fueled generators and other users, the differences in timing of short-term operations and markets between the natural gas system and the power system, and the deepening penetration of variable renewable energy in the power system cause difficulties in operating the two systems economically and reliably. This dissertation consists of three papers which present different models and methods for the short-term operation of the natural gas and power systems considering different sources of uncertainty.

From the viewpoint of a centralized system operator, who can operate the power system and natural gas system simultaneously, we first compare two approaches to addressing the uncertainty in the joint scheduling of a combined natural gas and power system. A stochastic programming model and a deterministic model with reserves are formulated to minimize the daily operational cost and investigate the hourly unit commitment and economic dispatch decisions in the power system as well as the hourly working schedule of the natural gas system while satisfying all the operational constraints. In the deterministic model, the reserves proportional to the wind energy forecast are used to mitigate the effect of the uncertainty in wind energy, whereas in the stochastic programming model the day-ahead decisions are made while explicitly considering the wind energy uncertainty. To tackle the nonlinear constraints on the gas flows in pipelines, we approximately linearize those nonlinear constraints by adding multiple binary variables and constraints. Through numerical experimentation, the number of piecewise linear segments is chosen to balance accuracy and computational efficiency. The simulation results of two case studies indicate that, when the total wind capacity exceeds 15% of the conventional generation capacity, the stochastic programming model produces schedules with comparable or lower cost and energy shortages than the deterministic model with reserves.

The centralized system operator modeled in the first paper does not exist in the real U.S. energy market. From a more realistic viewpoint of the power system operator, in the second paper, we quantify the effect of the uncertainty in the gas spot price on power system dispatch cost in the absence of wind energy. The influence of the natural gas system is considered in terms of fixed or uncertain parameters in the power system daily economic dispatch problem. A benchmark distribution of the dispatch cost is generated by Monte Carlo simulation conducted with the gas price fixed at its expectation while sampling from the marginal distribution for the load. For comparison, another dispatch cost distribution is generated by sampling from a joint distribution for the gas price and the load. The risk from uncertainty in the gas price is quantified by the distance between dispatch cost distributions or, alternatively, by the difference between the values of a risk measure applied to each distribution. We demonstrate that this risk quantification method helps to select from among alternative risk-mitigation strategies, such as providing dual-fuel capability or adding gas storage facilities at the system level.

In the third paper, we investigate the use of a reliability unit commitment (RUC) conducted after the day-ahead market unit commitment to manage the natural gas cost in the power system operations, where the operations of the two systems are separately optimized to minimize their own net cost. This separately optimized model incorporates the interruptible contract and the real-time market for gas, where an iterative process between the electricity and gas operations determines the real-time gas flows and prices. An ideal co-optimized model, where a centralized system operator optimizes the two systems simultaneously, is taken as a benchmark for comparison. By numerical studies, we demonstrate the ability of the RUC step to reduce power system cost, maintain a low real-time gas price, and avoid real-time gas supply deficiency.

# CHAPTER 1. GENERAL INTRODUCTION

## 1.1 Background

An electric power system is a network of electrical components that supply, transmit and deliver electric power. It consists of generators that supply the power, the transmission system that transmits electric power from the generating units to the load centers, and the load distribution system that feeds the power to nearby customers. The electricity demand, as projected by the U.S. Energy Information Administration (EIA), will increase by 0.9% per year from 3,826 billion kilowatt-hours (kWh) in 2012 to 4,954 billion KWh in 2040 [70]. This increase is mainly supported by natural gas as a fuel. According to EIA's projection, the share of natural gas in the total electric power generation will rise from 27% in 2012 to 31% in 2040 [70]. This increase originates from the retirement of coal-fired generators, development of high-efficiency natural gas-fueled generators, the increase of relatively low price natural gas supply since 2009, and potential emission regulations.

This fuel mixture change not only provides the power system with more generating capabilities to satisfy the increasing demand but also causes some short-term operational issues, such as dealing with the uncertainties from the natural gas system, the extra operating constraints added to the power system, and the difficulty of coordinating the operations of the natural gas and power systems. The natural gas system operator experiences difficulties with optimizing and operating the large scale dynamic natural gas network. Natural gas is traded in a more competitive market than other fossil fuels because of its fast procurement and low price. Compared with residential, commercial and industrial natural gas consumers, many gas generators have low priority in the gas market and face possible gas flow cutoff because of the low price they are willing to pay. These operational difficulties of the gas network and the low priority of many gas-fueled generators contribute to some

gas availability uncertainties, which can limit their generating capabilities in the power system in some situations. The lack of efficient communications between the natural gas operator and the independent system operator (ISO) of the power system may result in real-time infeasibility of the day-ahead scheduling decisions made by the ISO. All of these issues lead to possibly high electricity and natural gas spot prices along with blackout, as were experienced in the eastern U.S. during early January 2018; the 2013-14 Polar Vortex events [65]; and earlier severe-weather events in Texas, New England, and Colorado [64].

## 1.2 Problem Statement

To maintain a reliable and efficient operation of the power system given the high share of generation by natural gas, we must consider the effect of incorporating natural gas uncertainties and the interdependency of the operations of the natural gas and power systems. Numerous studies of the short-term joint operation of the power system and the natural gas system have been conducted to investigate their interdependency with and without uncertainties using robust optimization, stochastic optimization and simulation. However, there are few comparisons between these models and more realistic models that corresponds to actual operations. For example, deterministic models for scheduling on the day ahead deal with uncertainty by adding some reserves requirements proportional to the uncertainty level. In addition, most of the recent research studies assumed the level of uncertainty remains constant, but the performance of stochastic optimization models given various levels of uncertainty remains uninvestigated. The uncertainty factors the recent research studies investigated include wind energy, contracted gas price and gas availability, but of these, only wind energy probability models have been estimated from realistic data. It is critical to conduct analysis based on real data for gas price and availability. What's more, a new formulation describing a realistic operation process between the natural gas system and the power system is requisite.

This dissertation addresses the short-term electric power operation problem including the unit commitment problem (UC) and the economic dispatch problem (ED) incorporating the natural gas

system. From the alternative viewpoints of the ISO alone, of an assumed operator who can optimize both the natural gas and power system simultaneously or of the viewpoints where the natural gas system and power system are operated separately, we investigate the effect on the power system of incorporating the natural gas system considering the uncertainty of the gas price, gas availability, and wind energy.

## 1.3 Dissertation Structure

The dissertation consists of three papers. The first examines the short-term scheduling of a combined natural gas and power system with wind energy. It compares a stochastic programming model and a deterministic model with reserves to investigate the optimal hourly unit commitment and economic dispatch decisions in the power system as well as the hourly working schedule of the natural gas system. The deterministic model uses reserves proportional to the wind energy forecast to mitigate the effect of uncertain wind energy, while the stochastic programming model makes the day-ahead decisions considering uncertainties. The study addresses the following issues:

- The formulation of a deterministic model with reserves for the combined day-ahead scheduling of the natural gas and power systems and the corresponding stochastic program, from the viewpoint of a centralized operator of both systems.
- The performance comparison between a stochastic program and a deterministic optimization with reserve constraints when confronted with different levels of wind energy uncertainty on different days.
- Experimentation for selection of the number of piecewise linear segments to approximate the nonlinear natural gas flow constraints while maintaining accuracy and computational efficiency.

The first paper assumes that there is a single entity who can operate both the natural gas and the power systems, which is not the case in many part of the world, including the U.S. Natural gas is an essential fuel in the power system, and its price and availability influence the power system operational scheduling and costs directly. Thus, from a more practical viewpoint of the power

system, we take the natural gas status as a set of input parameters to the power system. The second paper quantifies the effect of the gas system on the economic dispatch cost of the power system and includes the following:

- The formulation of an economic dispatch model incorporating the gas availability and prices from both the spot market and contracts.
- The estimate of a joint probability function of temporal and weather conditional daily electric load and gas spot price by segmentation, transformation, and fitting a bivariate normal ditribution in each segment.
- The quantification of the effect on the economic dispatch cost of uncertainties in the availability of contracted natural gas as well as its price in the spot market using the Wasserstein distance (WD) metric and a conditional value-at-risk (CVaR) metric.
- The employment of this uncertainty quantification methodology to select from among alternative risk-mitigation strategies; namely, dual fuel capability conversion and the addition of gas storage facilities.

In the third paper, we propose a model of the current daily working schedules optimized separately for the power and natural gas system, and focus on the communication of information about gas flows and prices between them. To help manage the natural gas cost in this separately optimized model, we include the reliability unit commitment step between the day-ahead market and the real-time market. A co-optimized model is also formulated and considered to provide a lower bound on the cost for the separately optimized model with and without reliability unit commitment. The co-optimized model assumes that there exists a centralized system operator who has full information about the two systems and can operate them simultaneously. The performance of these three models is compared with respect to the operational level decisions. The major contributions of this paper are as follows:

- The formulation of a daily separately optimized model for the operation of the natural gas and power systems while incorporating the interruptible gas contracts and the gas from the real-time market and characterizing the real operation process.

- The addition of the reliability unit commitment step to the separately optimized model to enable the power system to adjust the unit commitment decisions according to the gas availability information from the gas system and manage the natural gas cost in the power system operations.

- Comparisons conducted for various combinations of interruptible contract gas price and non-electric gas demand between these two proposed models and the co-optimized model, with respect to the detailed operational decisions, including the unit commitment decisions, gas price, and gas flow in the real-time market, and the power system cost breakdown as startup and shutdown cost, non-gas-fired generator cost, payment for the gas fuel, and the unserved energy cost.

The dissertation consists of three papers. The first paper, published in the *International Journal of Electrical Power & Energy Systems*, is reproduced in Chapter 2. The second paper, under second round review by the *Energy Systems*, is presented in Chapter 3. The third paper is in preparation for submission to the *IISE Transactions* and is presented in Chapter 4. Finally, Chapter 5 summarizes the conclusions, contributions and future research suggestions of this dissertation.

# CHAPTER 2. STOCHASTIC VS. DETERMINISTIC SCHEDULING OF A COMBINED NATURAL GAS AND POWER SYSTEM WITH UNCERTAIN WIND ENERGY

A paper published in the *International Journal of Electrical Power & Energy Systems*

## Abstract

We compare approaches for addressing uncertainty in the joint scheduling of a combined power and gas system, with the goal of minimizing the total cost of meeting demands for gas and electricity, while satisfying operational and equilibrium constraints. A stochastic programming model and a deterministic model with reserves are formulated to investigate the hourly unit commitment and economic dispatch in the power system as well as the hourly working schedule of the natural gas system. The deterministic model uses reserves proportional to the wind energy forecast to mitigate the effect of the uncertainty in wind energy, whereas the stochastic programming model makes the day-ahead decisions while explicitly considering the wind energy uncertainty. Nonlinear constraints on the gas flows in pipelines are linearized with binary variables where, based on numerical experimentation, the number of piecewise linear segments is chosen to balance accuracy and computational efficiency. A six-bus power system with seven-node gas system and the IEEE 24-bus power system with adjusted Belgian 20-node gas system are analyzed. The simulation results indicate that, when the total wind capacity exceeds 15% of the conventional generation capacity, the stochastic programming model produces schedules with comparable or lower cost and energy shortages than the deterministic model with reserves.

**Keywords :** Natural gas system, Power system, Short-term unit commitment and economic dispatch, Wind energy.

According to a U.S. government forecast, the share of natural gas in the total electricity generation will rise from 27% in 2012 to 31% in 2040, while the share from coal will decrease from 39% to 34% [69]. This change results from the retirement of coal-fired generators, the development of high-efficiency natural gas fueled power generators (NGPGs), the increase of natural gas supply with a relatively stable gas price since 2009, and potential emission regulations. To maintain a reliable power system, more research about how to make unit commitment (UC) and economic dispatch (ED) decisions for the increasing numbers of NGPGs is needed.

Wind energy, with a low operational cost, can be added into the power grid directly and thus relieve some of the pressure on NGPGs. Meanwhile, NGPGs can ramp their production up and down quickly according to the variable wind energy. The cooperation of the wind generators and NGPGs can not only decrease the operational cost but also increase the reliability of the grid. Due to the pre-schedule scheme of natural gas and power systems, ahead of the actual operating day, decisions about the supply of natural gas must be made on the basis of wind power output forecasts. If the actual wind output is less than the forecast, load shedding may occur if too few units are committed or not enough gas is available. Thus, it is important to plan the operation of the natural gas and power systems accounting for the uncertainty of wind energy.

Currently in many parts of the world, the natural gas and power systems are operated independently. As natural gas claims a higher share of generation capacity, more generating companies consider signing firm contracts with the natural gas suppliers to make sure they have sufficient fuel. Because the peak gas and electricity loads may overlap and coincide with extreme weather, the current independent operation of the natural gas and power systems makes it hard to react to these conditions. Recently, the U.S. Federal Energy Regulatory Commission, which regulates both systems, mandated adjustments in the timing of day-ahead wholesale electricity markets to permit better coordination with the gas market. Here, we examine the combined operation of the

electric power and natural gas systems to minimize the total operational cost including penalties on non-served energy.

In this paper, we focus on comparing the stochastic and the deterministic scheduling of the combined natural gas and power system with uncertain wind energy. We formulate the problem with a centralized direct current (DC) power flow model and static natural gas system, neglecting some complicated dynamic power and natural gas constraints for the sake of tractability. Uncertainty in the wind energy is incorporated by adding fixed reserves in the deterministic model or by probabilistic scenarios in the stochastic programming (SP) model. Here we quantify *risk* as the expected unserved energy (in the form of either gas or electricity) and *cost* as the UC and expected production cost in the combined system. While some previous comparisons of stochastic and deterministic scheduling of these systems together have focused on expected cost, we examine risk impacts more closely. We compare the cost and risk in numerical case studies, illustrating that under deep penetration of wind power, the SP model reduces both cost and risk compared to the deterministic model with reserves.

## 2.1 Literature Review

Many researchers have discussed approaches to modeling the combined natural gas and power system. The effects of gas infrastructure and gas unit price on power generation scheduling were addressed by using security-constrained unit commitment (SCUC) [62]. Dual decomposition, Lagrangian relaxation and dynamic programming were used to solve a large scale integrated electricity-gas optimal short-term planning problem with a hydrothermal system included, formulated as a nonlinear mixed-integer program [68], while a day-ahead integrated SCUC model is applied incorporating the natural gas network constraints and fuel diversity as an effective peak shaving strategy [41]. Reference [43] applied Benders decomposition in the SCUC problem with natural gas transmission constraints and reference [44] formulated a bi-level model in which the upper level problem includes the unit commitment (UC) and economic dispatch (ED) problems while the lower level problem concerns the natural gas system. With a focus on component outages, or contingencies, a

coordinated stochastic model, including scenarios of random generating unit and line outages, was proposed to demonstrate that hourly economic demand response would decrease the dependence on natural gas constraints for the optimal operation of the electric power system [77]; a two-stage stochastic programming model of the UC with natural gas constraints, in which the first stage optimizes the UC and gas production decisions, was developed [15]; and reference [17] applied the corresponding linear sensitivity analysis to adjust decisions in advance for system security in the event of a single contingency. The Alternating Direction Method of Multipliers (ADMM) was used not only to solve the gas-electric integrated optimal power flow model and compare the results with and without a coordinating operator [73] but also to coordinate the gas-electric systems and demonstrate the algorithm efficiency, under electric load uncertainty [5]. In [14], second-order cone constraints are employed as a relaxation for the non-convex gas flow through pipelines and a sensitivity analysis of the wind energy forecast error is conducted. Reference [26] applied the energy modeling method to the different energy systems including the natural gas system, power system, gas-to-power units, gas-to-power units and line pack of the natural gas. Reference [35] proposed a genetic algorithm based hybrid model for a power system distribution network, a natural gas network and the energy centers including the combined heat and power units, different energy conversion devices and demand responsive load to minimize the day-ahead operational cost of the integrated urban energy system, but the optimality is not guaranteed. Moreover, it is difficult to extend these methodologies to multiple scenarios due to their low computational efficiency. A study of a distribution system including reverse power management focuses on the operation of the power-to-gas and gas-to-power facilities [37]. Reference [42] investigated the micro integrated electric power, natural gas and heat delivery system and focused on minimizing the total operation and environmental cost, and reference [75] proposed a robust optimization model of the integrated natural gas and power system model with uncertain wind energy and focused on the worst cases. None of references [37], [42] and [75] modeled the detailed non-convex gas flow through pipelines.

Several papers presented models of gas flows in pipelines. For the most general case of transient flow, the laws of conservation of mass, energy and momentum were applied to find three partial

differential equations (PDEs) [52]. However, although the gas state condition could be added to those three PDEs to help identify a closed form of the solution, more equations are required due to the large number of variables in the transient model. The theoretical and some experimental results of the unsteady and transient flow of compressible fluids in pipelines were reviewed in [67]. Given the special physical characteristics of gas pipelines, they proposed a unidirectional flow model and developed various derivative models of different thermal conditions. A one-dimensional, non-isothermal gas flow model was solved to simulate the slow and fast fluid transients and address the effect of various thermal models on the flow rate, pressure and temperature in the pipelines [12]. Given a one dimensional homo-thermal steady state flow condition, the PDEs for transient state flow could be simplified and the Weymouth equation (WE) was proposed to model gas flow in passive pipelines [44]. A theoretical and computational comparison of piecewise linear models for approximating the WEs led to the conclusion that the incremental method, where continuous variables are introduced to represent the portion of each segment and binary variables force all intervals to its left must be completely used if a segment is chosen, is the fastest [16]. The non-convex Weymouth gas flow equation was relaxed to convexified quadratic constraints to enable solution of the optimal gas flow by an iterative second-order cone programming procedure with a greater efficiency than traditional nonlinear methods [72]. A robust co-optimization scheduling model was proposed to study the coordinated natural gas and power system while considering key power system uncertainties [27], which only mentions incremental method is used for linearizing nonlinear constraints but the computational efficiency and accuracy for different numbers of segments were not discussed.

UC and ED formulations traditionally have been based on fixed reserve limits. With the power turbine technology development, the capacity of wind turbines has increased significantly and wind power has become an important energy resource. Thus, methodologies for incorporating increasing amounts of wind energy into the power system attract more attention. Although many research studies have been done on scheduling the combined natural gas and power system as well as on the UC/ED problems with uncertain wind energy, there are few studies on the combined

natural gas and power system that also include uncertain wind energy. Reference [2] formulated a coordinated stochastic day-ahead scheduling model of the electricity infrastructure with costs and constraints imposed by the gas system and examined its ability to firm the uncertain wind energy. This study did not compare the stochastic programming approach against traditional methods of adding reserves and did not analyze different levels of wind uncertainty. Reference [55] describes the study that, to our knowledge, is most similar to this one. The authors compared deterministic, two-stage, and multi-stage stochastic formulations of commitment and dispatch of an integrated gas and electricity network. However, they separately solved a (stochastic) mixed-integer program to schedule the electricity generators and a nonlinear program to determine if gas demands could be satisfied under that schedule, then iteratively applied a heuristic method to constrain the gas generators' output, re-solving both models until feasibility could be achieved.

We apply linear approximations to the gas constraints and integrate the decisions for both systems in a single optimization model. By penalizing energy- and gas-balance constraint violations in the objective function, we quantify the risk of load shedding in either system. The contributions of this paper are:

(1) We model the combined day-ahead scheduling of the natural gas and power systems with reserves. The current deterministic models for the integrated natural gas and power system in the literature include only the wait-and-see model and the expected value model, which are special cases of the stochastic programming model. There is a theoretically guaranteed relationship among the optimal expected costs of solution to stochastic model, wait-and-see model and the expected value model. However, our proposed deterministic model with reserves is a different and more practical model, where reserves are added in the day ahead market, and there is no guarantee that the stochastic programming model dominates it. Thus, it is important to compare the results of the deterministic model with reserves and the stochastic programming model. In numerical case studies, the stochastic program results in less cost and risk when the wind uncertainty is high.

(2) We compare the performance of a stochastic program and a deterministic optimization with reserve constraints (called a DR model) when confronted with different levels of wind energy

uncertainty on different days. Current research only tests one or two cases of uncertainty using sensitivity analysis, which does not guarantee the generality of the conclusions.

(3) We experiment with different numbers of segments when linearizing the nonlinear Weymouth equation, to identify a number of segments that best balances computational efficiency with accuracy. Because the past publications each use a single number of piecewise segments, which varies among them, it is hard to compare their results. The number of segments we identify can serve as a standard for future studies.

The remainder of this paper has the following structure. The two models are presented along with a perfect information (wait and see) model to evaluate their effectiveness in Section 2.2. Section 2.3 describes the scenario generation process and numerical simulations to compare the operational cost and risk of the SP and DR models. Finally, the conclusions are summarized in Section 2.4.

## 2.2 Model

Although gas and electricity can flow in either direction through a pipeline or transmission line, respectively, we model those components as directed arcs either from or to a node, where negative values for corresponding flow variables indicate flows in the reverse direction. Define the notation as follows:

**Sets and indices**

$\mathcal{J}$ Gas nodes, indexed by $j$

$\mathcal{J}'(j)$ Gas nodes connected to $j$ by passive pipelines from $j$, indexed by $j'$

$\mathcal{J}''(j)$ Gas nodes connected to $j$ by passive pipelines to $j$, indexed by $j''$

$\mathcal{C}'(j)$ Gas nodes connected by active pipelines from $j$, indexed by $c'$

$\mathcal{C}''(j)$ Gas nodes connected by active pipelines to $j$, indexed by $c''$

$\Lambda(j)$ Gas wells in node $j$, indexed by $\lambda$; $\Lambda = \bigcup_{j\in\mathcal{J}} \Lambda(j)$ is the set of all gas wells

$\Psi(j)$ Storage facilities in node $j$, indexed by $\psi$; $\Psi = \bigcup_{j\in\mathcal{J}} \Psi(j)$ is the set of all storage facilities.

$\mathcal{I}$ Electricity nodes, indexed by $i$ and $i'$

$\mathcal{I}'(i)$ Electricity nodes connected to $i$ by a transmission line from $i$, indexed by $i'$

$\mathcal{I}''(i)$ Electricity nodes connected to $i$ by a transmission line to $i$, indexed by $i''$

$\mathcal{G}(i,j)$ Gas-fired generators at power node $i$ and gas node $j$, indexed by $g$; $\mathcal{G} = \bigcup_{i\in\mathcal{I},j\in\mathcal{J}} \mathcal{G}(i,j)$ is the set of all gas-fired generators.

$\mathcal{N}(i)$ Non-gas-fired conventional generators at node $i$, indexed by $n$; $\mathcal{N} = \bigcup_{i\in\mathcal{I}} \mathcal{N}(i)$ is the set of all non-gas-fired generators.

$\mathcal{W}(i)$ Wind turbines at node $i$, indexed by $w$; $\mathcal{W} = \bigcup_{i\in\mathcal{I}} \mathcal{W}(i)$ is the set of all wind turbines

$\mathcal{M}$ Set of all gas-fired and non-gas-fired generators, indexed by $m$; $\mathcal{M} = \mathcal{G} \cup \mathcal{N}$

$\mathcal{T}$ Hours from 1 to $|\mathcal{T}|$, indexed by $t$

$\mathcal{S}$ Wind energy scenarios, indexed by $s$

$\mathcal{K}$ Piecewise segments of gas flow quantities, indexed by $k$

**Binary Decision Variables**

$u_{g,t}, u_{n,t}, u_{m,t}$ Unit commitment indicator: equals 1 if unit is online in hour $t$ and 0 otherwise

$y^k_{j,j',t}$ Linearization segment indicator

**Nonnegative Continuous Decision Variables**

| | |
|---|---|
| $v^u_{g,t}, v^u_{n,t}, v^u_{m,t}$ | Unit start-up indicator: equals 1 if the unit is started up in hour $t$ and 0 otherwise |
| $v^d_{g,t}, v^d_{n,t}, v^d_{m,t}$ | Unit shut-down indicator: equals 1 if the unit is shut down in hour $t$ and 0 otherwise |
| $p^{ng}_{\lambda}$ | Daily natural gas production level [kcf/day] |
| $\pi_{j,t}$ | Gas pressure squared [Psig$^2$] |
| $\delta^k_{j,j',t}$ | Linear approximating coefficients for passive pipelines |
| $\alpha^-_{j,t,s}$,$\alpha^+_{j,t,s}$ | Unserved/excess gas in gas node $j$ [kcf] |
| $l_{\psi,t,s}$ | Storage level [kcf] |
| $q^{out}_{\psi,t,s}, q^{in}_{\psi,t,s}$ | Out/in-flow of storage facility [kcf/h] |
| $p_{g,t,s}, p_{n,t,s}, p_{m,t,s}$ | Electricity production [MWh] |
| $\mu_{g,t,s}$ | Gas demand for electricity generation [kcf/h] |
| $p^{wind}_{w,t,s}$ | Wind energy output [MWh] |
| $r_{g,t}, r_{n,t}, r_{m,t}$ | Operating reserves [MWh] |
| $\beta^-_{i,t,s}$,$\beta^+_{i,t,s}$ | Unserved/excess electricity [MWh] |
| $\gamma^-_{t,s}$,$\gamma^+_{t,s}$ | Non-supplied/excess reserves [MWh] |

**Unrestricted Continuous Decision Variables**

| | |
|---|---|
| $\eta_{j,j',t}$ | Gas flow from $j$ to $j'$ [kcf] |
| $\Delta\pi_{j,j',t}$ | Gas squared pressure difference between $j$ and $j'$ [Psig$^2$] |
| $\theta_{i,t,s}$ | Phase angle [rad] |
| $f_{i,i',t,s}$ | Line flow from $i$ to $i'$ [MWh] |

**Fixed Parameters**

| | |
|---|---|
| $D^{ng}_{j,t}$ | Non-electric gas demand [kcf/h] |
| $\overline{P}^{ng}_{\lambda}, \underline{P}^{ng}_{\lambda}$ | Max/Min daily gas production [kcf/day] |
| $C^{ng}_{\lambda}, C^{stor}_{\psi}$ | Gas production/storage cost [$/kcf] |
| $C_{j,j'}$ | Passive pipeline constant [kcf/Psig] |
| $\tau_{j,c'}$ | Max squared pressure increase ratio of active pipelines |
| $\overline{\pi}_j, \underline{\pi}_j$ | Max/Min squared pressure [Psig$^2$] |
| $\Delta\pi^k_{j,j'}$ | Squared pressure gap of the segment |
| $\overline{L}_{\psi}, \underline{L}_{\psi}$ | Max/Min storage level [kcf] |
| $Q_{\psi}$ | Max net flow (outflow minus inflow) [kcf] |
| $\eta^k_{j,j'}$ | Gas flow of the $k^{th}$ piecewise segment on pipeline from $j$ to $j'$ |
| $\Gamma^-_{\alpha}, \Gamma^+_{\alpha}$ | Unserved/excess gas penalty [$/kcf] |
| $\phi_g$ | Efficiency of gas generator [kcf/MWh] |
| $C^{sd}_g, C^{su}_g, C^{sd}_n, C^{su}_n, C^{sd}_m, C^{su}_m$ | Shut-down/start-up cost [$] |
| $C^{prod}_n$ | Power production cost [$/MWh] |
| $\Gamma^-_{\beta}, \Gamma^+_{\beta}$ | Unserved/excess electricity penalty [$/MWh] |
| $\Gamma^-_{\gamma}, \Gamma^+_{\gamma}$ | Non-supplied/excess reserves penalty [$/MWh] |
| $\overline{P}_g, \underline{P}_g, \overline{P}_n, \underline{P}_n, \overline{P}_m, \underline{P}_m$ | Max/min electricity generation [MWh] |
| $R^{up}_g, R^{up}_n, R^{up}_m, R^{down}_g, R^{down}_n, R^{down}_m$ | Max ramp up/down rate [MW] |
| $X_{i,i'}$ | Transmission line impedance [pu] |
| $T^{on}_g, T^{on}_n, T^{on}_m, T^{off}_g, T^{off}_n, T^{off}_m$ | Min on/off time [h] |
| $D^e_{i,t}$ | Electricity demand forecast [MWh] |
| $\overline{F}_{i,i'}$ | Max line flow [MWh] |
| $\hat{P}^{wind}_{w,t}$ | Available wind energy forecast [MWh] |
| $WR$ | Reserve margin for wind energy [%] |

**Uncertain Parameters**

$\overline{P}^{wind}_{w,t,s}$ Available wind energy in scenario s [MWh]

$\xi_s$ Scenario probability

### 2.2.1 Stochastic Programming (SP) Model

We propose a two-stage stochastic mixed-integer linear programming (SP) model of scheduling the combined energy system to satisfy demands for electricity and gas under uncertain wind energy supply. The two stage model not only deals with the uncertainties in the short-term scheduling problem, but also reflects the difference in time scales for operating inflexible thermal units and adjusting to varying amounts of load and wind energy. As in many two-stage stochastic unit commitment models, we consider decisions on an hourly basis. To avoid the end of day distortions in the decisions, we minimize the expected cost over a 36-hour study horizon to be implemented over a 24-hour operating day. In the first stage, one day ahead of the operating day, we make decisions on the hourly binary unit commitment decisions, start-up and shut-down status of each thermal generator and the total gas supply quantity from wells, along with pressures at each gas node, gas flows in each pipeline and the gas compressor working schedule $x \equiv (u_{m,t}, v^u_{m,t}, v^d_{m,t}, p^{ng}_{\lambda}, \pi_{j,t}, \Delta\pi^k_{j,j',t}, \eta_{j,j',t}, y^k_{j,j',t}, \delta^k_{j,j',t})$. These decisions are made in advance because of minimum up- and down-times, ramping constraints, and the time required for gas to travel through pipelines. Then, for each scenario time series of wind energy availability, the hourly dispatch solution of the power system, including energy production and transmission quantities, as well as storage levels and flows in and out of gas storage facilities, $z_s \equiv (p^{wind}_{w,t,s}, p_{m,t,s}, l_{\psi,t,s}, \mu_{g,t,s}, q^{in}_{\psi,t,s}, q^{out}_{\psi,t,s}, \theta_{i,t,s}, f_{i,i',t,s}, \alpha^-_{j,t,s}, \alpha^+_{j,t,s}, \beta^-_{j,t,s}, \beta^+_{j,t,s}, \gamma^-_{j,t,s}, \gamma^+_{j,t,s})$, are determined. Thus, the second stage represents the ISO's real time dispatch decisions and natural gas system's real time working pattern of the storage facilities. To focus on the uncertainty from wind energy, equipment outages are not considered. Wind generators are modeled as dispatchable to reflect day-ahead market practices such as those in the Midcontinent Independent System Operator (MISO) in the US, where they participate as Dispatchable Intermittent Resources [46]. The model

is:

$$\zeta^{SP} = \min \sum_{t\in\mathcal{T}} \Bigg\{ \sum_{n\in\mathcal{N}} \left( C_n^{su} v_{n,t}^u + C_n^{sd} v_{n,t}^d \right) + \sum_{g\in\mathcal{G}} \left( C_g^{su} v_{g,t}^u + C_g^{sd} v_{g,t}^d \right) + \sum_{\lambda\in\Lambda} C_\lambda^{ng} p_\lambda^{ng} + \sum_{s\in\mathcal{S}} \xi^s \Bigg[ \sum_{n\in\mathcal{N}} C_n^{prod} p_{n,t,s} + \sum_{i\in\mathcal{I}} \left( \Gamma_\beta^+ \beta_{i,t,s}^+ + \Gamma_\beta^- \beta_{i,t,s}^- \right) + \sum_{j\in\mathcal{J}} \left( \Gamma_\alpha^+ \alpha_{j,t,s}^+ + \Gamma_\alpha^- \alpha_{j,t,s}^- \right) + \sum_{\psi\in\Psi} C_\psi^{stor} q_{\psi,t,s}^{out} \Bigg] \Bigg\} \tag{2.1}$$

$$s.t. \sum_{j\in\mathcal{J}} \sum_{g\in\mathcal{G}(i,j)} p_{g,t,s} + \sum_{n\in\mathcal{N}(i)} p_{n,t,s} + \sum_{w\in\mathcal{W}(i)} p_{w,t,s}^{wind} + \sum_{i''\in\mathcal{I}''(i)} f_{i'',i,t,s} + \beta_{i,t,s}^- = D_{i,t}^e + \sum_{i'\in\mathcal{I}'(i)} f_{i,i',t,s} + \beta_{i,t,s}^+, \quad \forall i,t,s \tag{2.2}$$

$$u_{m,t} - u_{m,t-1} = v_{m,t}^u - v_{m,t-1}^d, \quad \forall m\in\mathcal{M}, t \tag{2.3}$$

$$u_{m,t} \geq v_{m,t}^u, \quad \forall m\in\mathcal{M}, t \tag{2.4}$$

$$u_{m,t} \leq 1 - v_{m,t}^d, \quad \forall m\in\mathcal{M}, t \tag{2.5}$$

$$v_{m,t}^u + v_{m,t}^d \leq 1, \quad \forall m\in\mathcal{M}, t \tag{2.6}$$

$$\sum_{tt=t-T_m^{on}+1}^{t} v_{m,tt}^u \leq u_{m,t}, \quad \forall m\in\mathcal{M}, i, t \tag{2.7}$$

$$\sum_{tt=t-T_m^{off}+1}^{t} v_{m,tt}^d \leq 1 - u_{m,t}, \quad \forall m\in\mathcal{M}, i, t \tag{2.8}$$

$$p_{m,t,s} \geq \underline{P}_m \left( u_{m,t} - v_{m,t}^u \right), \quad \forall m\in\mathcal{M}, t, s \tag{2.9}$$

$$p_{m,t,s} \leq \overline{P}_m \left( u_{m,t} - v_{m,t}^u \right) + \underline{P}_m \left( v_{m,t}^d + v_{m,t}^u \right), \quad \forall m\in\mathcal{M}, t, s \tag{2.10}$$

$$p_{w,t,s}^{wind} \leq \overline{P}_{w,t,s}^{wind}, \quad \forall w\in\mathcal{W}_i, i, t, s \tag{2.11}$$

$$-R_m^{down} \leq p_{m,t,s} - p_{m,t-1,s} \leq R_m^{up}, \quad \forall m\in\mathcal{M}, t, s \tag{2.12}$$

$$-\overline{F}_{i,i'} \leq f_{i,i',t,s} \leq \overline{F}_{i,i'}, \quad \forall i'\in\mathcal{I}'(i), i, t, s \tag{2.13}$$

$$f_{i,i',t,s} = \frac{\theta_{i,t,s} - \theta_{i',t,s}}{X_{i,i'}}, \quad \forall i'\in\mathcal{I}'(i), i, t, s \tag{2.14}$$

$$\mu_{g,t,s} = \phi_g p_{g,t,s}, \quad \forall g\in\mathcal{G}, t, s \tag{2.15}$$

$$\alpha^{-}_{j,t,s} + \sum_{\lambda \in \Lambda(j)} \frac{p^{ng}_{\lambda}}{|\mathcal{T}|} + \sum_{\psi \in \Psi(j)} \left(q^{out}_{\psi,t,s} - q^{in}_{\psi,t,s}\right) + \sum_{j'' \in \mathcal{J}''(j)} \eta_{j'',j,t} + \sum_{c'' \in \mathcal{C}''(j)} \eta_{c'',j,t}$$
$$= D^{ng}_{j,t} + \sum_{j' \in \mathcal{J}'(j)} \eta_{j,j',t} + \sum_{c' \in \mathcal{C}'(j)} \eta_{j,c',t} + \sum_{i \in \mathcal{I}} \sum_{g \in \mathcal{G}(i,j)} \mu_{g,t,s} + \alpha^{+}_{j,t,s}, \forall j, t, s \quad (2.16)$$

$$\underline{L}_{\psi} \leq l_{\psi,t,s} \leq \overline{L}_{\psi}, \quad \forall \psi, t, s \quad (2.17)$$

$$-Q_{\psi} \leq \left(q^{out}_{\psi,t,s} - q^{in}_{\psi,t,s}\right) \leq Q_{\psi}, \quad \forall \psi, t, s \quad (2.18)$$

$$l_{\psi,t,s} = l_{\psi,t-1,s} - q^{out}_{\psi,t,s} + q^{in}_{\psi,t,s}, \quad \forall \psi, t, s \quad (2.19)$$

$$l_{\psi,t-1,s} - \overline{L}_{\psi} \leq q^{out}_{\psi,t,s} - q^{in}_{\psi,t,s} \leq l_{\psi,t-1,s} - \underline{L}_{\psi}, \quad \forall \psi, t, s \quad (2.20)$$

$$\underline{\pi}_{j} \leq \pi_{j,t} \leq \overline{\pi}_{j}, \quad \forall j, t \quad (2.21)$$

$$\frac{\pi_{j,t}}{\tau_{j,c'}} \leq \pi_{c',t} \leq \pi_{j,t}\tau_{j,c'}, \quad \forall c' \in \mathcal{C}'(j), t \quad (2.22)$$

$$\eta_{j,j',t} = sgn\left(\pi_{j,t} - \pi_{j',t}\right) C_{j,j'} \sqrt{|\pi_{j,t} - \pi_{j',t}|}, \quad \forall j' \in \mathcal{J}'(j), t \quad (2.23)$$

The objective (2.1) is to minimize the total expected cost which consists of the first stage cost, including the thermal generator start-up and shut-down costs and gas supply cost (first line), and the second stage cost (second line), including the expected electricity production costs of non-gas-fired conventional generators, penalties on unserved/excess electricity, penalties on unserved/excess gas and the net cost of gas flows from storage. Here we count the power production costs for non-gas-fired generators as the product of the production cost per unit electricity and the electricity production. The production costs of the gas-fired generators are the fuel costs coming from the gas production or storage facilities. Constraints (2.2) represent the energy balance at each electricity node in each hour. The UC constraints (2.3)–(2.6) describe the connection between start-up/shut-down and unit on/off status variables. Constraints (2.7)–(2.8) enforce generator minimum on/off times. Constraints (2.9)–(2.10) describe upper and lower limits for the generator production levels and constraints (2.11) impose upper bounds on the wind energy output according to the available wind energy for each hour. Constraints (2.12) specify generator ramping limits. Constraints (2.13)–(2.14) represent the lossless, linearized DC formulation of power flows, limited by the transmission line capacities.

The gas and power system are connected through the amount of gas consumed by gas-fired generators (2.15).

The gas flow constraints (2.16) describe the flow conservation for each scenario in each hour at each node. Constraints (2.17)–(2.18) enforce upper and lower bounds on the storage levels and flow rates into and out of each gas storage facility. Constraints (2.19) connect storage levels of consecutive hours with the flow rates. Constraints (2.20) impose limits on the flow rates to maintain storage levels within prescribed bounds. Because the gas flow through a pipeline, as described by the Weymouth equation, depends on the difference of squared pressure levels between its two end nodes, the gas flow model is formulated in terms of these squared pressures, $\pi_{j,t}$, which are bounded by constraints (2.21). According to a simplified compressor model, the squared pressure increase ratio in each active pipeline is bounded as in (2.22) [18]. It limits the gas pressure increase ratio through compressors. The WEs (2.23) are applied to characterize the gas flows in passive pipelines.

According to the WEs, the gas flow in a passive pipeline is a continuous, nonlinear and non-convex function of the squared pressures at the two end nodes of the pipeline. An incremental method is applied to approximate the nonlinear constraints as piecewise linear with additional binary variables because it is the fastest and most accurate linearization method for the nonlinear Weymouth equation [16]. We divide the squared pressure range into segments and introduce a continuous variable $\delta^k$ and a binary variable $y^k$ for each segment, $k$, where $\delta^k$ represents the portion of segment $k$ that is used and the values of $y^k$ ensure that if any part of a segment is used then all lower-valued segments must be completely used [45]. Upon dividing its domain into intervals with breakpoints $x^k, k \in \mathcal{K}$, a one-dimensional nonlinear function $h(x)$ can be approximated as (2.24)–(2.28).

$$h\left(x\right) \approx h\left(x^1\right) + \sum_{k \in \mathcal{K}} \left[h\left(x^{k+1}\right) - h\left(x^k\right)\right] \delta^k \tag{2.24}$$

$$x = x^1 + \sum_{k \in \mathcal{K}} \left(x^{k+1} - x^k\right) \delta_k \tag{2.25}$$

$$\delta^{k+1} \leq y^k \leq \delta^k, \quad \forall k \in \mathcal{K} - 1 \tag{2.26}$$

$$0 \leq \delta^k \leq 1, \quad \forall k \in \mathcal{K} \tag{2.27}$$

$$y^k \in \{0,1\}, \quad \forall k \in \mathcal{K} \tag{2.28}$$

Accordingly, we linearize constraints (2.23) as (2.29)–(2.35), where the quantities $\Delta\pi^k_{j,j',t}$ are fixed constants.

$$\Delta\pi_{j,j',t} = \pi_{j,t} - \pi_{j',t}, \quad \forall j' \in J'(j), j, t \tag{2.29}$$

$$\Delta\pi_{j,j',t} = \Delta\pi^1_{j,j',t} + \sum_{k\in\mathcal{K}} \left(\Delta\pi^{k+1}_{j,j',t} - \Delta\pi^k_{j,j',t}\right) \delta^k_{j,j',t} \tag{2.30}$$

$$\eta_{j,j',t} = \eta^1_{j,j',t} + \sum_{k\in\mathcal{K}} \left(\eta^{k+1}_{j,j',t} - \eta^k_{j,j',t}\right) \delta^k_{j,j',t} \tag{2.31}$$

$$\eta^k_{j,j',t} = sgn\left(\Delta\pi^k_{j,j',t}\right) C_{j,j'} \sqrt{|\Delta\pi^k_{j,j',t}|} \tag{2.32}$$

$$\delta^{k+1}_{j,j'} \leq y^k_{j,j'} \leq \delta^k_{j,j'}, \quad \forall k \in \mathcal{K} - 1 \tag{2.33}$$

$$0 \leq \delta^k_{j,j'} \leq 1, \quad \forall k \in \mathcal{K} \tag{2.34}$$

$$y^k_{j,j'} \in \{0,1\}, \quad \forall k \in \mathcal{K} \tag{2.35}$$

Overall, the SP model includes equations (2.1)–(2.22) and (2.29)–(2.35).

### 2.2.2 Deterministic Model with Reserves (DR)

The deterministic model with reserves has been implemented in the power system industry, but nobody implemented it for the integrated operation of the power and natural gas system operation. Here we incorporate a simple deterministic model with reserves as the comparable baseline for the SP model. The DR model includes constraints (2.2)–(2.9), (2.11), (2.13)–(2.22), and (2.29)–(2.35) with $\mathcal{S} = \{f\}, \xi_f = 1$ and $\overline{P}^{wind}_{w,t,f} = \hat{P}^{wind}_{w,t}, \forall w, t$. As in the traditional practice, day-ahead uncertainty in the wind energy is managed by including reserves. The objective function (2.36) includes an additional term for non-supplied/excess reserves, and the reserve limits are imposed by replacing the dispatch constraints (2.10) and (2.12) with (2.37)–(2.40). Here we model only operating reserves, which are proportional to the hourly total wind energy forecast as described in (2.38), to protect against wind energy forecast errors. This is consistent with the SP model including scenarios for uncertain wind energy only. Both the SP and the DR models could be

extended to include additional types of reserves including regulating, load-following, contingency, spinning and non-spinning reserves.

$$\min \sum_{t\in\mathcal{T}}\Bigg\{\sum_{n\in\mathcal{N}}\left(C_n^{su}v_{n,t}^{u}+C_n^{sd}v_{n,t}^{d}\right)+\sum_{g\in\mathcal{G}}\left(C_g^{su}v_{g,t}^{u}+C_g^{sd}v_{g,t}^{d}\right)+\sum_{\lambda\in\Lambda}C_\lambda^{ng}p_\lambda^{ng}+\sum_{n\in\mathcal{N}}C_n^{prod}p_{n,t,f}$$
$$+\sum_{i\in\mathcal{I}}\left(\Gamma_\beta^{+}\beta_{i,t,f}^{+}+\Gamma_\beta^{-}\beta_{i,t,f}^{-}\right)+\sum_{j\in\mathcal{J}}\left(\Gamma_\alpha^{+}\alpha_{j,t,f}^{+}+\Gamma_\alpha^{-}\alpha_{j,t,f}^{-}\right)+\sum_{\psi\in\Psi}C_\psi^{stor}q_{\psi,t,f}^{out}+\Gamma_\gamma^{+}\gamma_{t,f}^{+}+\Gamma_\gamma^{-}\gamma_{t,f}^{-}\Bigg\} \tag{2.36}$$

$$0\le p_{m,t,f}+r_{m,t,f}\le\overline{P}_m\left(u_{m,t}-v_{m,t}^{u}\right)+\underline{P}_m\left(v_{m,t}^{d}+v_{m,t}^{u}\right),\quad\forall m\in\mathcal{M},t \tag{2.37}$$

$$\sum_{m\in\mathcal{M}}r_{m,t,f}+\gamma_{t,f}^{-}-\gamma_{t,f}^{+}=WR\sum_{w\in\mathcal{W}}\hat{P}_{w,t}^{wind},\quad\forall t \tag{2.38}$$

$$-R_m^{down}\le p_{m,t,f}-p_{m,t-1,f},\quad\forall m\in\mathcal{M},t \tag{2.39}$$

$$p_{m,t,f}+r_{m,t,f}-p_{m,t-1,f}\le R_m^{up},\quad\forall m\in\mathcal{M},t \tag{2.40}$$

To test the performance of the day-ahead decisions made according to the DR model, we simulate real-time dispatch by fixing the day-ahead decisions and resolving the DR model for each wind energy scenario $s$ in the original set $S$ while replacing $f$ by $s$ in equations (2.36)–(2.40) and setting $r_{m,t,s}=\gamma_{t,s}^{+}=\gamma_{t,s}^{-}=0,\forall m\in\mathcal{M},t,s$. Denoting the optimal cost of the solution under scenario $s$ by $\zeta_s^{DR}$, the expected cost of the DR day-ahead decisions is given by $\zeta^{DR}=\sum_{s\in\mathcal{S}}\xi_s\zeta_s^{DR}$. Fig. 2.1 depicts the process for comparing the SP model with the DR model.

### 2.2.3 Lower Bound for Model Evaluation

A lower bound on the optimal cost from both models can be found by supposing it were possible to make day-ahead decisions with perfect knowledge of the wind energy. We refer to this as the wait and see (WS) model (2.41) . In the WS model, the decision maker makes no decisions until all random parameters $\overline{P}_{w,t,s}^{wind}$ are realized. The optimal values of all decision variables and the objective are scenario-dependent. Denoting the optimal objective value for scenario $s$ as $\zeta_s^{WS}$, the

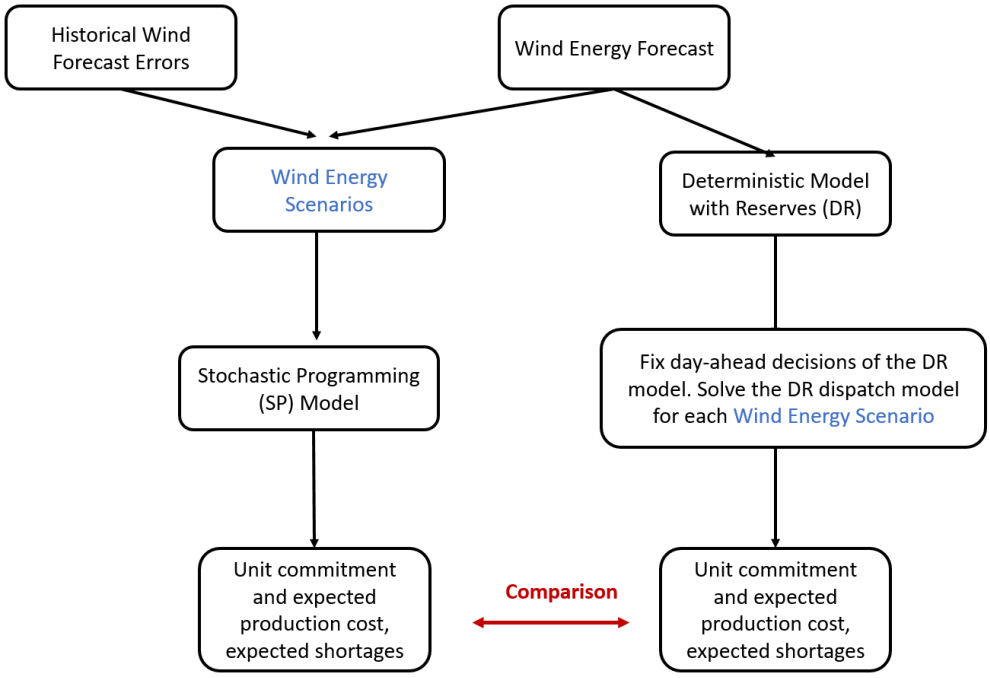


Figure 2.1: Flowchart of procedure for comparing the stochastic programming model and the deterministic model with reserves.

optimal objective value of the WS model is $\Sigma \xi_s \zeta_s^{WS} \leq \zeta^{SP} \leq \zeta^{DR}$.

$$\begin{aligned}\zeta_s^{WS} = \min \; \Bigg\{ & \sum_{t\in\mathcal{T}} \Bigg[ \sum_{n\in\mathcal{N}} \left( C_n^{su} v_{n,t}^u + C_n^{sd} v_{n,t}^d \right) + \sum_{g\in\mathcal{G}} \left( C_g^{su} v_{g,t}^u + C_g^{sd} v_{g,t}^d \right) + \sum_{\lambda\in\Lambda} C_\lambda^{ng} p_\lambda^{ng} \\ & + \sum_{n\in\mathcal{N}} C_n^{prod} p_{n,t,s} + \sum_{i\in\mathcal{I}} \left( \Gamma_\beta^+ \beta_{i,t,s}^+ + \Gamma_\beta^- \beta_{i,t,s}^- \right) + \sum_{j\in\mathcal{J}} \left( \Gamma_\alpha^+ \alpha_{j,t,s}^+ + \Gamma_\alpha^- \alpha_{j,t,s}^- \right) + \sum_{\gamma\in\Psi} C_\psi^{stor} q_{\psi,t,s}^{out} \Bigg] \\ & : (2.2) - (2.8), \\ & (2.9) - (2.22), (2.29) - (2.35) \;\; \text{enforced for this } s \text{ only} \Bigg\}\end{aligned} \tag{2.41}$$

## 2.3 Numerical Studies

We apply our models in two case studies consisting of a six-bus power system with a seven-node gas system [43] and the IEEE 24-bus system with a 20-node gas system. The purpose of the first case study is to compare the total cost distributions of the WS, SP and DR models. The second case study is used to find the scheduling differences of the SP and DR models and compare

the resulting risks and costs. We use a common set of wind energy scenarios, scaled to the wind capacity, in both cases. Because the wind energy scenarios depend on the uncertainty in the wind forecast and this uncertainty varies from day to day, we assess the performance in multiple days in each case study. We assume that 1 kcf of natural gas can generate 1 MBtu of energy in both cases. The mixed-integer programs are solved in their extensive form with GAMS/CPLEX 23.4.3 on a Linux workstation (40 CPU, 252GB RAM).

### 2.3.1 Scenario Generation

Various methods have been proposed for generating wind power scenarios. As this task is not the focus of this paper, we employ wind power scenarios generated for stochastic UC according to the approach described by [24, 57] and assessed by [61]. The important features of this approach are that it identifies a segment of similar historical days based on the characteristics of the day-ahead wind power forecast trajectory and then approximates the stochastic process for actual wind energy within that segment by conditional expectations within ranges of the forecast error distributions for different hours. As a result, a specified number of unequally likely scenario trajectories are generated with different amounts of dispersion on different days. This method can be extended to generate wind energy scenarios with whatever level of temporal detail is available in the forecast and actual wind data. For more details of the scenario generation process, please see [57]. Wind forecast data were obtained from the Bonneville Power Administration [6, 7]. The observed data and the wind generation capacity are available from [7] and [8], respectively. Data were collected for a recent year but, due to missing information for some days, scenarios were generated for only 340 days. A set of 27 scenarios was used for each day with probabilities ranging from 0.0001 to 0.5845. They were scaled according to specified wind capacity penetrations in each case study. To avoid end-of-study effects, the scheduling problems were solved over a 36-hour horizon. Deterministic loads for the first twelve hours were repeated to represent hours 25-36, while each wind power scenario was concatenated with the corresponding one for the following day.

### 2.3.2 Six-Bus System

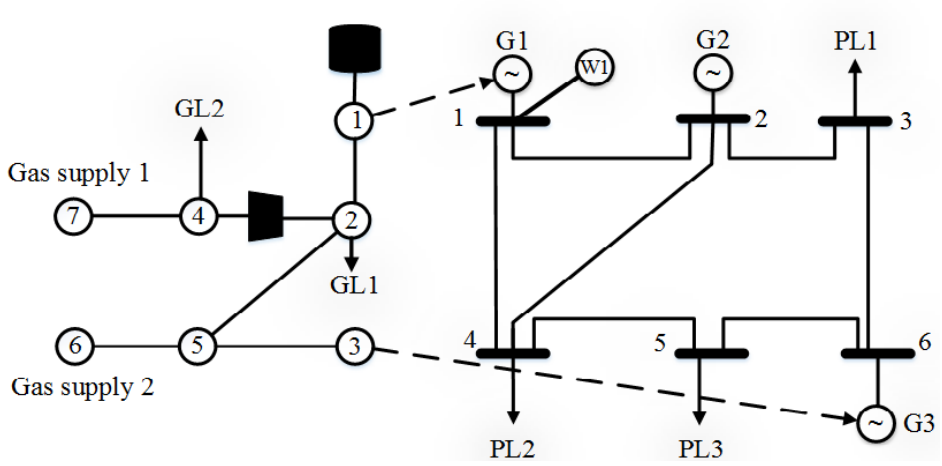


Figure 2.2: Six-bus power system with seven-node gas system. The natural gas system with gas loads (GL) shown on the left-hand side and the power system with power loads (PL), generators (G) and wind generators (W) is shown on the right-hand side. Dashed lines show connections between the two systems.

The six-bus power system with seven-node gas system has two NGPGs, one coal fueled generator, one wind generator (farm), three power loads, seven transmission lines, one storage facility, one active pipeline, five passive pipelines, two non-electric gas loads and two gas suppliers [43], as shown in Fig. 2.2. Hourly gross non-electric gas demand is 6000 kcf/h, divided between gas nodes 2 and 4 with the ratio of 2 to 1. The electric load is divided among power nodes 1, 2 and 3 with the ratio of 1:2:2. We set the hourly reserve margin for wind power WR to be 5% [53]. The wind generation capacity is 20% of the total thermal capacity. The start-up and shut-down cost of all the generators are zero for this case study.

Let $x_{d,s}^{MM}$ and $z_{d,s}^{MM}$ denote the optimal values of the first-stage variables and second-stage variables in scenario $s$ from model $MM$ for day $d$, respectively $MM \in \{DR, SP, WS\}$. The first-stage variables $x_{d,s}^{MM}, MM \in \{SP, DR\}$ are the same for all scenarios $s$; i.e., nonanticipative. Although the optimization process minimizes the total cost over 36 hours, only the optimal decisions of the 24 hours would be implemented. Let $f(x, z)$ denote the 24-hour cost. Expressions (2.42)–(2.43) define the daily expected cost and the cost standard deviation which are used to evaluate the expected total cost and the proxy measure of risk since it is mostly driven by the unserved energy

penalties for model $MM$. The mean expected cost and mean cost standard deviation for $|D|$=340 days are found by using equations (2.44)–(2.46).

$$E_d^{MM} = \sum_{s \in S} \xi_s f(x_{d,s}^{MM}, z_{d,s}^{MM}) \tag{2.42}$$

$$\sigma_d^{MM} = \sqrt{\sum_{s \in S} \xi_s \left[ f(x_{d,s}^{MM}, z_{d,s}^{MM}) - E_d^{MM} \right]^2} \tag{2.43}$$

$$\overline{E^{WS}} = \frac{1}{\mid D \mid} \sum_{d=1}^{|D|} E_d^{WS}, \overline{\sigma^{WS}} = \frac{1}{\mid D \mid} \sum_{d=1}^{|D|} \sigma_d^{WS} \tag{2.44}$$

$$\overline{E^{SP}} = \frac{1}{\mid D \mid} \sum_{d=1}^{|D|} E_d^{WS}, \overline{\sigma^{SP}} = \frac{1}{\mid D \mid} \sum_{d=1}^{|D|} \sigma_d^{SP} \tag{2.45}$$

$$\overline{E^{DR}} = \frac{1}{\mid D \mid} \sum_{d=1}^{|D|} E_d^{WS}, \overline{\sigma^{DR}} = \frac{1}{\mid D \mid} \sum_{d=1}^{|D|} \sigma_d^{DR} \tag{2.46}$$

Table 2.1: Mean expected cost and standard deviation comparison over 36 hours as well as the first 24 hours.

| | Mean expected cost, $\overline{E^{MM}}$ (\$) | | Mean standard deviation, $\overline{\sigma^{WS}}$ (\$) | |
|---|---|---|---|---|
| MM | 36 hours | 24 hours | 36 hours | 24 hours |
| WS | 670,351 | 456,755 | 3,819 | 2,737 |
| SP | 674,114 | 459,331 | 3,847 | 2,883 |
| DR | 886,309 | 623,264 | 5,168 | 3,514 |

Based on experimentation described in Section 2.3.3, we approximate the nonlinear functions with 20 piecewise linear segments. A similar approximation accuracy experiment is conducted in [74] based on Taylor series expansion to linearize the nonlinear constraints. Table 2.1 illustrates that the SP model has mean expected cost and standard deviation nearly as low as the WS model. The DR model results in 36% higher mean expected cost and 32% higher mean standard deviation than the SP model. Fig. 2.3 shows the relative frequency distributions for expected cost and cost standard deviation for the first 24 hours. Because the high cost values are driven by the penalties for unserved energy, we can conclude that the SP model makes more reliable decisions given different wind uncertainty.

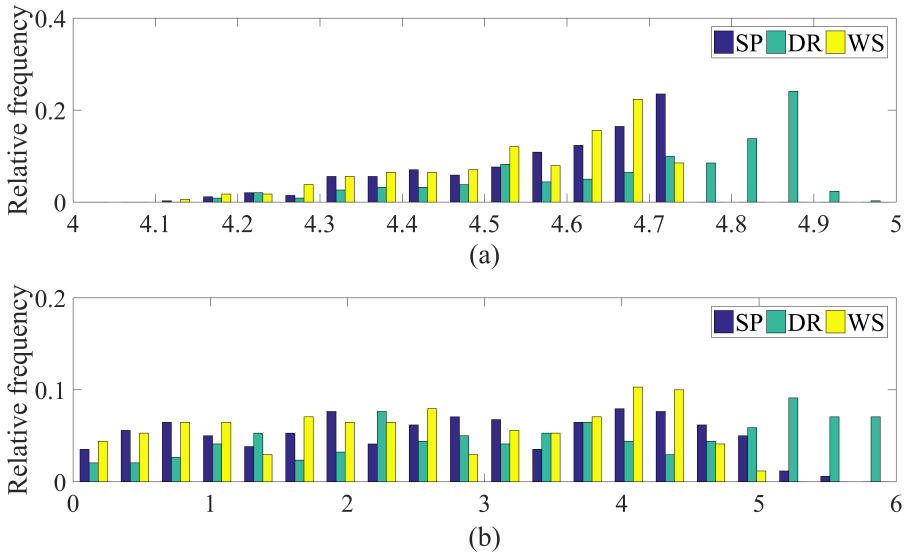


Figure 2.3: (a) Distribution of first 24 hour expected cost $E_d$ ($\$10^5$); (b) Distribution of first 24 hour cost standard deviation $\sigma_d$ ($\$10^3$).

### 2.3.3 24-Bus System

A modified IEEE 24-bus system and modified Belgian 20-node natural gas system are used according to [18] as shown in Fig. 2.4 with the ramp up and down rates and production cost revised in accordance with [66]. The system has 3 NGPGs, 4 coal-fired units, 3 hydro units, 2 wind generators, 38 transmission lines, 9 power loads, 2 gas suppliers (wells), 4 storage facilities, 21 passive pipelines, 3 active pipelines and 17 non-electric gas demands. The unserved energy and non-supplied reserves penalty cost are set to be \$3500/MWh and \$1100/MWh, respectively, as recommended by MISO [46]. The excess energy and reserve penalties are set to be \$350/MWh and \$110/MWh, respectively, while the unserved gas and excess gas penalties are set to be \$3500/kcf and \$350/kcf, respectively. Fig. 2.5 shows the electric load and gas load of 36 hours in which the electric peak load occurs at hour 18 and gas peak load occurs at hour 9. The total thermal generating capacity is 3453 MW, which is the sum of the capacities of all the thermal generators in the IEEE 24-bus system. Two wind generators with identical capacity are added at nodes 7 and 15. Energy production by these wind generators is uncertain in advance. To compare the SP model and the DR model representing different levels of wind energy penetration and resulting

uncertainty, we define the wind energy capacity penetration factor (WPF) to be the ratio of the total wind generation capacity to the total thermal generation capacity; i.e., WPF $= \frac{\sum_{w \in \mathcal{W}} \overline{P}_w^{wind}}{\sum_{m \in \mathcal{M}} \overline{P}_m}$. For example, given WPF=30%, the total wind energy capacity is $0.3 \times 3453\text{MW} = 1035.9\text{MW}$. This implies that each of the two wind generators has a capacity of 517.95 MW. As the WPF increases, the amount of uncertainty increases also; i.e., the variation of wind energy uncertainty given WPF=30% is six times that given WPF=5%.

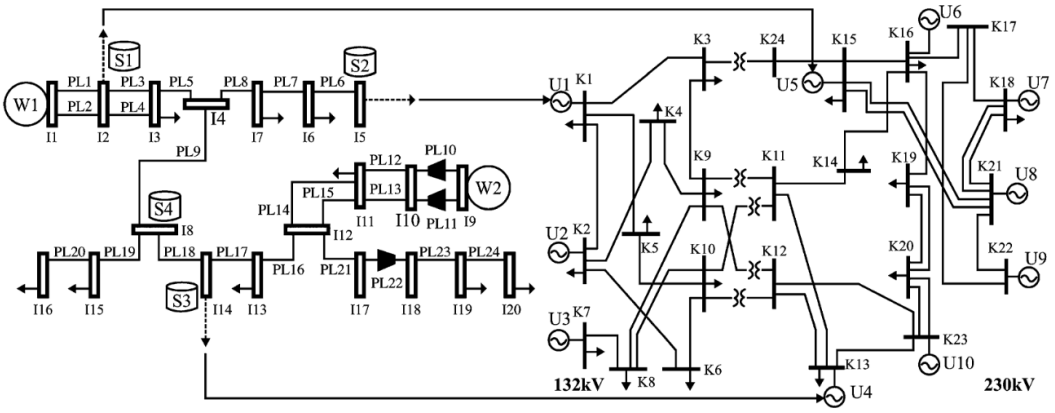


Figure 2.4: Modified IEEE 24-bus system and modified Belgian 20-node natural gas system [18]

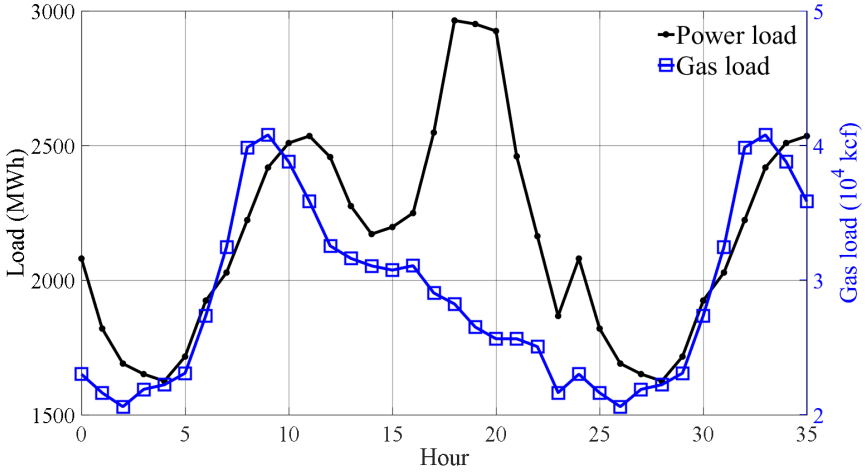


Figure 2.5: Power and gas load profiles.

We identify specific days to examine the results according to the dispersion of the scenarios. Because unserved energy is penalized at a higher rate than excess energy, we measure the dispersion

according to the amount of positive deviation, or *discrepancy*, of a scenario from the forecast. Define $\epsilon_s$ to be the discrepancy between the wind energy forecast and scenario $s$.

$$\epsilon_s = \sum_{t=1}^{36} \sum_{w \in \mathcal{W}} \max \left\{ \hat{P}_{w,t}^{wind} - \overline{P}_{w,t,s}^{wind}, 0 \right\} \tag{2.47}$$

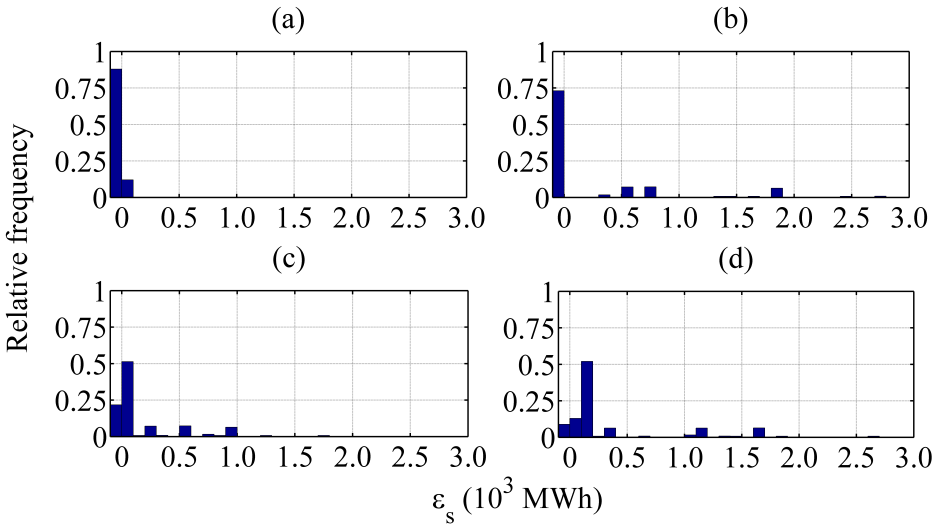


Figure 2.6: Discrepancy histogram of four days.

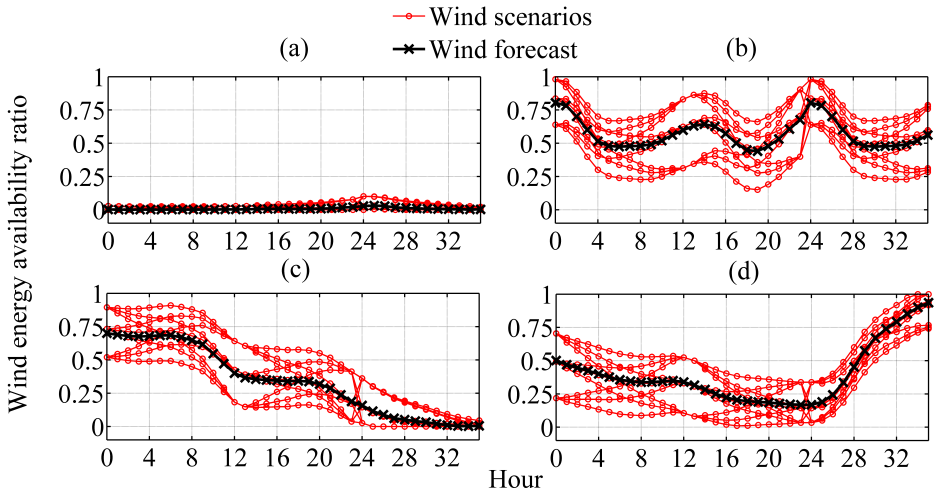


Figure 2.7: Hourly wind availability of scenarios and forecast for four selected days, scaled as a fraction of capacity.

Fig. 2.6 shows the discrepancy histograms of four days, selected based on diversity in the expected value and variance of the discrepancy. Fig. 2.7 shows the wind scenarios and forecast distribution of these four days.

*Day (a)*: Low expected discrepancy and low variance.

*Day (b)*: Low expected discrepancy and medium variance.

*Day (c)*: Medium expected discrepancy and medium variance.

*Day (d)*: Large expected discrepancy and large variance.

Table 2.2: SP model segment experiment result for day (d)

| | WPF=5% | | | | | | WPF=15% | | | | | | WPF=30% | | | | | |
|---|---|---|---|---|---|---|---|---|---|---|---|---|---|---|---|---|---|---|
| $\|K\|$ | 2 | 5 | 10 | 20 | 40 | 80 | 2 | 5 | 10 | 20 | 40 | 80 | 2 | 5 | 10 | 20 | 40 | 80 |
| Expected Cost ($10^3$\$) | 1,822 | 1,782 | 1,782 | 1,782 | 1,782 | 1,782 | 1,741 | 1,701 | 1,701 | 1,701 | 1,701 | 1,701 | 1,649 | 1,609 | 1,609 | 1,609 | 1,609 | 1,609 |
| Time ($10^3 s$) | 10.3 | 0.7 | 5.5 | 42.6 | 18.6 | 143.6 | 7.5 | 1.5 | 0.5 | 0.5 | 0.8 | 94.3 | 6.5 | 1.6 | 55.3 | 44.7 | 59.7 | 77.8 |

Table 2.3: DR model segment experiment result for day (d)

| | | WPF=5% | | | | | | WPF=15% | | | | | | WPF=30% | | | | | |
|---|---|---|---|---|---|---|---|---|---|---|---|---|---|---|---|---|---|---|---|
| | $\|K\|$ | 2 | 5 | 10 | 20 | 40 | 80 | 2 | 5 | 10 | 20 | 40 | 80 | 2 | 5 | 10 | 20 | 40 | 80 |
| | $WR$ | | | | | | | | | | | | | | | | | | |
| Expected Cost ($10^3$\$) | 0.1 | 1822 | 1782 | 1782 | 1790 | 1782 | 1782 | 1742 | 1728 | 1720 | 1720 | 1728 | 1728 | 1656 | 1622 | 1622 | 1622 | 1622 | 1622 |
| | 0.2 | 1822 | 1790 | 1790 | 1782 | 1790 | 1782 | 1765 | 1728 | 1741 | 1720 | 1741 | 1741 | 1658 | 1624 | 1624 | 1624 | 1624 | 1624 |
| | 0.3 | 1822 | 1782 | 1782 | 1782 | 1790 | 1782 | 1765 | 1728 | 1728 | 1741 | 1720 | 1728 | 1665 | 1630 | 1631 | 1630 | 1631 | 1630 |
| | 0.4 | 1822 | 1782 | 1782 | 1790 | 1782 | 1790 | 1765 | 1728 | 1720 | 1741 | 1728 | 1728 | 1668 | 1634 | 1634 | 1634 | 1634 | 1634 |
| | 0.5 | 1822 | 1782 | 1790 | 1790 | 1782 | 1782 | 1747 | 1708 | 1708 | 1708 | 1708 | 1708 | 1677 | 1628 | 1628 | 1628 | 1628 | 1628 |
| | 0.6 | 1831 | 1786 | 1786 | 1786 | 1786 | 1794 | 1747 | 1708 | 1708 | 1708 | 1708 | 1708 | 1670 | 1630 | 1630 | 1631 | 1630 | 1632 |
| | 0.7 | 1831 | 1782 | 1787 | 1782 | 1787 | 1787 | 1749 | 1708 | 1708 | 1708 | 1708 | 1708 | 1672 | 1632 | 1632 | 1632 | 1632 | 1632 |
| | 0.8 | 1831 | 1787 | 1787 | 1782 | 1782 | 1782 | 1749 | 1710 | 1710 | 1710 | 1710 | 1710 | 1683 | 1642 | 1642 | 1642 | 1642 | 1642 |
| | 0.9 | 1822 | 1787 | 1782 | 1782 | 1782 | 1782 | 1750 | 1711 | 1711 | 1711 | 1711 | 1711 | 1691 | 1644 | 1644 | 1644 | 1644 | 1644 |
| | 1 | 1822 | 1787 | 1782 | 1787 | 1787 | 1787 | 1757 | 1719 | 1719 | 1718 | 1719 | 1719 | 1698 | 1652 | 1654 | 1652 | 1652 | 1654 |
| Total Time ($10^3 s$) | | 1.21 | 1.87 | 2.89 | 4.95 | 9.93 | 27.32 | 1.32 | 1.61 | 2.51 | 4.95 | 12.84 | 22.72 | 1.32 | 1.84 | 2.94 | 5.54 | 12.77 | 231.61 |

Before we compare the simulation results of the SP and DR models, we conduct an experiment to study the effect of the number of linearization segments $|K|$ for both models for day (d) to choose an efficient approximation while maintaining a relatively accurate cost. Each segment has equal length. The minimum and maximum breakpoints of a passive pipeline from $j$ to $j'$ are $\underline{\pi}_j - \overline{\pi}_{j'}$ and $\overline{\pi}_j - \underline{\pi}_{j'}$, respectively. As illustrated in Tables 2.2 and 2.3, as $|K|$ increases from 2 to 80, the optimal costs of SP and DR model first change rapidly and become stable when $|K| \geq 40$, while

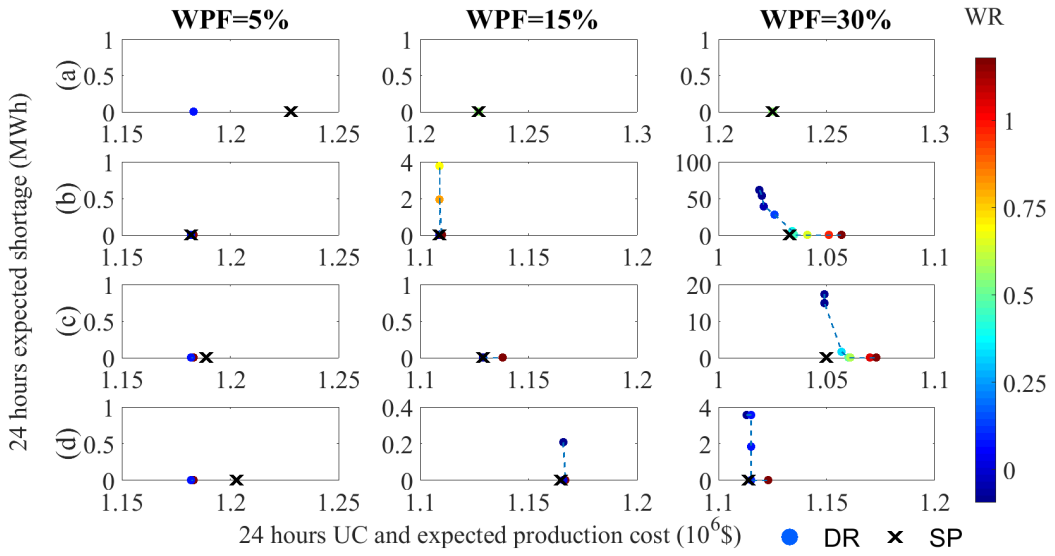


Figure 2.8: Expected total cost less penalty versus expected shortage of the first 24 hours with WPF of 5%, 15% and 30% and WR ranging from 10% to 100%. The scale of each subplot is adjusted for visibility of the results and the comparison between the DR model and the SP model within each subplot.

the computational time generally increases with $|K|$. In addition, it takes more than 24 hours to find the optimal solution when $|K|= 80$. Because the daily short-term operation of natural gas and power system requires solutions to be found quickly, we choose $|K|= 40$ for the following case study.

To compare the costs and risks from the SP and DR models, we plot the UC and expected production cost versus expected shortage across all 27 scenarios for the first 24 hours with WPF of 5%, 15% and 30% and WR of 10%, 20%, 30%, 40%, 50%, 60%, 70%, 80%, 90% and 100% in Fig. 2.8. The rows and columns contain plots for different cases and WPF levels, respectively. The SP model has no unserved energy in any of the 12 subplots. As the WPF increases from 5% to 30%, the 24-hour UC and expected production cost decreases for all four of the days and both models. The DR model has zero unserved energy and lower 24-hour UC and expected cost than the SP model given WPF equals to 5%. Here we minimize the expected cost including not only UC and expected production cost but also unserved and excess penalties for 36 hours. It is not guaranteed that the first 24-hour UC and expected cost of the SP model is less than that of the DR model.

For each of the four cases, the SP model has less expected shortage than the DR model when the WPF equals 15% or 30%, indicating that the SP model lowers the risk of operating the system while maintaining a low UC and expected production cost.

Table 2.4: Optimal unit commitment decisions for day (b) with WPF = 30% and WR = 40%.

| Unit | Fuel Type | SP model hours (1-24) |
|---|---|---|
| 1 | Gas | 1 1 1 1 1 1 0 0 0 0 1 1 1 1 1 1 1 1 1 1 1 1 |
| 4 | Gas | 1 1 1 1 1 1 1 1 1 1 1 1 1 1 1 1 1 1 1 1 1 1 1 1 |
| 5 | Gas | 1 1 1 1 1 1 1 1 0 0 0 0 1 1 1 1 1 1 1 1 1 1 1 |
| 2 | Coal | 0 0 0 0 0 0 0 1 1 1 1 1 1 1 1 1 1 1 1 1 0 0 0 |
| 3 | Coal | 1 1 1 1 1 1 1 1 1 1 1 1 1 1 1 1 1 1 1 1 1 1 1 |
| 6 | Coal | 0 0 0 0 0 0 0 0 0 0 0 0 0 0 0 0 0 0 0 0 0 0 0 0 |
| 7 | Coal | 1 1 1 1 1 1 1 1 1 1 1 1 1 1 0 0 0 0 0 0 0 0 0 0 |

| Unit | Fuel Type | DR model hours (1-24) |
|---|---|---|
| 1 | Gas | 1 1 1 1 1 1 1 1 1 1 1 1 1 1 1 1 1 1 1 1 1 1 1 1 |
| 4 | Gas | 1 1 1 1 1 1 1 1 1 1 1 1 1 1 1 1 1 1 0 0 0 0 0 0 |
| 5 | Gas | 1 1 1 1 1 1 1 0 0 0 0 0 0 0 0 0 0 1 1 1 1 1 1 1 |
| 2 | Coal | 0 0 0 0 0 0 0 0 0 0 0 0 0 0 0 0 0 0 0 0 0 0 0 0 |
| 3 | Coal | 1 1 1 1 1 1 1 1 1 1 1 1 1 1 1 1 1 1 1 1 1 1 1 1 |
| 6 | Coal | 0 0 0 0 0 0 0 0 0 0 0 0 0 0 0 0 0 0 0 0 0 0 0 0 |
| 7 | Coal | 1 1 1 1 1 1 1 1 1 1 1 1 1 1 1 1 1 1 1 0 0 0 0 0 |

Day (b) has the largest difference between the SP and DR models, as illustrated in Fig. 6(b). As the WPF increases to 30%, the expected energy shortage of the DR model increases dramatically while that of the SP model remains at zero. In addition, as the WR increases from 10% to 100%, the expected shortage of the DR model decreases. When WR is greater than 80%, there is no unserved energy in the DR model, and the UC and expected production cost of the SP model is less than that of the DR model. Table 2.4 displays the hourly UC schedule for day (b) with WPF of 30%, selected based on the greatest difference between the results of the two models, and WR of 40%. Among the seven thermal units, units 1, 4 and 5 are NGPGs, while units 2, 3, 6 and 7 are coal fueled. Units 8, 9 and 10 are hydro generators which are assumed free and always on. Here the NGPGs are cheaper than the coal fueled generators and the SP model always commits one unit more than the DR model does in hour 7–21. Production levels of well 1 of the SP and DR models are identical and equal to 861,983 kcf/day, while those of well 2 are 0 kcf/day for both models. The corresponding 24 hour UC and expected production costs are $1,032,629 and

$1,025,947, respectively, for the SP and DR models, while the respective expected shortage amounts are 0 and 28 MWh. The SP model commits more units in each hour to increase the committed capacity and assure that sufficient electricity can be produced in case less wind energy is available than forecast. The SP model is able to firm the variable wind energy by committing more units and supplying more gas since DR model makes the day-ahead decisions only on the basis of the wind energy forecast and reserve margins.

Table 2.5: Comparison of shortages in the first 24 hours for different scenarios day (b) with 30% wind capacity penetration factor (WPF) and 40% wind reserve margin (WR).

| **Scenario** | 1 | 2 | 3 | 4 | 5 | 6 | 7 | 8 | 9 |
|---|---|---|---|---|---|---|---|---|---|
| **Probability** | 0.0010 | 0.0079 | 0.0010 | 0.0079 | 0.0634 | 0.0080 | 0.0010 | 0.0080 | 0.0010 |
| **SP shortage** | 20 | 0 | 0 | 0 | 0 | 0 | 0 | 0 | 0 |
| **DR shortage** | 344 | 327 | 327 | 0 | 0 | 0 | 0 | 0 | 0 |
| **Scenario** | 10 | 11 | 12 | 13 | 14 | 15 | 16 | 17 | 18 |
| **Probability** | 0.0079 | 0.0636 | 0.0080 | 0.0636 | 0.5110 | 0.0647 | 0.0080 | 0.0646 | 0.0082 |
| **SP shortage** | 0 | 0 | 0 | 0 | 0 | 0 | 0 | 0 | 0 |
| **DR shortage** | 293 | 276 | 276 | 0 | 0 | 0 | 0 | 0 | 0 |
| **Scenario** | 19 | 20 | 21 | 22 | 23 | 24 | 25 | 26 | 27 |
| **Probability** | 0.0010 | 0.0080 | 0.0010 | 0.0080 | 0.0647 | 0.0082 | 0.0010 | 0.0082 | 0.0010 |
| **SP shortage** | 0 | 0 | 0 | 0 | 0 | 0 | 0 | 0 | 0 |
| **DR shortage** | 155 | 239 | 239 | 0 | 0 | 0 | 0 | 0 | 0 |

C

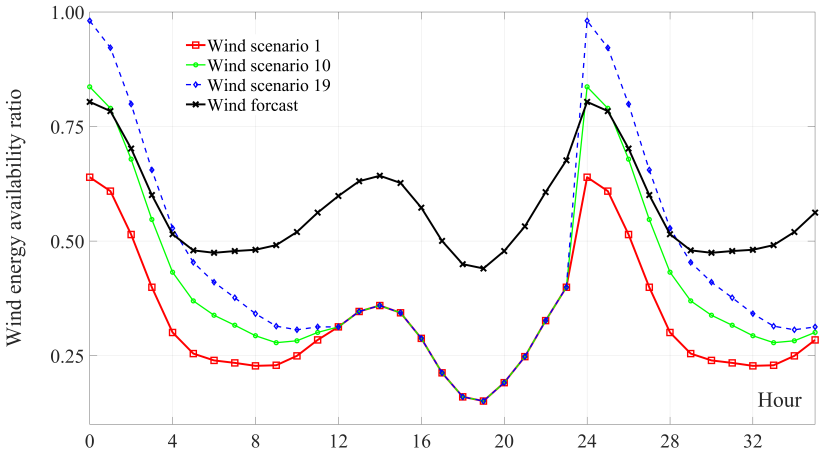


Figure 2.9: Hourly wind availability, scaled to capacity, of scenarios and forecast for day (b).

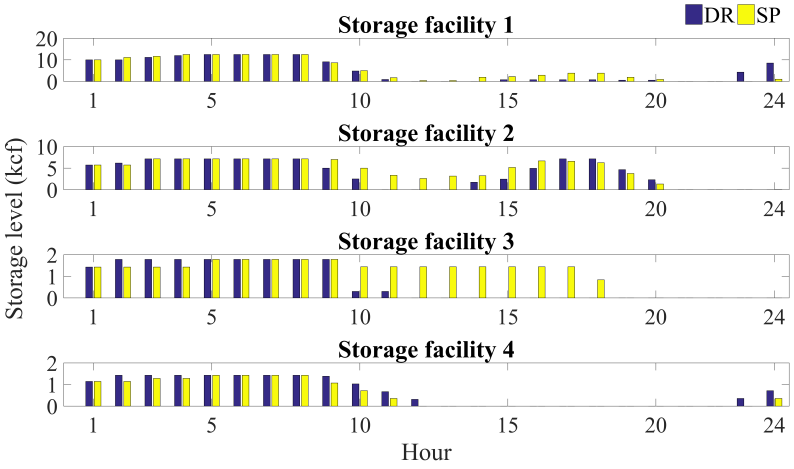


Figure 2.10: Hourly storage level of four storage facilities with 30% wind capacity penetration factor and 40% wind reserve margin for day (b) for scenario 1.

To explore the reliability comparison further, Table 2.5 reports shortages in different scenarios from using the SP and DR models in day (b) with 30% wind capacity penetration and 40% WR, reported for the first 24 hours. Scenario 1 has one of the most different shortage between the SP and DR models, where the shortages of the two models are 20 MWh and 344 MWh, respectively. Fig. 2.9 shows the wind energy availability time series of the scenarios 1, 10 and 19 as well as forecast for day (b), expanded from Fig. 7(b). In hour 20, the wind energy availability of scenario 1 is only 21% less than forecast, whereas at hour 1, the wind energy availability of scenario 1 is 80% less than forecast. On average the wind energy availability of scenario 1 is 55% of the forecast. The DR model resorts to 327 MW of electric load shedding in scenario 1 during hours 11–13 because of the high electric and gas loads and large wind energy discrepancy. A WR of 40% still results in considerable shortage because all four storage facilities run out of gas as listed in Fig. 2.10 and line congestion occurs. Specifically, for example, under scenario 1, power node 17 has the most non-served energy of 196.60 MWh in hour 12. There are three lines connecting to power node 17. Both line 28 from power node 16 to 17 and line 29 from power node 17 to 18 reach the maximum flow of -500 MWh. Line 31 from power nodes 17 to 22 has a flow of 196.60 MWh. In other words, among all the three lines connecting to power node 17, the optimal solution has only one power

flow into power node 17 through line 29 and both the other two lines have power flows out of power node 17. Power flow constraints through line 29 are binding and congestion occurs. As the WR increases to 50%, the 24 hour expected unserved energy is reduced to 6 MWh and the UC and expected production cost increases to $\$1.035 \times 10^6$, whereas the cost of the SP model is $\$1.026 \times 10^6$. In general, the SP model is able to make day-ahead and real time decisions with a better cost-risk trade-off for the integrated natural gas and power system while accounting for network constraints, including crucial limitations on gas storage capacity, as well as the uncertain discrepancy between actual and forecast wind energy.

## 2.4 Conclusion

We compare a two-stage stochastic program (SP) and a deterministic model with forecast-based wind reserves (DR) to model the short-term combined scheduling of the natural gas and power systems while minimizing the total operational cost with uncertain wind energy. Simulation results are compared with multiple wind uncertainty scenarios in two case studies. In the smaller case study of a six-bus power system and seven-node natural gas system, we simulate a year's worth of days to capture the variability of the daily wind energy forecast and the resulting wind energy scenarios. The simulation results indicate that the SP model yields a much lower standard deviation and mean cost, suggesting that probabilistic-scenario-based scheduling of the combined system is better able to maintain a stable cost.

The two models are further compared using a 24-bus power system and 20-node natural gas system in four days that differ according to discrepancy between the wind energy scenarios and forecast, three WPF of 5%, 15% and 30%, and various wind reserve margins (WR). With WPF=5%, the DR model maintains no expected unserved energy and has less expected cost than the SP model. When the WPF equals 15% or 30%, the combination of expected cost and expected unserved energy resulting from the SP model consistently dominates that from the DR model. By adjusting the thermal unit commitments along with the gas supply and pipeline working schedule on the day

ahead to the level of uncertainty present in the scenarios, the SP model avoids shortages (high risks) while achieving low costs given relatively high wind penetration level.

Linearization experiments were done for both the small and large case studies to choose a number of segments that balances accuracy and computational efficiency. The details of the large system segment experiment indicates that the SP model is more robust to the number of segments. In this paper we modeled the unit commitment and economic dispatch process of the power system in two stages. Alternatively, more stages may be included with, for example, a third stage that explicitly addresses the intra-hourly dispatch process. Security constraints could be added to protect against equipment failure. Finally, more efficient stochastic programming solution algorithms such as progressive hedging could be applied to improve time and memory efficiency.

In future work, investigation of a good method to choose breakpoints in the piecewise linear formulation can improve approximation accuracy. To improve computational efficiency, use of the three-binary model [48] for unit commitment should be investigated also.

# CHAPTER 3. QUANTIFYING THE EFFECT OF UNCERTAINTY IN THE GAS SPOT PRICE ON POWER SYSTEM DISPATCH COSTS WITH ESTIMATED CORRELATED UNCERTAINTIES

A paper under review by the *Energy Systems*

## Abstract

Electricity generation increasingly relies on natural gas for fuel. The competing demands for gas by other users who may have higher priority, the lack of coordination between gas and electricity markets, and extreme weather events all pose risks to systems with high dependence on gas. When the gas supply on which generators have planned is limited, operators may dispatch more costly units and generators may switch to alternative fuels or procure gas at high spot prices. All these efforts to avoid load-shedding result in higher electricity costs. To assess this economic risk we approximate the distribution of the daily operational cost to satisfy demand for electricity by conducting simulations of dispatch. Input parameters are sampled from a temporal and weather conditional joint distribution of daily electric load and spot price of gas. To isolate the impact of uncertainty in the gas price, we generate a benchmark distribution of the dispatch cost by fixing the gas price at its expectation while sampling from the marginal distribution for load, and compare the distribution generated from uncertainty in both the gas price and the load against this benchmark. The risk is quantified by alternatively computing the distance between dispatch cost distributions or by the difference between the values of a risk measure applied to each distribution. In a numerical case study we demonstrate how such risk quantification can be used to evaluate alternative risk-mitigation strategies at the system level.

**Keywords :** Economic dispatch, natural gas, bivariate normal distribution, Wasserstein distance, conditional value-at-risk

## 3.1 Introduction

Due to the retirements of coal-fired and nuclear generators, the development of highly efficient gas-fired generators, the increase of natural gas supply with a relatively stable gas price over the last decade, and potential emission regulations, natural gas and renewable energy sources have taken a rapidly increasing share of electricity production. Natural gas experiences a more competitive market than other fossil fuels because of its fast procurement and low price. Although increased reliance on natural gas decreases operational cost and environmental pollution, it also increases the fuel risk in the power system. Short-term dispatch decisions by the power system operator determine the cost of serving the realized electric demand under increasingly constrained gas supply and uncertain spot prices. Natural gas consumers usually sign contracts, consisting of either interruptible or firm contracts, with the pipeline companies. Residential, industrial, and commercial entities usually are willing to pay higher prices for firm contracts in exchange for guaranteed supply. However, many electricity generators in competitive wholesale markets rely on interruptible contracts, which carry lower prices but make the generators vulnerable to disruptions in fuel delivery. Such a disruption may occur in case of a contingency in the gas system or a dramatic increase in demand by the firm contract holders. The gas generators may then have no alternative but to acquire fuel from the spot market at a high price caused by the same supply disruption or demand spike. High wholesale electricity prices result from these efforts to avoid outages, as were seen in the eastern U.S. during early January, 2018; the 2013-14 Polar Vortex events [65]; and earlier severe-weather events in Texas, New England, and Colorado [64]. For the longer term, understanding the risk imposed by dependence on interruptible contracts and exposure to the volatile spot market can help generators and system operators to evaluate potential investments to mitigate the risk.

Our goal in this paper is to present approaches for quantifying the risk imposed by limited natural gas availability and price uncertainty in terms of the probability distribution of daily dispatch cost based on the joint distribution of load and gas spot prices. We generate discrete scenarios for natural gas price jointly with electric load. The impact of uncertainty in natural gas availability is assessed through sensitivity analysis. An electricity system operator can use the quantification methods to evaluate alternative risk-mitigation strategies according to the tradeoff between investment cost and risk reduction.

Previous research has investigated various aspects of the effect of gas system uncertainties on the power system. For evaluating bidding strategies and efficiencies of an integrated gas-fired unit and power-to-gas conversion facility, the financial risk introduced by the uncertain price gap between electricity and natural gas was assessed according to the conditional value at risk (CVaR) [42]. The effect of gas supply uncertainty and gas price variability on unit commitment has been investigated by stochastic programming with a small number of discrete scenarios [78]. However, both references [42] and [78] consider only a single natural gas price parameter. In fact, the current gas-fired generators acquire gas from both contracts and the spot market at different prices. While the contracted natural gas price is fixed, that from the spot market has high uncertainty. In addition, the scenarios in the literature are frequently generated without any validation using actual data. Some papers discuss methodologies to assess the forecast uncertainty associated with gas prices; for example, based on weekly data [34]. At the same time, substantial research has been aimed at generating point or probabilistic forecasts of the electric load [23]. The gas spot price is highly correlated with electric load, especially in severe cold weather. But few studies have investigated their joint distribution. To our knowledge, no previous work has addressed the dispatch cost risk resulting from these uncertainties or their influence on the selection of a risk-mitigation strategy.

In this paper, from the viewpoint of an independent system operator (ISO), we propose a dispatch model incorporating the gas availability from both contracts and the spot market. Extending the work in [29], we estimate a joint distribution of daily electric load and gas spot price for use as input to the probabilistic simulation of the dispatch. The objective of this research is to quantify

the effect of uncertainties in the availability of natural gas from contracts, as well as its price in the spot market, on the economic dispatch cost. We compare the dispatch cost distributions obtained with and without uncertainty in the spot price for various levels of available contracted gas with the same marginal distribution for electric load. The contributions of this paper are summarized as follows:

- Formulate an economic dispatch model considering gas availability and prices from both contracts and the spot market;
- Estimate the joint distribution functions of temporal and weather conditional daily electric load and natural gas spot price by segmentation, transformation, and fitting bivariate normal distributions in each segment;
- To quantify the effect of uncertain natural gas spot price on the dispatch cost, apply the Wasserstein distance metric and CVaR difference to characterize the disparity between the cost distribution functions generated from two simulations, where one simulation uses a point estimate for gas spot price and the other one uses the spot price distribution;
- Demonstrate how to employ the uncertainty quantification, as well as the CVaR of the cost distribution directly, to inform choices among alternative risk-mitigation strategies; namely, dual fuel capability conversion and the addition of a gas storage facility, in a case study.

In the remainder of this paper, the economic dispatch model is formulated in Section 3.2. In Section 3.3, we describe how to estimate the joint distribution functions for the daily electric load and the daily gas spot price for different weather conditions and seasons. Section 3.4 describes the detailed steps to quantify the effect of uncertain natural gas spot price on dispatch cost. Section 3.5 revises the dispatch cost model of Section 3.2 according to alternative risk-mitigation strategies. Case studies and numerical results are shown in Section 3.6, and finally Section 3.7 concludes.

## 3.2 Economic Dispatch Model (ED) with Natural Gas Availability Constraints

We formulate a linear programming (LP) model of the daily economic dispatch problem with hourly time steps considering gas price and availability from both contracts and the spot market. To focus on the risk imposed by reliance on interruptible contracts, we assume all gas-fired generators choose such contracts for fuel delivery. First we introduce the following notation:

**Sets**

| | |
|---|---|
| $\mathcal{J}$ | Gas nodes, indexed by $j$ |
| $\mathcal{J}'(j)$ | Gas nodes connected to $j$ by passive pipelines from $j$, indexed by $j'$ |
| $\mathcal{J}''(j)$ | Gas nodes connected to $j$ by passive pipelines to $j$, indexed by $j''$ |
| $\Lambda(j)$ | Gas wells in node $j$, indexed by $\lambda$; $\Lambda = \bigcup_{j\in\mathcal{J}} \Lambda(j)$ is the set of all gas wells |
| $\Psi(j)$ | Storage facilities in node $j$, indexed by $\psi$; $\Psi = \bigcup_{j\in\mathcal{J}} \Psi(j)$ is the set of all storage facilities |
| $\Psi'(j)$ | Added storage facilities in node $j$, indexed by $\psi$; $\Psi' = \bigcup_{j\in\mathcal{J}} \Psi'(j)$ is the set of all added storage facilities |
| $\mathcal{I}$ | Electricity nodes, indexed by $i$ |
| $\mathcal{I}'(i)$ | Electricity nodes connected to $i$ by a transmission line from $i$, indexed by $i'$ |
| $\mathcal{I}''(i)$ | Electricity nodes connected to $i$ by a transmission line to $i$, indexed by $i''$ |
| $\mathcal{G}(i,j)$ | Gas-fired generators at power node $i$ and gas node $j$, indexed by $g$; $\mathcal{G} = \bigcup_{i\in\mathcal{I},j\in\mathcal{J}} \mathcal{G}(i,j)$ is the set of all gas-fired generators |
| $\mathcal{G}'(i,j)$ | Gas-fired generators converted to dual fuel units at power node $i$ and gas node $j$, indexed by $g'$; $\mathcal{G}'(i,j) \in \mathcal{G}(i,j)$; $\mathcal{G}' = \bigcup_{i\in\mathcal{I},j\in\mathcal{J}} \mathcal{G}'(i,j)$ is the set of all gas-fired generators converted to dual fuel units |
| $\mathcal{N}(i)$ | Conventional non-gas-fired generators at node $i$, indexed by $n$; $\mathcal{N} = \bigcup_{i\in\mathcal{I}} \mathcal{N}(i)$ is the set of all non-gas-fired generators |
| $\mathcal{K}$ | Set of all gas-fired and non-gas-fired generators, indexed by $k$; $\mathcal{K} = \mathcal{G} \cup \mathcal{N}$ |
| $\mathcal{T}$ | Hours from 1 to $\lvert\mathcal{T}\rvert$, indexed by $t$ |

**Fixed Parameters**

| | |
|---|---|
| $u_{g,t}, u_{n,t}, u_{k,t}$ | Unit commitment indicator: equals 1 if unit is online in hour $t$ and 0 otherwise |
| $v^u_{g,t}, v^u_{n,t}, v^u_{m,t}$ | Unit start-up indicator: equals 1 if the unit is started up in hour $t$ and 0 otherwise |
| $v^d_{g,t}, v^d_{n,t}, v^d_{m,t}$ | Unit shut-down indicator: equals 1 if the unit is shut down in hour $t$ and 0 otherwise |
| $\lambda^C_g$ | Gas price from contract [$/kcf] |
| $\lambda^\Lambda_\lambda$ | Gas price of the storage outflow [$/kcf] |
| $\overline{L}_\psi, \underline{L}_\psi$ | Maximum and minimum storage level [kcf] |
| $\Delta\overline{L}_\psi$ | Increased storage capacity [kcf] |
| $\overline{q}_\psi$ | Max net flow (outflow minus inflow) [kcf] |
| $\phi_g$ | Efficiency of gas generator [kcf/MWh] |
| $\phi^{oil}_{g'}$ | Cost of using oil as dual fuel [$/MWh] |
| $C^{prod}_n$ | Power production cost [$/MWh] |
| $\Gamma^-_\beta, \Gamma^+_\beta$ | Unserved/excess electric penalty [$/MWh] |
| $\Gamma^-_\alpha, \Gamma^+_\alpha$ | Unserved/excess gas penalty [$/kcf] |
| $\overline{P}_g, \underline{P}_g, \overline{P}_n, \underline{P}_n, \overline{P}_k, \underline{P}_k$ | Max/min electricity generation [MWh] |
| $\overline{F}_{i,i'}$ | Max line flow from $i$ to $i'$ [MWh] |
| $x_{i,i'}$ | Transmission line impedance from $i$ to $i'$ [pu] |
| $\overline{G}_{j,t}$ | Nominal available gas from gas contract for the power system as planned in day-ahead unit commitment [kcf] |

**Uncertain Parameters**

| | |
|---|---|
| $D_{i,t}$ | Electric load [MWh] |
| $\Lambda^M$ | Gas price in the spot market [$/kcf] |

**Nonnegative Decision Variables**

| | |
|---|---|
| $\alpha^-_{j,t}$,$\alpha^+_{j,t}$ | Unserved/excess gas [kcf] |
| $l_{\psi,t}$ | Storage level [kcf] |
| $p_{g,t}, p_{n,t}, p_{k,t}$ | Electricity production [MWh] |
| $\beta^-_{i,t}$,$\beta^+_{i,t}$ | Unserved/excess electricity [MWh] |
| $q^{out}_{\psi,t}, q^{in}_{\psi,t}$ | Out/in-flow of storage facility [kcf/h] |
| $m_{j,t}$ | Gas from spot market for the power system [kcf] |
| $\eta^C_{g,t}$ | Consumed gas from pipeline contract [kcf] |
| $\eta^M_{g,t}$ | Consumed gas from spot market [kcf] |

**Unrestricted Decision Variables**

| | |
|---|---|
| $\theta_{i,t}$ | Phase angle [rad] |
| $f_{i,i',t}$ | Line flow from $i$ to $i'$ [MWh] |

The economic dispatch model including constraints on contracted gas availability and prices from both contract and the spot market is formulated as follows:

$$\min \sum_{t\in\mathcal{T}} \Bigg\{ \sum_{g\in\mathcal{G}} \lambda^C_g \eta^C_{g,t} + \sum_{j\in\mathcal{J}} \Lambda^M m_{j,t} + \sum_{n\in\mathcal{N}} C^{prod}_n p_{n,t} + \sum_{\psi\in\Psi} \lambda^{\Psi}_{\psi,t} q^{out}_{\psi,t} + \sum_{i\in\mathcal{I}} \left( \Gamma^+_\beta \beta^+_{i,t} + \Gamma^-_\beta \beta^-_{i,t} \right) + \sum_{j\in\mathcal{J}} \left( \Gamma^+_\alpha \alpha^+_{j,t} + \Gamma^-_\alpha \alpha^-_{j,t} \right) \Bigg\} \tag{3.1}$$

s.t.

$$\sum_{j\in\mathcal{J}} \sum_{g\in\mathcal{G}(i,j)} p_{g,t} + \sum_{n\in\mathcal{N}(i)} p_{n,t} + \sum_{i''\in\mathcal{I}''(i)} f_{i'',i,t} + \beta^-_{i,t} = D_{i,t} + \sum_{i'\in\mathcal{I}'(i)} f_{i,i',t} + \beta^+_{i,t}, \quad \forall i,t \tag{3.2}$$

$$p_{k,t} \geq \underline{p}_k \left( u_{k,t} - v^u_{k,t} \right), \quad \forall k \in \mathcal{K}, t \tag{3.3}$$

$$p_{k,t} \leq \overline{p}_k \left( u_{k,t} - v^u_{k,t} \right) + \underline{p}_k \left( v^d_{k,t} + v^u_{k,t} \right), \quad \forall k \in \mathcal{K}, t \tag{3.4}$$

$$f_{i,i',t} = \frac{\theta_{i,t} - \theta_{i',t}}{x_{i,i'}}, \quad \forall i' \in \mathcal{I}'(i), i, t \tag{3.5}$$

$$-\overline{F}_{i,i'} \leq f_{i,i',t} \leq \overline{F}_{i,i'}, \quad \forall i' \in \mathcal{I}'(i), i, t \tag{3.6}$$

$$\phi_g p_{g,t} = \eta^C_{g,t} + \eta^M_{g,t} + \eta^{out}_{g,t}, \quad \forall g, t \tag{3.7}$$

$$\sum_{i \in \mathcal{I}} \sum_{g \in \mathcal{G}(i,j)} \eta^C_{g,t} \leq \rho \overline{G}_{j,t}, \quad \forall j, t \tag{3.8}$$

$$\sum_{i \in \mathcal{I}} \sum_{g \in \mathcal{G}(i,j)} \phi_g p_{g,t} + \alpha^+_{j,t} \leq \rho \overline{G}_{j,t} + m_{j,t} + \sum_{\psi \in \Psi(j)} \left(q^{out}_{\psi,t} - q^{in}_{\psi,t}\right) + \alpha^-_{j,t}, \quad \forall j, t \tag{3.9}$$

$$\underline{L}_\psi \leq l_{\psi,t} \leq \overline{L}_\psi, \quad \forall \psi, t \tag{3.10}$$

$$-\overline{q}_\psi \leq \left(q^{out}_{\psi,t} - q^{in}_{\psi,t}\right) \leq \overline{q}_\psi, \quad \forall \psi, t \tag{3.11}$$

$$l_{\psi,t} = l_{\psi,t-1} - q^{out}_{\psi,t} + q^{in}_{\psi,t}, \quad \forall \psi, t \tag{3.12}$$

The daily economic dispatch (ED) problem finds production quantities for the committed thermal units for each hour that minimize the total cost, including the production cost and penalties for energy imbalances, while satisfying the electric load, transmission and other operational constraints. The objective (3.1) is to minimize the total daily dispatch cost, including the fuel cost from contracts and the spot market for gas-fired generators, the production cost of the non-gas generators, the net cost of gas flows from storage and the penalties on non-served or excess electricity and gas demands. Constraints (3.2) enforce the power balance at each electricity node for each hour. Constraints (3.3)–(3.4) limit the minimum and maximum production by each generator based on its commitment status in each hour. Constraints (3.5)–(3.6) compute and limit the flows through transmission lines according to a linear DC approximation. Constraints (3.7) compute the gas consumption, which comprises gas from contracts, the spot market and storage facilities. Constraints (3.8) dictate that the total gas quantity consumed by the gas-fired generators does not exceed the current available gas quantity from the contracts. To assess the effect of uncertainty in the gas availability on the dispatch cost, a contracted gas availability factor, $\rho$, and nominal available gas quantities from contracts for the power system, $\overline{G}_{j,t}$, are defined as parameters. The latter are determined along with the unit commitment status parameters in a prior optimization. Thus, $\rho\overline{G}_{j,t}$ represents various levels of contracted gas availability. Any $\rho < 1$ indicates that less gas than desired is available, and thus the committed gas-fired generators cannot obtain enough gas from contracts and must acquire it from the spot market. Meanwhile, some non-gas-fired generators might have to be dispatched

at higher levels. Any $\rho > 1$ indicates a surplus, in which case the gas-fired generators have more flexibility of obtaining gas from the spot market if the spot price is low or as contracted from the pipeline if the spot price is high. Constraints (3.9) express the gas balance for each hour at each gas node where a linear function is applied to describe the input-output curve [38]. Constraints (3.10)–(3.11) define the upper and lower limits on the storage levels and flow rates of each gas storage facility. Constraints (3.12) connect storage levels of consecutive hours.

## 3.3 Uncertainty Identification

We view the electric load and natural gas spot price as the two uncertain input parameters for the economic dispatch model formulated in Section 3.2. Given a specific realization of electric load and spot price, we can obtain the corresponding dispatch cost by solving (3.1) – (3.12). Thus, it is crucial to estimate the joint distribution of daily electric load and natural gas spot price. Historical electric load and natural gas spot price data, along with the corresponding weather data, can be obtained from system operator and local natural gas hub records. Our goal in this section is to use the available data to generate discrete realizations that can be used individually as input to the ED model formulated in Section 3.2. The simulated dispatch cost distribution can be constructed from the outputs of multiple simulation replications.

To improve the accuracy of estimating the correlation and generating scenarios, similar weather days in the same season are clustered using the K-means method. The details of the K-means method and definition of a distortion metric which helps to decide the number of clusters can be found in [63]. Within each cluster, a joint distribution of electric load and gas price is generated. Among parametric approaches to fitting continuous bivariate observations, the bivariate normal distribution is frequently used [3]. The Box-Cox transformation is the most common approach to transforming observations to achieve normality [10]. A nonnegative observation $y = \left(y_1, ..., y_Z\right)$ of dimension $Z$ can be transformed to $y^{(\tau)} = \left(y_1^{(\tau_1)}, ..., y_Z^{(\tau_Z)}\right)$ by applying Eq. (3.13), where $\tau = (\tau_1, ..., \tau_Z)$ is a vector with the same dimension as the observation. Based on the assumption

that $y^{(\tau)}$ follows a bivariate normal distribution, the maximum-likelihood estimate of $\tau$ can be obtained according to the detailed steps described in [10].

$$y_z^{(\tau_z)} = \begin{cases} \dfrac{y_z^{\tau_z} - 1}{\tau_z} & (\tau_z \neq 0) \\ \log y_z & (\tau_z = 0) \end{cases}, \forall z \in \{1, ..., Z\} \tag{3.13}$$

One of the several tests for bivariate normality such as the Mardia, Henze-Zirkler and Royston tests, as well as the graphical approach of constructing a chi-square quantile-quantile (Q-Q) plot [39], may then be applied to test goodness of fit. The best number of clusters is chosen considering distortion [63] and the results of the goodness-of-fit tests within each cluster.

As the generated bivariate normal distribution is continuous, to obtain a tractable number of input scenarios for the dispatch simulation in each cluster, we first generate a large sample of realized (gas price, electricity load) pairs from the fitted distribution for that cluster. Much research has been done on scenario generation and reduction as well as continuous distribution discretization. Because this is not the focus of this research, we simply construct a bivariate histogram of the randomly sampled observations. The center of each bin of the histogram is adopted as one scenario and the relative frequency for that bin is taken as the scenario probability. More accurate and tractable scenario generation and reduction methods can be found in [20, 63].

## 3.4 Quantification Metrics

Given the model presented in Section 3.2 and the discrete scenarios generated by the methods in Section 3.3, this section presents methodologies to quantify the effect of natural gas spot price uncertainty on the economic dispatch cost uncertainty. We review and apply the Wasserstein distance metric and the CVaR risk measure in Sections 3.4.1 and 3.4.2, respectively. The Wasserstein distance is frequently used in scenario reduction for stochastic programming [20]. Here, it quantifies the difference between distribution over all scenarios including both the worst and best cases. The CVaR metric is a coherent risk measure that characterizes the worst cases only and is also

frequently incorporated in stochastic programming formulations. The detailed quantification steps are illustrated in Section 3.4.3.

### 3.4.1 Review of the Wasserstein Distance (WD)

The Wasserstein distance was proposed to measure the distance between probability distributions [56]. If $\boldsymbol{H}$ and $\boldsymbol{R}$ are discrete probability distributions having finitely many scenarios $\xi_s$ (with probabilities $h_s$), $s = 1, ..., S$, and $\tilde{\xi}_{s'}$ (with probabilities $r_{s'}$), $s' = 1, ..., S'$, respectively, we obtain the Wasserstein distance as Eq. (3.14). This is a minimum cost flow problem on a bipartite graph, where nodes represent scenarios and $d(\xi_s, \tilde{\xi}_{s'})$ is the distance between scenario $\xi_s$ in $\boldsymbol{H}$ and $\tilde{\xi}_{s'}$ in $\boldsymbol{R}$ according to some norm [28].

$$\text{WD} = inf\Big\{ \sum_{s=1}^{S}\sum_{s'=1}^{S'} d(\xi_s, \tilde{\xi}_{s'}) y_{s,s'} : \quad y_{s,s'} \geq 0, \quad \sum_{s'=1}^{S'} y_{s,s'} = h_s, \quad \sum_{s=1}^{S} y_{s,s'} = r_{s'} \Big\} \tag{3.14}$$

### 3.4.2 Review of Conditional Value at Risk (CVaR)

The CVaR was described in [58] as a coherent risk measure. For a cost probability density function $f_X(x)$ and a confidence level $\gamma \in (0, 1)$, which usually is set to be 0.95 or 0.99, the value at risk (VaR) and CVaR are defined as follows:

**Definition 1.** (VaR) The value-at-risk measure for a random variable with cumulative distribution function (cdf) F is defined as:

$$\text{VaR}_\gamma(\text{F}) = inf\{x : \text{F}(x) \geq \gamma\}. \tag{3.15}$$

**Definition 2.** (CVaR) The conditional value-at-risk measure is defined as:

$$\text{CVaR}_\gamma(\text{F}) = \frac{1}{1-\gamma} \int_{\text{VaR}_\gamma(\text{F})}^{\infty} x d\text{F}(x). \tag{3.16}$$

**Definition 3.** (CVaR for discrete probability distributions) The conditional value-at-risk measure for discrete probability distribution F such that $f_X(x) = \Pr(X = x) = \Pr(\{\omega \in \Omega : X(\omega) = x\})$ is defined as:

$$\text{CVaR}_\gamma(\text{F}) = \frac{1}{1-\gamma} \sum_{\omega \in \Omega} \Big\{ \Pr(\omega) \Big( \text{VaR}_\gamma(\text{F}) + [X(\omega) - \text{VaR}_\gamma(\text{F})]^+ \Big) \Big\}. \tag{3.17}$$

Algorithm 1 is a procedure to compute CVaR according to Eq. (3.17).

**Algorithm 1:** CVaR Evaluation for a Discrete Probability Distribution.

**Input:** Discrete probability distribution F, sorted mass points $x^1 \leq x^2 \leq ... \leq x^N$ and the corresponding probabilities $p^1, p^2, ..., p^N$, confidence level $\gamma$

**Output:** The CVaR of distribution F : $\text{CVaR}_\gamma(\text{F})$

$i = 1$

**while** $\sum_{n=1}^{i} p^n < \gamma$ **do**
  $i = i + 1$

$i^* = i$, $\text{VaR}_\gamma(\text{F}) = x^{i^*}$

$$\text{CVaR}_\gamma(\text{F}) = \frac{1}{\sum_{n=i^*}^{N} p^n} \sum_{n=i^*}^{N} (x^n p^n)$$

**Return** $\text{CVaR}_\gamma(\text{F})$

### 3.4.3 Quantifying Steps

We use the WD and CVaR metrics to compare the cost distributions resulting from the economic dispatch with price estimate (ED-PE) simulation, where the load uncertainty is considered but the price uncertainty is not, and the economic dispatch with price distribution (ED-PD) simulation, where both uncertainties are included, as illustrated in Fig. 3.1. The method can be applied to each segment of each season and is summarized as follows:

**Step 1:** Obtain input parameter values, including unit commitment/start-up/shut-down indicators $(u_{k,t}, u^u_{k,t}, v^d_{k,t})$ and available gas from contracts $(\overline{G}_{j,t})$ by solving the day-ahead unit commitment (UC) problem. The detailed formulation of the UC model can be found in [32]. The UC model includes a reserve requirement and natural gas network constraints of pipelines as well as storage facilities using the 24-hour electric load point estimates and contracted gas only. Set the optimal UC decisions and hourly schedule of the gas network as the input parameters of the ED model.

**Step 2: (ED-PE simulation)** Solve the ED model for each scenario from the electric load probability distribution $P_{i,t}(D)$ and the **point estimate of the gas spot price**. Construct the corresponding discrete dispatch cost probability distribution $\boldsymbol{H}$ having finitely many scenarios

$\xi_s$ (with probabilities $h_s$), $s = 1, ..., S$, where $\xi_s$ denotes optimal cost of scenario $s$ for the ED-PE simulation.

**Step 3: (ED-PD simulation)** Solve the ED model for each scenario of the joint probability distribution of the electric load and the gas spot price. Construct the corresponding discrete dispatch cost probability distribution $\boldsymbol{R}$ having finitely many scenarios $\tilde{\xi}_{s'}$ (with probabilities $r_{s'}$), $s = 1, ..., S'$, where $\tilde{\xi}_{s'}$ denotes optimal cost of scenario $s'$ for the ED-PD simulation.

**Step 4:** Compare the two dispatch cost probability distribution, $\boldsymbol{H}$ and $\boldsymbol{R}$. Calculate the Wasserstein distance (WD) as the optimal cost of model (3.14). Calculate $\text{CVaR}_\gamma$ of $\boldsymbol{H}$ and $\boldsymbol{R}$ using Algorithm 1. Then the CVaR difference between the ED-PD simulation and the ED-PE simulation can be assessed as $\Delta\text{CVaR}_\gamma = \text{CVaR}_\gamma(\boldsymbol{R}) - \text{CVaR}_\gamma(\boldsymbol{H})$.

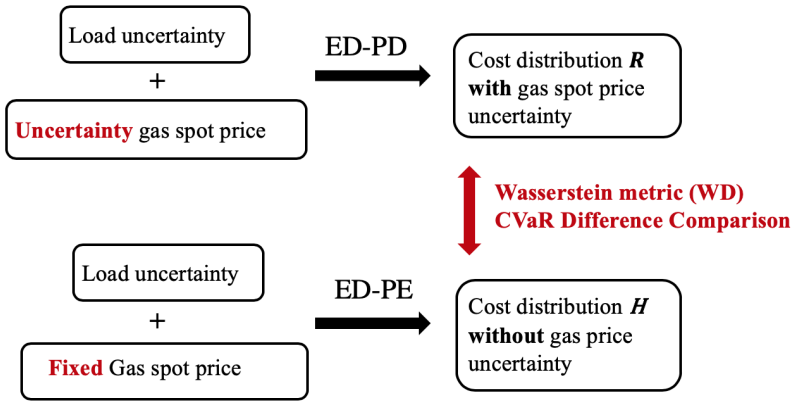


Figure 3.1: Illustration of procedure to quantify impact of gas price uncertainty.

## 3.5 Applying Risk Metrics to Select a Risk-Mitigation Strategy

The previous sections discuss how to compute the WD and CVaR metrics to quantify the effect of gas spot price uncertainty on the risk of dispatch cost for the daily short-term operation. To reduce this risk, the ISO can coordinate or suggest to generator owners some risk-mitigation strategies, such as converting natural gas fueled units into dual-fuel units and building new gas storage facilities. Both of these strategies potentially are able to reduce risk but also will result

in conversion and installation costs. In this section we present revisions to the daily short-term dispatch model to reflect the adoption of either risk-mitigation strategy. Using these revised models, modified values of the WD and CVaR metrics can be assessed by the methods described in Section 3.4.3.

### 3.5.1 Strategy 1: Dual Fuel Conversion

Adding dual fuel, such as fuel oil, capability is a useful strategy to mitigate the effect of natural gas price volatility. Conversion of natural gas fueled generators to be able to operate on an alternate fuel requires building fuel storage tanks, which results in a one-time conversion cost. For the operation of a dual fuel generator, it takes some time, ranging from 4 to 72 hours, to switch between fuels. Here we assume that within one day, a converted generator can only use one kind of fuel. The effect of having dual fuel capability on the economic dispatch model is to include fuel-switching decisions based on the cost minimization shown in Eq. (3.18), where $\zeta_g$ is the daily production cost of a converted generator, $g$.

$$\zeta_g = inf\left\{\sum_{t\in\mathcal{T}}\left(\lambda_g^C\eta_{g,t}^C + \Lambda^M\eta_{g,t}^M + \lambda_\psi^\Psi\eta_{g,t}^{out}\right), \sum_{t\in\mathcal{T}}\phi_g^{oil}p_{g,t}\right\}, \forall g\in\mathcal{G}'(i,j), \psi\in\Psi(j) \tag{3.18}$$

The gas balance constraint (3.9) becomes (3.19). The first expression of the left hand side of (3.9) is divided into two parts in (3.19) where the first part is the gas consumption by the non-converted gas generators and the second part represents the gas consumption by the converted gas generators. Here for each converted generator, we use $b_g(\eta_{g,t}^C+\eta_{g,t}^M+\eta_{g,t}^{out}) = b_g\phi_g p_{g,t}$ to indicate the gas consumption, where $b_g$ is a binary variable indicating whether natural gas results in a smaller cost, compared with the alternate fuel. While producing a fixed amount of power, $b_g = 1$ if the gas fuel cost is lower and $b_g = 0$ otherwise, as illustrated in Eq. (3.20a)–(3.20b).

$$\sum_{i\in\mathcal{I}}\sum_{g\in\mathcal{G}(i,j)\setminus\mathcal{G}'(i,j)}\phi_g p_{g,t} + \sum_{i\in\mathcal{I}}\sum_{g\in\mathcal{G}'(i,j)} b_g\phi_g p_{g,t} + \alpha_{j,t}^+ \le \rho\overline{G}_{j,t} + m_{j,t} + \sum_{\psi\in\Psi(j)}\left(q_{\psi,t}^{out} - q_{\psi,t}^{in}\right) + \alpha_{j,t}^-, \forall j,t \tag{3.19}$$

where

$$b_g = 1, \text{if} \quad \sum_{t\in\mathcal{T}}\left(\lambda_g^C\eta_{g,t}^C + \Lambda^M\eta_{g,t}^M + \lambda_\psi^\Psi\eta_{g,t}^{out}\right) \le \sum_{t\in\mathcal{T}}\phi_g^{oil}p_{g,t}, \forall g\in\mathcal{G}'(i,j), \psi\in\Psi(j) \tag{3.20a}$$

$$b_g = 0, \text{if} \quad \sum_{t\in\mathcal{T}} \left( \lambda_g^C \eta_{g,t}^C + \Lambda^M \eta_{g,t}^M + \lambda_\psi^\Psi \eta_{g,t}^{out} \right) > \sum_{t\in\mathcal{T}} \phi_g^{oil} p_{g,t}, \forall g \in \mathcal{G}'(i,j), \psi \in \Psi(j). \tag{3.20b}$$

Constraints (3.18)–(3.20b) are nonlinear and may introduce solutions that are locally but not globally optimal. Thus we transform them into mixed integer linear constraints via the disjunctive method. Constraints (3.18) can be linearized as (3.21a)–(3.21e), where $b_g$ can be assessed and $M_1$ is a big number. Constraints (3.22) are added to determine the exact amount of gas the converted generator consumes from the storage facility, which influences the objective function. Constraints (3.19) are linearized as Eq. (3.23a)–(3.23e) where another big number $M_2$ is used and a new variable $z_{g,t} \equiv b_g(\eta_{g,t}^C + \eta_{g,t}^M + \eta_{g,t}^{out}) = b_g \phi_g p_{g,t}$, is introduced.

$$\zeta_g \leq \sum_{t\in\mathcal{T}} (\lambda_g^C \eta_{g,t}^C + \Lambda^M \eta_{g,t}^M + \lambda_\psi^\Psi \eta_{g,t}^{out}), \forall g \in \mathcal{G}'(i,j), \psi \in \Psi(j) \tag{3.21a}$$

$$\zeta_g \leq \sum_{t\in\mathcal{T}} \phi_g^{oil} p_{g,t}, \forall g \in \mathcal{G}'(i,j), \psi \in \Psi(j) \tag{3.21b}$$

$$\zeta_g \geq \sum_{t\in\mathcal{T}} (\lambda_g^C \eta_{g,t}^C + \Lambda^M \eta_{g,t}^M + \lambda_\psi^\Psi \eta_{g,t}^{out}) - M_1(1-b_g), \forall g \in \mathcal{G}'(i,j), \psi \in \Psi(j) \tag{3.21c}$$

$$\zeta_g \geq \sum_{t\in\mathcal{T}} \phi_g^{oil} p_{g,t} - M_1 b_g, \forall g \in \mathcal{G}'(i,j), \psi \in \Psi(j) \tag{3.21d}$$

$$b_g \in \{0,1\}, \forall g \in \mathcal{G}'(i,j) \tag{3.21e}$$

$$\sum_{i\in\mathcal{I}} \sum_{g\in\mathcal{G}(i,j)} \eta_{g,t}^{out} = \sum_{\psi\in\Psi(j)} q_{\psi,t}^{out}, \forall t \tag{3.22}$$

$$\sum_{i\in\mathcal{I}} \sum_{g\in\mathcal{G}(i,j)\setminus\mathcal{G}'(i,j)} \phi_g p_{g,t} + \sum_{i\in\mathcal{I}} \sum_{g\in\mathcal{G}'(i,j)} z_{g,t} + \alpha_{j,t}^+ \leq \rho \overline{G}_{j,t} + m_{j,t} + \sum_{\psi\in\Psi(j)} \left( q_{\psi,t}^{out} - q_{\psi,t}^{in} \right) + \alpha_{j,t}^-, \quad \forall j,t \tag{3.23a}$$

$$z_{g,t} \leq M_2 b_g, \forall g \in \mathcal{G}'(i,j), t \tag{3.23b}$$

$$z_{g,t} \leq \phi_g p_{g,t}, \forall g \in \mathcal{G}'(i,j), t \tag{3.23c}$$

$$z_{g,t} \geq \phi_g p_{g,t} - M_2(1-b_g), \forall g \in \mathcal{G}'(i,j), t \tag{3.23d}$$

$$z_{g,t} \geq 0, \forall g \in \mathcal{G}'(i,j), t \tag{3.23e}$$

Finally, the revised ED model with dual fuel conversion strategy is formulated as follows. The objective function (3.24) is revised based on (3.1). The difference is that the fuel cost is computed

separately for the converted generators and non-converted generators. Since all the storage outflow costs are considered in the fourth expression, we must take care with the definition of the first expression. According to the previous discussion, if $b_g = 0$, the alternate fuel is used, and $\zeta_g$ in the first expression represents the fuel cost of using the alternate fuel. However, for this converted generator, the storage outflow variable still has some nonnegative values because we are comparing the costs of using the alternate fuel and natural gas, and choosing the fuel with a cheaper cost. The fourth expression, the total storage outflow cost, includes the storage outflow cost of the converted generator, which is not actually used. So we have to deduct the storage outflow cost from the converted generator when the alternate fuel is selected. If $b_g = 1$, then natural gas is used, and the first expression represents the total production cost minus the storage outflow cost for the converted generators since all the storage outflow costs are calculated in the fourth expression. The revised dispatch model is:

$$\begin{aligned}\min \sum_{g\in\mathcal{G}'}(\zeta_g - \sum_{t\in\mathcal{T}}\lambda^{\Psi}_{\psi}\eta^{out}_{g,t}) + \sum_{t\in\mathcal{T}}\Bigg\{ \sum_{g\in\mathcal{G}\setminus\mathcal{G}'}\left(\lambda^{C}_{g}\eta^{C}_{g,t} + \Lambda^{M}\eta^{M}_{g,t}\right) + \sum_{n\in\mathcal{N}} C^{prod}_{n}p_{n,t} \\ + \sum_{\psi\in\Psi}\lambda^{\Psi}_{\psi}q^{out}_{\psi,t} + \sum_{i\in\mathcal{I}}\left(\Gamma^{+}_{\beta}\beta^{+}_{i,t} + \Gamma^{-}_{\beta}\beta^{-}_{i,t}\right) + \sum_{j\in\mathcal{J}}\left(\Gamma^{+}_{\alpha}\alpha^{+}_{j,t} + \Gamma^{-}_{\alpha}\alpha^{-}_{j,t}\right)\Bigg\} \\ \text{s.t.}(3.2)-(3.8),(3.10)-(3.12),(3.21a)-(3.21e),(3.22),(3.23a)-(3.23e).\end{aligned} \tag{3.24}$$

### 3.5.2 Strategy 2: Adding Gas Storage Facilities

Adding gas storage facilities is another strategy to mitigate risk. Here we define $\Psi'(j)$ as the set of added gas storage facilities at gas node $j$. The only difference between the following revised model and the ED model from Section 3.2 is that all the expressions involving $\Psi(j)$ and $\Psi$ are replaced with $\Psi(j) \cup \Psi'(j)$ and $\Psi \cup \Psi'$, respectively, to reflect the presence of the additional gas storage facilities.

$$\begin{aligned}\min \sum_{t\in\mathcal{T}}\Bigg\{ \sum_{g\in\mathcal{G}}\lambda^{C}_{g}\eta^{C}_{g,t} + \sum_{j\in\mathcal{J}}\Lambda^{M}m_{j,t} + \sum_{n\in\mathcal{N}}C^{prod}_{n}p_{n,t} + \sum_{\psi\in\Psi\cup\Psi'}\lambda^{\Psi}_{\psi,t}q^{out}_{\psi,t} + \sum_{i\in\mathcal{I}}\left(\Gamma^{+}_{\beta}\beta^{+}_{i,t} + \Gamma^{-}_{\beta}\beta^{-}_{i,t}\right) \\ + \sum_{j\in\mathcal{J}}\left(\Gamma^{+}_{\alpha}\alpha^{+}_{j,t} + \Gamma^{-}_{\alpha}\alpha^{-}_{j,t}\right)\Bigg\}\end{aligned} \tag{3.25}$$

s.t.

(3.2)-(3.8)

$$\sum_{i\in\mathcal{I}}\sum_{g\in\mathcal{G}(i,j)}\phi_g p_{g,t}+\alpha^{+}_{j,t}\le\rho\overline{G}_{j,t}+m_{j,t}+\sum_{\psi\in\Psi(j)\cup\Psi'(j)}\left(q^{out}_{\psi,t}-q^{in}_{\psi,t}\right)+\alpha^{-}_{j,t},\quad\forall j,t \tag{3.26}$$

$$\underline{L}_{\psi}\le l_{\psi,t}\le\overline{L}_{\psi},\quad\forall\psi\in\Psi\cup\Psi',t \tag{3.27}$$

$$-\overline{q}_{\psi}\le\left(q^{out}_{\psi,t}-q^{in}_{\psi,t}\right)\le\overline{q}_{\psi},\quad\forall\psi\in\Psi\cup\Psi',t \tag{3.28}$$

$$l_{\psi,t}=l_{\psi,t-1}-q^{out}_{\psi,t}+q^{in}_{\psi,t},\quad\forall\psi\in\Psi\cup\Psi',t \tag{3.29}$$

### 3.5.3 Comparison of Risk-Mitigation Strategies

The daily cost distributions of each strategy can be obtained using the discrete scenarios generated in Section 3.3 and quantification method in Section 3.4 along with the revised ED model in Sections 3.5.1 and 3.5.2. A comparison between the quantification measures in the form of the WD and CVaR metrics and the corresponding conversion or installation costs informs the choice of the better strategy. This method can be extended to other risk-mitigation strategies including building new pipelines and signing firm gas transportation contracts.

Now we have two strategies of dual fuel conversion and adding storage facilities. We assume the dual fuel conversion cost is $C^D$ (\$/MW). Suppose one option is to convert a specific natural gas generator with a capacity of $\bar{P}_g$ into a dual fuel generator. If the installation cost of a new storage facility is $C^S$ (\$/kcf) at the same location, then the investment cost of dual fuel conversion could alternatively be used to build a storage facility with a maximum capacity of $\bar{P}_g C^D/C^S$. With the same investment, the strategy that results in a greater reduction of the gas price uncertainty impact, as quantified by the WD metric or CVaR difference between the ED-PD result and the ED-PE result, is preferred. We also directly compare the CVaRs of the ED-PD distributions that result from implementing each risk-mitigation strategy. Use $\Theta^1, \Theta^2$ to indicate the risk measures for strategy 1 and 2, respectively. Strategy 1 is preferred if $\Theta^1 < \Theta^2$ and strategy 2 is preferred otherwise, where $\Theta \in \left\{\text{WD}, \Delta\text{CVaR}_\gamma, \text{CVaR}_\gamma(\boldsymbol{R})\right\}$ as defined in Eqs. (3.30a)–(3.30b). Since the risk-mitigation strategies have different results for each segment and each contracted gas availability

factor, we assign each segment risk a weight $a_c$, where $c \in \mathcal{C}$ is a segment index, and each contracted gas availability factor case a weight $b_\rho$, where $\rho$ is the contracted gas availability factor. Let $\Theta^1_{c,\rho}, \Theta^2_{c,\rho}$ indicate the risk measures for strategies 1 and 2 for segment $c$ and contracted gas availability factor $\rho$, respectively. Then the composite risk measures are constructed as:

$$\Theta^1 = \sum_{\rho} \sum_{c \in \mathcal{C}} b_\rho a_c \Theta^1_{c,\rho}, \tag{3.30a}$$

and

$$\Theta^2 = \sum_{\rho} \sum_{c \in \mathcal{C}} b_\rho a_c \Theta^2_{c,\rho}. \tag{3.30b}$$

## 3.6 Case Study

Currently there are no available large test cases of the coordinated operation of a real natural gas and power system. We provided an extensive literature review of the current available test cases, all of which are artificial, in [60]. The IEEE 24-bus power system with Belgian 20-node natural gas system has been used frequently as a large system tested in previous papers including [76]. We apply our models in a case study of a modified IEEE 24-bus system with a modified Belgian 20-node natural gas system [18]. The cost function is revised according to [54]. The non-served energy penalty cost is set to be \$3500/MWh, as recommended by Midcontinent Independent System Operator [46]. The excess energy penalty cost is set to be \$350/MWh, while the non-served gas and excess gas penalties are set to be \$3500/kcf and \$350/kcf, respectively. The gas price from contracts is set to be \$2.0/kcf and we assume for simplicity that 1 kcf of natural gas can generate 1 MBtu of energy. ISO New England (ISO–NE) provided the electric load data for each of its eight zones including Connecticut (CT), North Central Massachusetts, West Central Massachusetts, Southeast Massachusetts, Maine, New Hampshire, Rhode Island and Vermont. Since CT accounts for the greatest share, about 25% of the electricity assumption of ISO–NE, we apply a case study for CT only. The total for the system is set to be that for CT and is allocated to buses according to the same proportions as in the IEEE 24-bus system load data. The non-electric natural gas demand is set to equal that of the Belgian 20-node natural gas system. The Algonquin Citygate natural

gas price for ISO–NE is taken as the gas price for the Belgian 20-node natural gas system. The optimal unit commitment decisions and natural gas network schedules of the day-ahead short-term scheduling model of the combined natural gas and power system with reserves of 3% are fixed to be the initial values of the unit commitment parameters $u_{k,t}, v^u_{k,t}, v^d_{k,t}$ and gas availability from gas contract $\overline{G}_{j,t}$. The linear programs are solved with GAMS/CPLEX 23.4.3 on a Linux workstation (24 CPU, 94GB RAM).

### 3.6.1 Uncertainty Identification

As explained in Section 3.3, we generate discrete scenarios for correlated electric load and natural gas price for each weather information segment. This section describes the sources of historical data for the uncertain parameters and shows the best clustering result. For each segment of each season, the joint distribution of the electric load and the natural gas spot price is generated, where bivariate normal distributions are seen to be valid after data transformation. Lastly, we present the generated discrete scenarios for correlated electric load and gas price.

#### 3.6.1.1 Data Sources

Hourly electric load data can be obtained from ISO–NE for each year [33]. ISO–NE also provided weather data including temperature, dew point and wind speed from 2012–12–31 to 2016–11–07 for each hour of each day. We use Algonquin Citygate natural gas spot price as the reference natural gas spot price index for the ISO–NE area, available from 2014–03–17 to 2017–01–03 [71]. Because the natural gas spot price is recorded daily, we sum the hourly electric load data to find the corresponding daily electric loads. A similar process is followed for the daily average weather information. According to the regression result of [23] and because each season has its own typical electric load pattern, the electric load data are divided into three seasons, spring/fall (April 1–May 14 and September 15–November 30), summer (May 15–September 14) and winter (December 1–March 31). Altogether we had available data for daily weather information (temperature, dew point and wind speed), the daily electric load and the daily natural gas spot price for ISO–NE from

2014-03-17 to 2016–11–07. We display results only for winter in CT because in winter natural gas price intends to have high uncertainty. This study can be replicated easily for each season and zone within the ISO–NE region.

#### 3.6.1.2 Clustering According to Weather

We cluster the weather information using the K-means method. As illustrated in Fig. 3.2, for each additional cluster beyond three, the distortion decreases by less than one. There are no clear ways of choosing the best number of clusters. For this case, three is chosen as the best because it results in acceptable transformed bivariate normality goodness of fit, as illustrated in Table 3.1, whereas using four clusters does not. Fig. 3.3 compares the original and the clustered weather data for winter, where the three segments labeled 0, 1 and 2 represent the coldest, merely cold and moderate winter days, respectively.

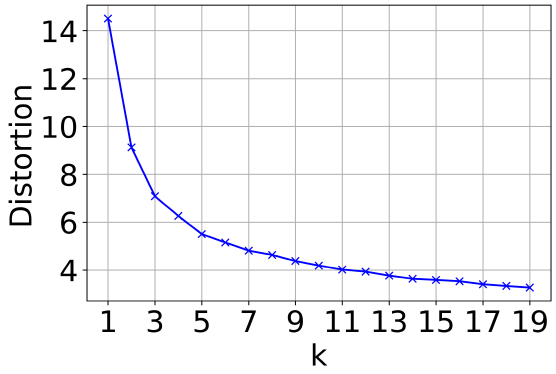


Figure 3.2: Clustering optimization distortion of the K-means method.

#### 3.6.1.3 Joint Distribution of Electric Load and Gas Price

Fig. 3.4 displays scatterplots of the natural gas price and electric load for each segment of the winter season. The coldest days tend to combine high natural gas price and high electric load, while the moderate days in the winter have relatively low values for both quantities.

Table 3.1 illustrates the results of bivariate normality tests for each segment of winter. Segments 0 and 1 pass all the bivariate normality tests while Segment 2 passes more than half of the tests.

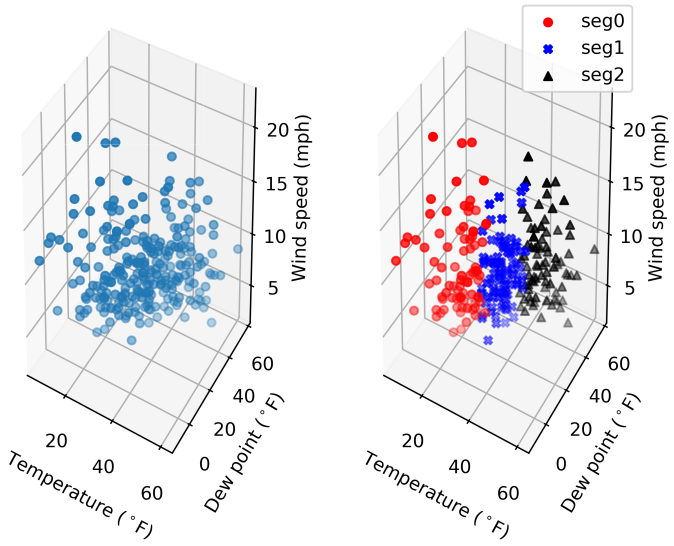


Figure 3.3: Winter weather data for CT (a) original; (b) clustered.

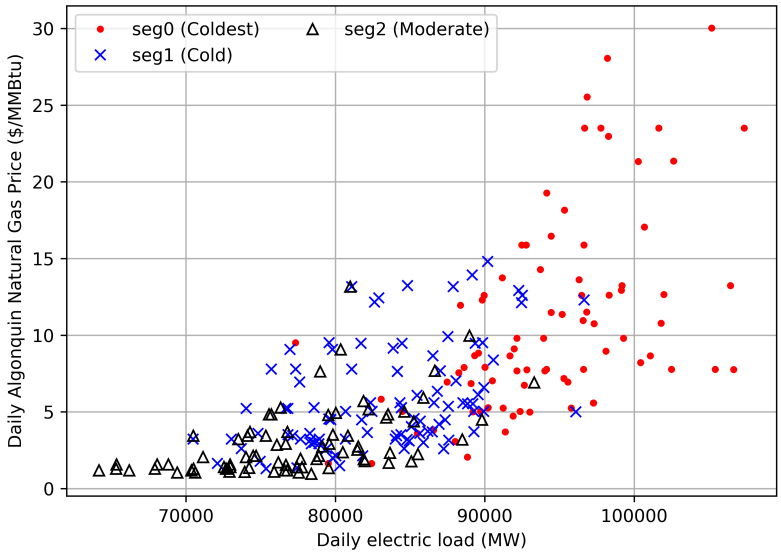


Figure 3.4: Winter daily Algonquin price vs. load in CT.

The column labeled "Result" indicates whether normality is accepted (i.e., YES or NO) at a significance level of 0.05. Figs. 3.5–3.7 show the test results using Q-Q plots, from which we can make two observations. The first is that the histograms of the marginal distributions are approximately bell-shaped and the corresponding univariate Q-Q plots fall close to straight lines, both indicating normality of the marginal distributions. The second observation, from panels (c), is that the bivariate Q-Q plots are nearly linear for most data points except several points at the top right. The Adjusted Mahalanobis distance metric indicates that none of these points are outliers. In addition, a similar process has been followed using the bivariate gamma distribution and the statistical results suggest that the bivariate normal distribution fits better [25]. Thus, we selected the bivariate normal distribution to represent the joint uncertainty of daily electric load and natural gas price. In future research, other theoretical or empirical bivariate distributions can also be tested. After obtaining the maximum-likelihood estimate of $\tau$, $y^{(\tau)}$ can be back-transformed to the original scale of observations. The corresponding results as well as the relevant statistical values are listed in Table 3.2. The coldest segment has the highest expected load and gas price, while the moderate days have the lowest expected load and gas price. Also, each cluster has a different correlation between the transformed load and price.

Table 3.1: Bivariate normal distribution test results for each segment of the winter season in CT at the 0.05 significance level.

| | Segment 0 | | | Segment 1 | | | Segment 2 | | |
|---|---|---|---|---|---|---|---|---|---|
| Test | Test Statistic | p-value | Result | Test Statistic | p-value | Result | Test Statistic | p-value | Result |
| Univariate Normality | | | | | | | | | |
| Shapiro-Wilk | | | | | | | | | |
| Load$^{(\tau_1)}$ | 0.990 | 0.735 | YES | 0.989 | 0.635 | YES | 0.995 | 0.988 | YES |
| Price$^{(\tau_2)}$ | 0.982 | 0.290 | YES | 0.976 | 0.079 | YES | 0.956 | 0.009 | NO |
| Bivariate Normality | | | | | | | | | |
| Mardia | | | | | | | | | |
| Skewness | 1.117 | 0.892 | YES | 1.474 | 0.831 | YES | 0.244 | 0.993 | YES |
| Kurtosis | 0.466 | 0.641 | YES | -1.756 | 0.079 | YES | -2.101 | 0.036 | NO |
| Henze-zirkler | 0.381 | 0.825 | YES | -1.756 | 0.059 | YES | 0.778 | 0.129 | YES |
| Royston | 1.228 | 0.544 | YES | 3.331 | 0.191 | YES | 6.811 | 0.033 | NO |
| E-statistic | 0.547 | 0.744 | YES | 0.875 | 0.111 | YES | 0.769 | 0.211 | YES |

Table 3.2: Box-Cox transformation maximum-likelihood estimate and bivariate normal fit results for each segment of winter in CT.

| Cluster | $\tau$ | | Means | | | | Transformed Covariance Matrix | Transformed Correlation |
|---|---|---|---|---|---|---|---|---|
| | Load | Price | Transformed Load (MWh) | Transformed Price ($/MMBtu) | Load (MWh) | Price ($/MMBtu) | | |
| 0 (Coldest) | 1.019 | 0.096 | 115,408 | 2.501 | 94,253 | 9.415 | $\begin{bmatrix} 5.364 \times 10^7 & 2.956 \times 10^3 \\ 2.956 \times 10^3 & 5.187 \times 10^{-1} \end{bmatrix}$ | 0.560 |
| 1 (Cold) | 0.682 | 0.048 | 3,486 | 1.700 | 89,501 | 5.128 | $\begin{bmatrix} 2.588 \times 10^4 & 5.017 \times 10^1 \\ 5.017 \times 10^1 & 4.055 \times 10^{-1} \end{bmatrix}$ | 0.490 |
| 2 (Moderate) | 0.797 | -0.464 | 9,845 | 0.667 | 77,388 | 2.212 | $\begin{bmatrix} 3.732 \times 10^5 & 1.490 \times 10^2 \\ 1.490 \times 10^2 & 1.658 \times 10^{-1} \end{bmatrix}$ | 0.599 |

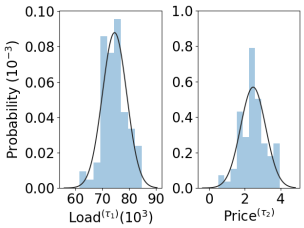


(a) Univariate histogram.

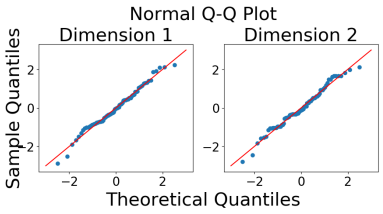


(b) Univariate Q-Q plot.

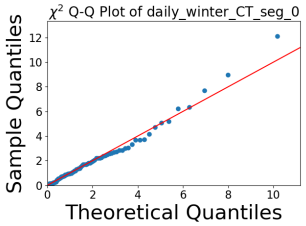


(c) Bivariate Q-Q plot.

Figure 3.5: Bivariate normal distribution validation for winter segment 0 in CT.

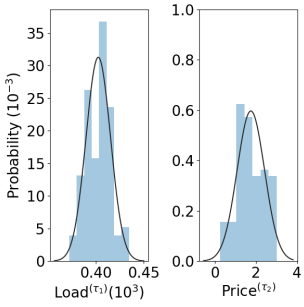


(a) Univariate histogram

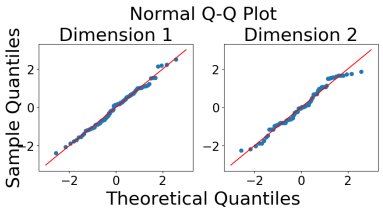


(b) Univariate Q-Q plot.

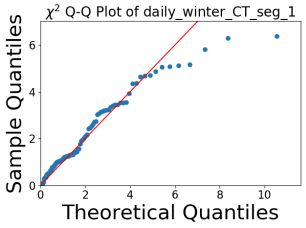


(c) Bivariate Q-Q plot.

Figure 3.6: Bivariate normal distribution validation for winter segment 1 in CT.

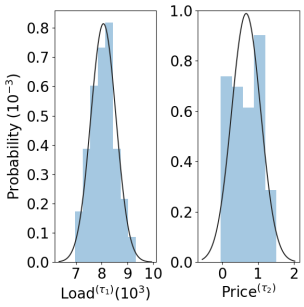


(a) Univariate histogram.

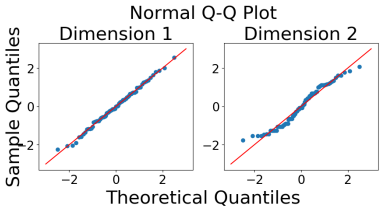


(b) Univariate Q-Q plot.

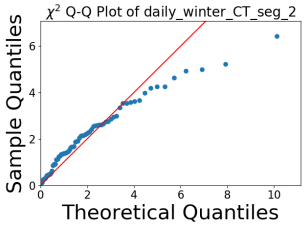


(c) Bivariate Q-Q plot.

Figure 3.7: Bivariate normal distribution validation for winter segment 2 in CT.

#### 3.6.1.4 Discrete Scenarios Generation

We randomly sample 100,000 observations from the fitted bivariate normal distributions for each segment. Each run of the ED model takes about 3 seconds. For each observation, we have 11 gas availability factors, and thus, simulating ED with 100,000 observations will take approximately 920 hours. We instead use fewer discrete scenarios to represent the uncertainty characteristics of the bivariate normal distribution. We select $30^2$ discrete scenarios as described in Section 3.3. More accurate and tractable scenario generation and reduction methods can be found in [20].

### 3.6.2 Effect of Natural Gas Price Uncertainty in Base Case

The case studies are conducted for each segment of winter because past electricity price spikes have been experienced in cold weather events. To demonstrate the influence of the contracted gas availability on the simulation results, we use $\rho\overline{G}_{j,t}$ to represent various levels of contracted gas availability by increasing $\rho$ from 0.5 to 1.5 by increments of 0.1. Fig. 3.8 summarizes the center and spread (mean +/− standard error) of costs from the ED-PE simulation and the ED-PD simulation for each winter segment. For each segment, both the mean and the standard deviation of the total cost from ED-PD simulation are greater than those from the ED-PE simulation, as a result of gas price uncertainty. Specifically, the cost of winter segment 0 (coldest days) has the maximum standard deviation and mean. As the contracted gas availability factor increases, the mean total cost from each simulation first decreases and then stabilizes, illustrating that low

contracted gas availability increases the effect of the gas price uncertainty. This happens because given low contracted gas availability, the committed natural gas generator is not able to acquire enough gas from contracts and must acquire gas from the spot market with a possibly high price.

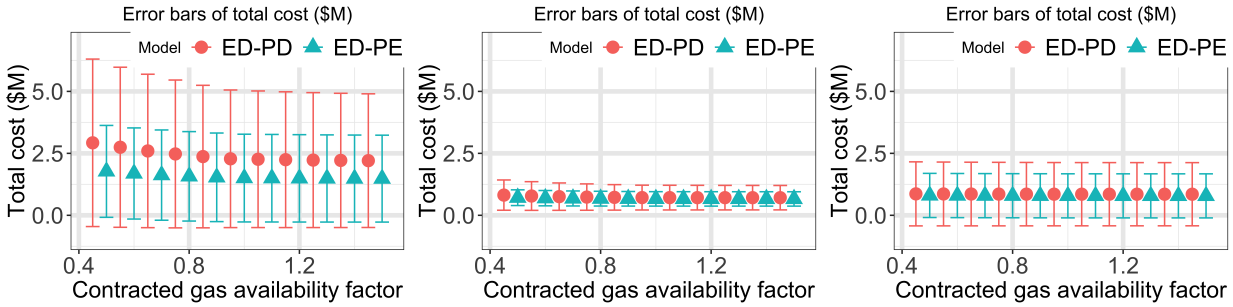


(a) Segment 0. (b) Segment 1. (c) Segment 2.

Figure 3.8: Error bars of the total cost for each segment of winter in CT.

However, the error bars cannot quantify the difference between the ED-PE simulation and the ED-PD simulation. In Fig. 3.9, the bars for strategy N/A (no strategy applied) illustrate the WD measure comparison for various contracted gas availability values $\rho$ of each segment. As $\rho$ increases from 0.5 to 1.0, the WD of each segment decreases dramatically. When $\rho$ exceeds 1.0, the WD remains stable. When the actual available gas quantity is less than the nominal value, the dispatch cost has high uncertainty due to the uncertain gas price. The CVaR difference between the ED-PD simulation and the ED-PE simulation, indicating the risk coming from gas price uncertainty, shows a pattern of change similar to WD (see Fig. 3.10). Segment 0 (coldest days) has the largest WD and CVaR difference, compared with segments 1 and 2, indicating the gas price uncertainty has the most impact on dispatch cost distribution risk in the coldest days.

### 3.6.3 Comparison of Risk-Mitigation Strategies

We compare the two risk-mitigation strategies of dual fuel conversion and adding a gas storage facility. The idea here is to compare the WD and CVaR difference metrics while applying different risk-mitigation strategies given a fixed investment cost. The strategy that reduces the WD or

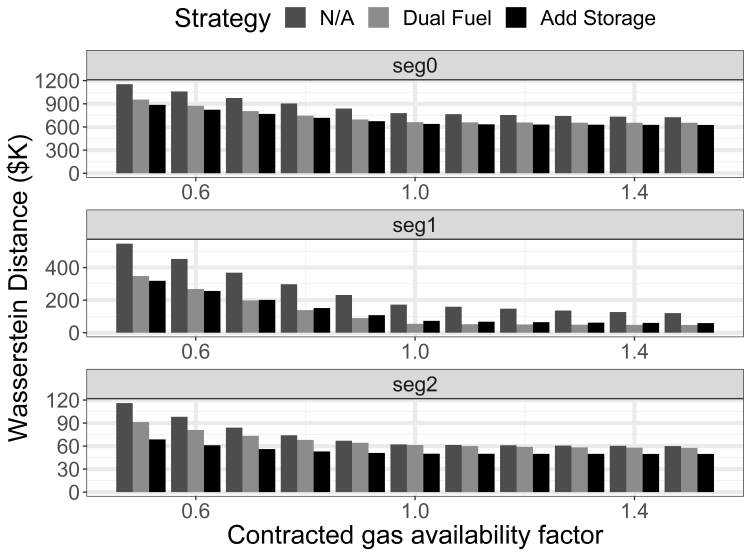


Figure 3.9: Wasserstein distance comparison between applying expansion strategies of adding storage, dual fuel conversion and N/A (no strategy applied) for each segment of winter season.

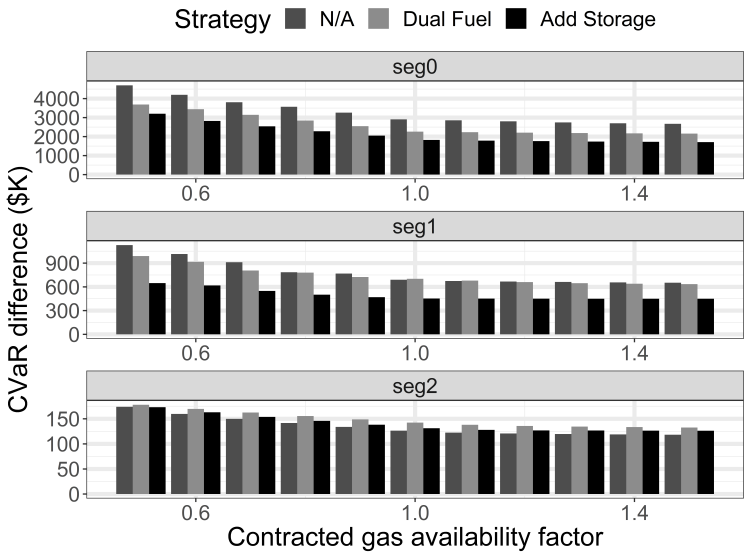


Figure 3.10: Conditional value at risk difference ($\gamma = 0.95$) due to gas price uncertainty comparison between applying strategies of adding storage, dual fuel conversion and N/A (no strategy applied) for each segment of winter season.

CVaR difference more dominates the other one. Here we use a simple example to demonstrate the comparison process.

The general dual fuel conversion cost is approximately \$7,500 – \$16,000/MW [1]. We assume the dual conversion cost is \$10,000/MW and totals \$3.15 million for the selected generator. The production cost of using the alternate fuel is \$26.91/MWh. The Inner City Fund expects that it takes \$30 million to construct a storage facility with a capacity of 1.1 Bcf in New England [21]. In addition, we set the cost of filling storage facility as \$2.5/kcf. Then the cost of constructing and filling a new storage facility is $\frac{\$30 \times 10^6}{1.1 \times 10^6 \text{kcf}} + \$2.5/\text{kcf} = \$29.77/\text{kcf}$. Thus the \$3.15 million could alternatively be used to construct and fill one storage facility with capacity $\frac{\$3.15 \times 10^6}{\$29.77/\text{kcf}} = 105,811\text{kcf}$. The hourly maximum outflow is 2,500 kcf [21]. This new storage facility is added at gas node 2 (as strategy 2), where alternatively the connected gas fuel generator is converted to dual fuel in strategy 1. The storage outflow cost is set to be the same as storage facility 1 which is located at gas node 2 as well.

Fig. 3.9 compares the WD measures while applying various strategies for each segment, displaying the difference between the cost distributions of the ED-PD simulation and the ED-PE simulation. Compared with the status quo, either adding storage or converting to dual fuel capability always results in a smaller WD metric, indicating that the effect of gas price uncertainty on the dispatch cost decreases. Moreover, adding the storage facility always results in a smaller WD metric than dual fuel conversion for a fixed investment cost except several days in segment 1 with a very minor reverse effect. That is, using WD in the risk measure defined in Section 3.5.3, we find $\text{WD}^1 \leq \text{WD}^2$. From the WD metric aspect, which indicates the effect of natural gas price uncertainty on the dispatch cost uncertainty, adding a storage facility dominates the dual fuel conversion strategy. The weighted WD metric, defined in Section 3.5.3, can be used to verify this.

Fig. 3.10 compares the CVaR difference between the ED-PD and ED-PE simulation which indicates the CVaR risk coming from the gas price uncertainty. For segments 0 and 1, adding either a storage facility or dual fuel capability results in a smaller CVaR difference than no strategy, while for segment 2 both these two strategies result in a larger CVaR difference. This anomaly occurs

mainly because we incorporate the risk-mitigation strategies in the unit commitment optimization also and, thus, the inputs of the dispatch problem differ between strategies. Thus, in the moderate days (segment 2), the risk-mitigation strategies do not guarantee reducing the risk coming from natural gas price uncertainty. The risk-mitigation strategies have the most effect on the coldest days, as we can see in Fig. 3.10 that the CVaR difference for segment 0 is the largest compared with segments 1 and 2. The effect of the risk-mitigation strategies on the CVaR difference decreases as the contracted gas availability factor increases. In other words, as expected, given less available natural gas from pipelines, the effects of risk-mitigation strategies are more obvious. Specifically, taking the risk measures defined in Section 3.5.3, the ISO can choose the corresponding values for parameters $b_\rho$ and $a_c$ according to its preference.

Table 3.3: CVaR difference ($\gamma = 0.95$) comparison among various strategies given different combinations of weight parameters.

| $a_c$ | $b_\rho$ | CVaR difference ($M) | | |
|---|---|---|---|---|
| | | $\Delta\text{CVaR}^0_\gamma$ N/A | $\Delta\text{CVaR}^1_\gamma$ Dual Fuel | $\Delta\text{CVaR}^2_\gamma$ Add Storage |
| [0.36, 0.36, 0.28] | [1/11, 1/11, 1/11, 1/11, 1/11, 1/11, 1/11, 1/11, 1/11] | 1.50 | 1.25 | 0.99 |
| | [0.025, 0.025, 0.05, 0.10, 0.15, 0.3, 0.15, 0.10, 0.05, 0.025, 0.025] | 1.42 | 1.18 | 0.92 |
| [0.20, 0.20, 0.60] | [1/11, 1/11, 1/11, 1/11, 1/11, 1/11, 1/11, 1/11, 1/11] | 0.90 | 0.76 | 0.61 |
| | [0.025, 0.025, 0.05, 0.10, 0.15, 0.3, 0.15, 0.10, 0.05, 0.025, 0.025] | 0.85 | 0.72 | 0.57 |
| [0.05, 0.05, 0.90] | [1/11, 1/11, 1/11, 1/11, 1/11, 1/11, 1/11, 1/11, 1/11] | 0.33 | 0.30 | 0.26 |
| | [0.025, 0.025, 0.05, 0.10, 0.15, 0.3, 0.15, 0.10, 0.05, 0.025, 0.025] | 0.31 | 0.29 | 0.24 |

We can estimate the value of $b_\rho$ using historical data. Here, from 2015-01-01 to 2016-12-31, we find 75, 75 and 61 days in segment 0, 1, and 2 of the winter season, respectively. Hence we can approximate $a_0 = a_1 = 0.36$ and $a_2 = 0.28$. As shown in Table 3.3, we examined two more cases of $a_c = [0.2, 0.2, 0.6]$ and $a_c = [0.05, 0.05, 0.9]$, where the first one indicates a moderately warm winter and the second one represents a very warm winter. Also, we tested two cases of $b_\rho$. The first one has $b_\rho = 1/11, \forall\rho$, and the second one sets $b_\rho = [0.025, 0.025, 0.05, 0.10, 0.15, 0.3, 0.15, 0.10, 0.05, 0.025, 0.025]$, which approximates a bell shape. Table 3.3 compares the CVaR difference for various strategies for different combinations of parameters $a_c$ and $b_\rho$. We observe that in all the cases, adding storage dominates dual fuel conversion and the status quo since it results in the smallest CVaR difference.

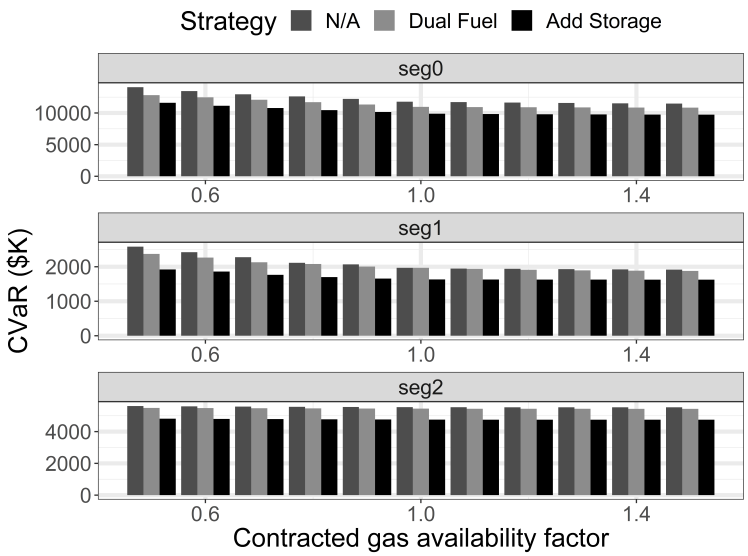


Figure 3.11: Comparison of dispatch cost CVaR ($\gamma = 0.95$) due to uncertainty in both electric load and gas price among applying strategies of adding storage, dual fuel conversion and N/A (no strategy applied) for each segment of winter season.

Fig. 3.11 compares the CVaR values of the dispatch cost distribution generated from the ED-PD simulation. For each segment, adding the storage facility or dual fuel capability results in a smaller CVaR than no strategy, and adding the storage facility yields the smallest CVaR. Applying the same method of estimating the $b_\rho$ and $a_c$ values, Table 3.4 compares the values of $\text{CVaR}_{0.95}(\boldsymbol{R})$ among various strategies given different combinations of weight parameters, and demonstrates that adding a storage facility consistently dominates the other two strategies for reducing the risk resulting from the combined uncertainty in both gas price and electric load.

Overall, given a fixed investment cost, the storage facility strategy best reduces the risk coming from natural gas price uncertainty and limiting the exposure to high dispatch costs caused by concurrent high values of both natural gas price and electric load. Other combinations of values for $b_\rho$ and $a_c$ can be substituted according to the estimated likelihood and severity of gas constraints, and judgment by the decision-maker of the relative importance of different segments, respectively.

Table 3.4: Dispatch cost CVaR ($\gamma = 0.95$) comparison among various strategies given different combinations of weight parameters.

| $a_c$ | $b_\rho$ | CVaR ($M) | | |
|---|---|---|---|---|
| | | $\text{CVaR}^0_\gamma(\boldsymbol{R})$ N/A | $\text{CVaR}^1_\gamma(\boldsymbol{R})$ Dual Fuel | $\text{CVaR}^2_\gamma(\boldsymbol{R})$ Add Storage |
| [0.36, 0.36, 0.28] | [1/11, 1/11, 1/11, 1/11, 1/11, 1/11, 1/11, 1/11, 1/11] | 6.73 | 6.37 | 5.64 |
| | [0.025, 0.025, 0.05, 0.10, 0.15, 0.3, 0.15, 0.10, 0.05, 0.025, 0.025] | 6.61 | 6.28 | 5.56 |
| [0.2, 0.2 0.4] | [1/11, 1/11, 1/11, 1/11, 1/11, 1/11, 1/11, 1/11, 1/11] | 6.21 | 5.96 | 5.25 |
| | [0.025, 0.025, 0.05, 0.10, 0.15, 0.3, 0.15, 0.10, 0.05, 0.025, 0.025] | 6.14 | 5.91 | 5.21 |
| [0.05, 0.05, 0.9] | [1/11, 1/11, 1/11, 1/11, 1/11, 1/11, 1/11, 1/11, 1/11] | 5.71 | 5.58 | 4.89 |
| | [0.025, 0.025, 0.05, 0.10, 0.15, 0.3, 0.15, 0.10, 0.05, 0.025, 0.025] | 5.69 | 5.56 | 4.87 |

## 3.7 Conclusion

In this paper, we proposed a daily economic dispatch model with natural gas fuel costs from contracts and the spot market while considering the natural gas availability constraints. Data are clustered based on weather information and, within each cluster, a bivariate normal joint distribution of daily electric load and gas spot market price is estimated by transforming the data, using maximum likelihood estimation to identify a parameter for the transformation. To quantify the effect of uncertain gas spot price on dispatch cost, two cost probability distributions are obtained by simulation. The first one fixes the gas spot price at its point estimate, while the second one incorporates the estimated gas spot price probability distributions. The results for different days clustered according to weather information in winter show that the effect of gas spot price uncertainty is weakened as the contracted gas availability increases. Based on the investment cost and risk reduction comparison, this quantification method can be applied to help choose the most effective risk-mitigation strategy for a given investment cost. Our case study suggests that adding a gas storage facility is preferred over dual fuel conversion. However, since the results are based on an artificial test case, this conclusion is not universal. A system operator could conduct its own case study based on its available data in order to select a better strategy according to the risk metrics.

In future work, this study could be extended to generate probability distributions of the hourly, rather than daily, electric load and spot gas price, and a regression model that relates hourly

electric load and spot gas price to a function of weather data could also be investigated. These extensions require hourly gas price data, which so far we have been unable to obtain. Using discrete scenarios to indicate different levels of contracted gas availability and repeating solving the ED problem with various parameter values is a straightforward way to estimate the cost distribution, but either a larger scenario set or a larger test system results in longer computation time. Developing more efficient methods to simulate the cost distribution given different parameters is necessary. Lastly, how to select the number of discrete scenarios to represent the uncertainty pattern of the transformed bivariate normal distribution could also be investigated in the future.

Economic dispatch models such as the one used here frequently form the second stage, which represents the decisions taken after uncertain parameters are realized, of stochastic unit commitment models. Most such models in the literature consider uncertainty only in the electric load or renewable generation. The results in this paper demonstrate the importance of also modeling uncertainty in the gas spot price, especially when there is a risk of deliveries from interruptible contracts being curtailed. The methods developed in this paper could be used to generate joint scenarios of gas spot price and net load. The linearized formulation of the dispatch cost CVaR can also be included in the objective function to represent risk aversion in the optimization [36].

# CHAPTER 4. RELIABILITY UNIT COMMITMENT TO MANAGE NATURAL GAS COST IN POWER SYSTEM OPERATIONS

A paper in preparation for submission to the *IISE Transactions*

## Abstract

The growing proportion of electric power generated from natural gas motivates greater coordination between the two energy markets. Many natural gas-fueled power generators rely on interruptible contracts with gas suppliers. The resulting uncertainty of contracted gas availability, combined with volatility in gas spot prices and availability, can result in high wholesale electricity prices. We formulate optimization models for the day-ahead and real-time electricity markets having different types of interactions with gas market models. An ideal co-optimized model for the natural gas and power systems provides a lower bound for the cost. To assess the role of the reliability unit commitment in managing the natural gas cost in power system operations, we compare the performance of three models, including the separately optimized model, the separately optimized model with reliability unit commitment, and the co-optimized model, in terms of operational decisions, real-time gas price and cost through two case studies. The simulation results demonstrate that, by adjusting the unit commitment decisions according to the most updated gas availability information, the reliability unit commitment step yields a smaller cost compared with the separately optimized model without a reliability unit commitment step. A large case study is used to demonstrate the impact of the interruptible contract gas price and non-electric gas load on the cost. The difference between the separately optimized models with and without reliability unit

commitment step is the largest when the interruptible contract gas price is low and the non-electric gas load is high.

## 4.1 Introduction

The role of natural gas in electric power generation is projected to increase over the next decades [70]. The natural gas customers are categorized into residential, commercial, industrial and electric power generation. These customers either sign contracts with the gas pipeline companies or purchase gas from the real-time spot market. The gas contracts are classified as firm or interruptible. Firm contract users generally are able to use as much as gas they need. As a result of this high priority in gas supply restriction situations, the firm contract has a relatively high price, while the interruptible contract users have low priority and can only use the remaining gas in the pipeline once the firm contract users' demand is satisfied. Currently, many electric power generators hold interruptible contracts because of their low price, which helps them submit competitive offers in wholesale electricity markets. However, these generators also experience some risk of their contracted fuel supply being cut off. As a recourse, they may purchase fuel in the spot market instead. Additionally, because the natural gas-fueled power generators (NGFGs) usually are dispatched in the peak load time and the gas price affects the electricity price, the possible high real-time spot market gas price will lead to high electricity price. To maintain a reliable and economically efficient power system, more research about the coordination and interdependency between the power and natural gas systems considering gas priorities, including the contract and real-time spot market, is needed.

Many researchers have investigated the gas and electric interdependency from the viewpoint of a centralized system operator who is able to cooperate these two systems simultaneously. These studies involve models to minimize the operational costs for both systems while satisfying all the operational constraints and coupling them through the NGFGs. Unsihuay formulated a mixed-integer nonlinear programming problem for the integrated natural gas-electricity model and employed a dual decomposition based Lagrangian relaxation and dynamic programming method to obtain the

optimal solution [68]. Correa-Posada and Sánchez-Martin [18] formulated the first mixed-integer linear programming integrated model and applied sensitivity analysis for the pipeline line-pack. Based on these deterministic models, several new models with uncertain parameters were proposed. In [15], the same authors formulated a two-stage stochastic optimization model for the contingency analysis including the pipeline and transmission contingencies, based on which a security-constrained optimal power and natural-gas flow model was proposed and solved by using a linear sensitivity factor based iterative methodology [17] as well as Bender's decomposition approaches [43, 19], respectively. Hu and Ryan demonstrated the dominance of the stochastic programming model over the deterministic model with reserves with respect to expected cost and energy shortage under various levels of wind energy uncertainty [32]. Robust scheduling has been studied considering pipeline and transmission N-1 contingencies [4]. With respect to the coupling components between natural gas and power systems, Chen et al. considered not only the NGFGs but also the electric-driven compressors and energy hubs integrated with power-to-gas units [13].

Other research has been aimed at investigating the interdependency between the natural gas and power system using multilevel optimization models. Li et al. designed a bi-level economic dispatch (ED) model for the integrated power and natural gas system, where the upper level is an ED model for the power system and the lower level is a scheduling problem for the gas system [40]. Byeon and Van Hentenryck designed a tri-level program for the unit commitment problem with gas network awareness, where the ED problem and the gas scheduling model constitute the second and third level, respectively [11].

However, the centralized system operator does not exist in the U.S. and many other part of the world. Multilevel models generally assume that the operator of at least one of the power and natural gas systems has full information about the other. To reflect more realistic conditions, several works examine the daily operation of the power system while taking gas network conditions, including fuel availability and price, as fixed or uncertain parameters to the power system. In [51], the gas price adjustment is optimized to increase the market efficiency and flexibility of incorporating renewable energy. The effect of the uncertain gas spot price and the gas availability from contracts was assessed

using the probability mass transportation distance and conditional value-at-risk measure [29, 30]. Zhao et al. applied a stochastic programming model for the unit commitment to investigate the effect of uncertainty of gas supply and gas price in case studies of ISO New England and California ISO [78].

Currently, the natural gas system and the power system are operated by different entities. The natural gas system is operated by the natural gas extraction company, the pipeline company and the local distribution company (LDC), whereas in many regions the power system is operated by the independent system operator (ISO). As discussed above, many recent studies investigated the interdependency and coordination between the natural gas and power systems by assuming full information about both systems. However, only the information exchange about the gas prices and flows between the natural gas and power systems are possible. This paper proposes a separately optimized model for the natural gas and power systems, where the operator of each system minimizes its cost or maximizes its profit while exchanging gas price and flow information with the other operator. Both the interruptible gas contract and the real-time spot market are incorporated as sources of gas for NGFGs. In addition, a separately optimized model with an additional reliability unit commitment step is proposed to deal with the possible high real-time gas price and gas deficiency. Some ISOs, such as the California ISO (CAISO), incorporate a Resource Adequacy (RA) program to ensure RA resources remain available to meet demand. But RA focuses on the load uncertainty, while our RUC step focuses on the gas fuel only. As a benchmark, a co-optimized model, which assumes there exists a centralized system operator optimizing the decisions for natural gas and power systems simultaneously, is formulated. The major contributions of this paper are summarized as follows:

- We formulate a separately optimized model for the daily operation of the natural gas and power systems, which incorporates the interruptible gas contract and the gas from the real-time market. The daily operation is categorized into day-ahead and real-time markets. The availability of gas from the interruptible contract is decided in the day-ahead gas market, and the real-time market

settles on the optimal real-time gas flow and price through an iterative process between the real-time gas scheduling problem and the power system ED problem.

- We add a reliability unit commitment step to the separately optimized model to decrease the possible risk from the gas system. The unit commitment optimization occurring between the day-ahead and the real-time electricity markets enables the power system to adjust the unit commitment decisions according to the gas availability information from the gas system.

- We compare these two models with the co-optimized model with respect to the operational decisions and cost for a baseline case as well as different combinations of the interruptible contract gas price and the non-electric gas load. Numerical studies demonstrate that the reliability unit commitment step can adjust the unit commitment decisions and yield a smaller cost, compared with the separately optimized model without reliability unit commitment step. In addition, the reliability unit commitment step is significant when the interruptible contract gas price is high and the non-electric gas load is high.

The remainder of this paper is organized as follows. Section 4.2 presents the co-optimized model, the separately optimized model, and the separately optimized with the reliability unit commitment model for the operation of the natural gas and power systems. Case studies and numerical results are shown in Section 4.3. Section 4.3.1 uses a small case study to illustrate and compare these three models at the detailed operational level, and Section 4.3.2 investigates the impact of the interruptible contract gas price and the non-electric load on the cost comparison among three models. Finally, the conclusions are summarized in Section 4.4.

## 4.2 Model

This section provides the detailed formulations of the proposed models. We start with describing the current operating process of the power system and natural gas system in the U.S. regions with wholesale electricity markets. Then we describe our simplified model and list the modeling assumptions. After that, the formulations for the three proposed models are given.

In 2015, the Federal Energy Regulatory Commission (FERC) approved the final rule to improve gas-electric coordination [22]. The current daily operating process of natural gas and power systems is shown in Fig. 4.1. The North American Energy Standards Board (NAESB) has issued the updated gas nomination schedule as shown in the lower portion of Fig. 4.1. There are three gas nomination processes including the timely, evening and intraday nomination cycles. The intraday nomination cycles consist of the intraday 1 (ID1), 2 (ID2) and 3 (ID3) nomination cycles. Within each nomination cycle, a gas shipper requests a pipeline to schedule a contract for gas transportation between two locations of a pipeline to arrange storage inflow or outflow. Following that, a series of processes consisting of confirmation, scheduling, and balancing are conducted by the gas system to guarantee the contract. The power system market is conducted in steps including the day-ahead (DA) unit commitment (UC) optimization problem, which is a mixed-integer program, and the real-time (RT) economic dispatch (ED) optimization problem, which is a linear program. Each ISO has its own time schedule for the ay-ahead and real-time markets. The top portion in Fig. 4.1 shows the operational schedule of a typical ISO.

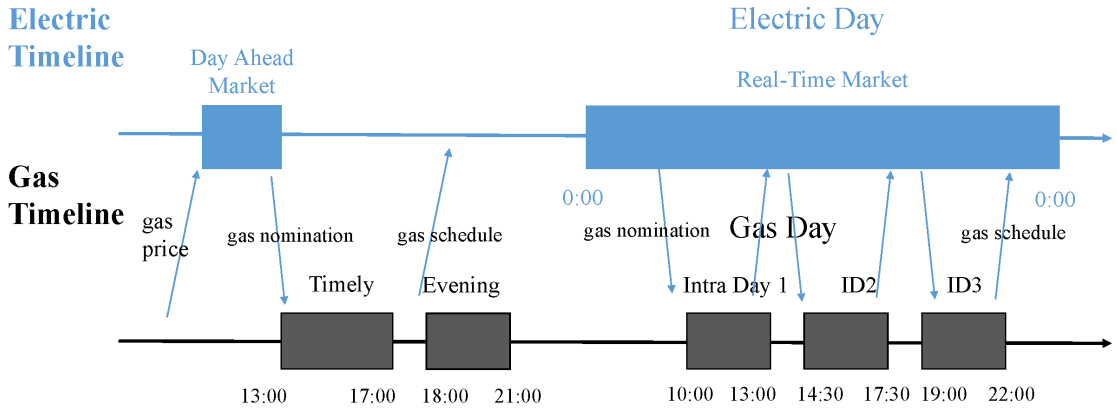


Figure 4.1: Current gas-electric decision cycles [59, 80, 49]. Blue arrows indicate the information exchange between the natural gas and power systems.

The NGFGs, as a critical component in both the power and gas systems, produce electricity using gas, which comes from one of the gas nomination cycles. However, there are two major gas-electric coordination issues in the current operation. The first issue is the NGFGs' unawareness of the gas availability in the DA UC problem. Since majority of the NGFGs hold interruptible gas

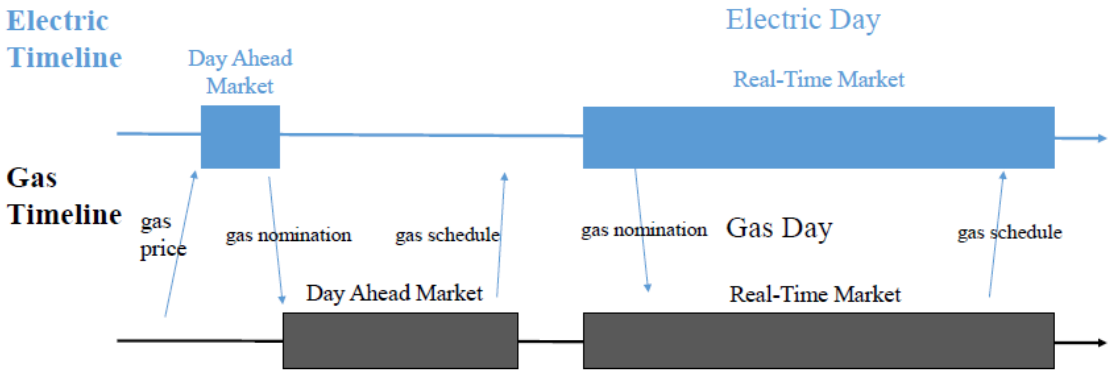


Figure 4.2: Simplified gas-electric decision cycles. Blue arrows indicate the information exchange between the natural gas and power systems.

contracts with the pipeline companies, the pipeline companies tend to serve the firm gas demands of non-electric customers first. When the gas pipeline condition becomes constrained due to the high non-electric gas demand or gas system contingencies, these interruptible generator customers may not be able to obtain enough gas. Furthermore, the day-ahead UC problem is solved before the timely and evening gas nomination cycles, and the UC decisions will be fixed based on their solution for the following real-time ED problem. In other words, the ISO makes binary day-ahead UC decisions without any awareness or confirmation of the gas availability. This unawareness or loss of confirmation could result in infeasibility of the ED problem. The other issue is the failure to characterize the gas demand by price. A possible approach in reality is a biddable capacity release, which is designed to allow a customer holding firm contracts to resell its capacity to another party on either temporarily or permanently, and the corresponding bid price represents the gas demand [50].

To model this unawareness of gas availability in the DA UC decisions and the possible way of using gas price to reflect gas demand, we simplify the daily operating process as in Fig. 4.2 and make the following assumptions:

- The timely and evening gas nomination processes are combined in one day-ahead market. The day-ahead market is open from 13:00 to 21:00 on the day before the target day. The intraday 1, 2 and 3 gas nomination cycles are combined in one real-time market. The real-time market time

horizon is the same as the power system ranging from 0:00 on the target day to 0:00 on the day after. Prices and quantities for all hours are settled simultaneously.

- The NGFGs are able to acquire gas from both interruptible contracts and the real-time market. The day-ahead gas market settlement determines the amount of gas available from the interruptible contracts. The real-time market decides the amount of gas available from the real-time market, and the real-time gas price reflects the demand for gas. The NGFGs know that they may acquire gas from the real-time market, but not the real-time gas price or quantity available. The DA UC problem is solved based on the interruptible contract gas price and forecast real-time price while assuming unlimited gas availability.

- Both the day-ahead and the real-time market are solved for all hours at once. To avoid end-of-study effects, the scheduling problems are solved over a 36-h horizon, but only the costs over the first 24-h are assessed.

- No electricity or gas imports from other regions are possible.

Generally, for the simplified operating process, DA UC decisions are made one day ahead of the target day, based on the interruptible contract gas price and the forecast real-time gas price. Then the committed NGFGs are supposed to acquire interruptible contract gas from the day-ahead market. In the real-time market, an iterative process between the power and gas systems, where the ED problem reports the requested real-time gas quantity and willing-to-pay price to the gas system and the gas system reports the gas availability and the willing-to-sell gas price back to the power system, decides the real-time gas flow and price. We discuss the details of the co-optimized model, the separately optimized model and the separately optimized model with reliability unit commitment step in the following sections. For the convenience of mathematics and expressions, we give the formulation for the co-optimized model first, and then present the formulations of the other two models.

### 4.2.1 Co-optimized Model

The co-optimized model represents an ideal situation where the power and gas systems are operated by a single entity such that all the decisions made are the best as a whole. This single regional operator is able to adjust the gas and power flows simultaneously. Here we list the formulation for a co-optimized model of scheduling the combined energy system to satisfy the demand for electricity and gas based on [32]. Decisions made on the day ahead of the operating day include the hourly on/off status of each thermal generator. Then, in real time, the hourly ED solution, including energy production and transmission quantities, gas supply amount, pressures at each gas node, gas flows in each pipeline, the gas compressor working schedules, as well as flows in and out of gas storage facilities, are determined. Wind generators are modeled as dispatchable to reflect day-ahead market practices such as those in the Midcontinent Independent System Operator (MISO), where they participate as Dispatchable Intermittent Resources. To focus on the interactions between gas and power systems, we assume wind power forecasts are perfect and do not consider equipment outages. We minimize the cost over a 36-h study horizon to be implemented over a 24-h operating day for the purpose of avoiding the end of day distortions in the decisions. We introduce the following notation:

**Sets**

$\mathcal{J}$ Gas nodes, indexed by $j$

$\mathcal{J}'(j)$ Gas nodes connected to $j$ by passive pipelines from $j$, indexed by $j'$

$\mathcal{J}''(j)$ Gas nodes connected to $j$ by passive pipelines to $j$, indexed by $j''$

$\mathcal{C}'(j)$ Gas nodes connected by active pipelines from $j$, indexed by $c'$

$\mathcal{C}''(j)$ Gas nodes connected by active pipelines to $j$, indexed by $c''$

$\Lambda(j)$ Gas wells in node $j$, indexed by $\lambda$; $\Lambda = \bigcup_{j\in\mathcal{J}} \Lambda(j)$ is the set of all gas wells

$\Psi(j)$ Storage facilities in node $j$, indexed by $\psi$; $\Psi = \bigcup_{j\in\mathcal{J}} \Psi(j)$ is the set of all storage facilities

$\mathcal{I}$ Electricity nodes, indexed by $i$ and $i'$

$\mathcal{I}'(i)$ Electricity nodes connected to $i$ by a transmission line from $i$, indexed by $i'$

$\mathcal{I}''(i)$ Electricity nodes connected to $i$ by a transmission line to $i$, indexed by $i''$

$\mathcal{G}(i,j)$ Gas-fired generators at power node $i$ and gas node $j$, indexed by $g$; $\mathcal{G} = \bigcup_{i\in\mathcal{I},j\in\mathcal{J}} \mathcal{G}(i,j)$ is the set of all gas-fired generators.

$\mathcal{N}(i)$ Non-gas-fired conventional generators at node $i$, indexed by $n$; $\mathcal{N} = \bigcup_{i\in\mathcal{I}} \mathcal{N}(i)$ is the set of all non-gas-fired generators.

$\mathcal{M}$ Set of all gas-fired and non-gas-fired generators, indexed by $m$; $\mathcal{M} = \mathcal{G} \cup \mathcal{N}$

$\mathcal{W}(i)$ Wind turbines at node $i$, indexed by $w$; $\mathcal{W} = \bigcup_{i\in\mathcal{I}} \mathcal{W}(i)$ is the set of all wind turbines

$\mathcal{T}$ Hours from 1 to 36, indexed by $t$

**Binary Decision Variables**

$u_{g,t}, u_{n,t}, u_{m,t}$ Unit commitment indicator: equals 1 if unit is online in hour $t$ and 0 otherwise

$y^{+}_{j,j',t}, y^{-}_{j,j',t}$ Gas pipeline flow direction indicator: $y^{+}_{j,j',t}$ equals 1 ($y^{-}_{j,j',t}$ equals 0) if the gas flow is from $j$ to $j'$ and $y^{+}_{j,j',t}$ equals 0 ($y^{-}_{j,j',t}$ equals 1) otherwise

**Nonnegative Continuous Decision Variables**

| | |
|---|---|
| $v^u_{g,t}, v^u_{n,t}, v^u_{m,t}$ | Unit start-up indicator: equals 1 if the unit is started up in hour $t$ and 0 otherwise |
| $v^d_{g,t}, v^d_{n,t}, v^d_{m,t}$ | Unit shut-down indicator: equals 1 if the unit is shut down in hour $t$ and 0 otherwise |
| $p^{ng}_{\lambda,t}$ | Hourly natural gas production level [kcf/hour] |
| $\pi_{j,t}$ | Gas squared pressure [Psig$^2$] |
| $\tilde{\pi}_{j,j',t}$ | Magnitude of the gas squared pressure difference [Psig$^2$] |
| $\alpha^-_{j,t}$,$\alpha^+_{j,t}$ | Unserved/excess gas in gas node $j$ [kcf] |
| $l_{\psi,t}$ | Storage level [kcf] |
| $q^{out}_{\psi,t}, q^{in}_{\psi,t}$ | Out/in-flow of storage facility [kcf/h] |
| $p_{g,t}, p_{n,t}, p_{m,t}$ | Electricity production [MWh] |
| $\mu_{g,t}$ | Gas demand for electricity generation [kcf/h] |
| $\mu^{\mathrm{DA}}_{g,t}$ | Requested gas quantity in the day-ahead unit commitment problem [kcf/h] |
| $\mu^{\mathrm{RT}}_{g,t}$ | Requested gas quantity from the real-time economic dispatch problem within the current gas availability limit [kcf/h] |
| $\mu^-_{g,t}$ | Additional requested gas quantity from the real-time economic dispatch problem beyond the current gas availability limit [kcf/h] |
| $\tilde{\mu}^{\mathrm{DA}}_{g,t}, \tilde{\mu}^{\mathrm{RT}}_{g,t}$ | Actual available gas quantity from the day-ahead and real-time markets [kcf/h] |
| $\rho_{g,t}$ | Real-time willingness-to-pay price for gas by the natural gas-fueled power generators [$/kcf] |
| $\mu_{j,t}$ | Real-time gas price [$/kcf] |
| $\kappa_{j,t}$ | Marginal gas price in the co-optimized model [$/kcf] |
| $p^{wind}_{w,t}$ | Wind energy output [MWh] |
| $\beta^-_{i,t}$,$\beta^+_{i,t}$ | Unserved/excess electricity [MWh] |

**Unrestricted Continuous Decision Variables**

$\eta_{j,j',t}$ Gas flow from $j$ to $j'$, unrestricted in sign [kcf]

$\theta_{i,t}$ Phase angle [rad]

$f_{i,i',t}$ Line flow from $i$ to $i'$ [MWh]

**Parameters**

| | |
|---|---|
| $D^{ng}_{j,t}$ | Baseline non-electric gas demand [kcf/h] |
| $\overline{P}^{ng}_{\lambda}, \underline{P}^{ng}_{\lambda}$ | Max/min hourly gas production [kcf/h] |
| $C^{ng}_{\lambda}, C^{stor}_{\psi}$ | Gas production/storage cost [$/kcf] |
| $C_{j,j'}$ | Passive pipeline constant [kcf/Psig] |
| $\tau_{j,c'}$ | Max squared pressure increase ratio of active pipelines |
| $\overline{\pi}_j, \underline{\pi}_j$ | Max/min squared pressure [Psig$^2$] |
| $\overline{L}_{\psi}, \underline{L}_{\psi}$ | Max/min storage level [kcf] |
| $Q_{\psi}$ | Max net flow (outflow minus inflow) [kcf] |
| $\Gamma^{-}_{\alpha}, \Gamma^{+}_{\alpha}$ | Unserved/excess gas penalty [$/kcf] |
| $\phi_g$ | Efficiency of gas generator [kcf/MWh] |
| $D^{e}_{i,t}$ | Electricity demand [MWh] |
| $C^{sd}_{g}, C^{su}_{g}, C^{sd}_{n}, C^{su}_{n}, C^{sd}_{m}, C^{su}_{m}$ | Shut-down/start-up cost [$] |
| $C^{prod}_{n}$ | Power production cost [$/MWh] |
| $\Gamma^{-}_{\beta}, \Gamma^{+}_{\beta}$ | Unserved/excess electricity penalty [$/MWh] |
| $\overline{P}_g, \underline{P}_g, \overline{P}_n, \underline{P}_n, \overline{P}_m, \underline{P}_m$ | Max/min electricity generation [MWh] |
| $R^{up}_{g}, R^{up}_{n}, R^{up}_{m}, R^{down}_{g}, R^{down}_{n}, R^{down}_{m}$ | Max ramp up/down rate [MW] |

| | |
|---|---|
| $T_g^{on}, T_n^{on}, T_m^{on}, T_g^{off}, T_n^{off}, T_m^{off}$ | Min on/off time [h] |
| $\overline{F}_{i,i'}$ | Max line flow [MWh] |
| $\overline{P}_{w,t}^{wind}$ | Available wind energy [MWh] |
| $X_{i,i'}$ | Transmission line impedance [pu] |
| $\chi$ | Non-electric load factor, default value of 1 |
| $C_{g,t}^{\text{gas,DA}}$ | Contract gas price [$/kcf] |
| $\hat{C}_{g,t}^{\text{gas,RT}}$ | Forecast real-time gas price [$/kcf] |

The co-optimized model is:

$$\zeta^{COM} = \min \sum_{t\in\mathcal{T}} \Bigg\{ \sum_{m\in\mathcal{M}} \left( C_m^{su} v_{m,t}^u + C_m^{sd} v_{m,t}^d \right) + \sum_{\lambda\in\Lambda} C_\lambda^{ng} p_{\lambda,t}^{ng} + \sum_{n\in\mathcal{N}} C_n^{prod} p_{n,t} + \sum_{i\in\mathcal{I}} \left( \Gamma_\beta^+ \beta_{i,t}^+ + \Gamma_\beta^- \beta_{i,t}^- \right) + \sum_{\gamma\in\Psi} C_\psi^{stor} q_{\psi,t}^{out} + \sum_{j\in\mathcal{J}} \left( \Gamma_\alpha^+ \alpha_{j,t}^+ + \Gamma_\alpha^- \alpha_{j,t}^- \right) \Bigg\} \tag{4.1}$$

$$s.t. \quad \sum_{j\in\mathcal{J}} \sum_{g\in\mathcal{G}(i,j)} p_{g,t} + \sum_{n\in\mathcal{N}(i)} p_{n,t} + \sum_{w\in\mathcal{W}(i)} p_{w,t}^{wind} + \sum_{i''\in\mathcal{I}''(i)} f_{i'',i,t} + \beta_{i,t}^- = D_{i,t}^e + \sum_{i'\in\mathcal{I}'(i)} f_{i,i',t} + \beta_{i,t}^+, \forall i,t \tag{4.2}$$

$$u_{m,t} - u_{m,t-1} = v_{m,t}^u - v_{m,t}^d, \quad \forall m \in \mathcal{G}\cup\mathcal{N}, t \tag{4.3}$$

$$u_{m,t} \geq v_{m,t}^u, \quad \forall m \in \mathcal{G}\cup\mathcal{N}, t \tag{4.4}$$

$$u_{m,t} \leq 1 - v_{m,t}^d, \quad \forall m \in \mathcal{G}\cup\mathcal{N}, t \tag{4.5}$$

$$v_{m,t}^u + v_{m,t}^d \leq 1, \quad \forall m \in \mathcal{G}\cup\mathcal{N}, t \tag{4.6}$$

$$p_{m,t} \geq \underline{P}_m \left( u_{m,t} - v_{m,t}^u - v_{m,t}^d \right), \quad \forall m \in \mathcal{G}\cup\mathcal{N}, t \tag{4.7}$$

$$p_{m,t} \leq \overline{P}_m \left( u_{m,t} - v_{m,t}^u \right) + \underline{P}_m \left( v_{m,t}^d + v_{m,t}^u \right), \quad \forall m \in \mathcal{G}\cup\mathcal{N}, t \tag{4.8}$$

$$-R_m^{down} \leq p_{m,t} - p_{m,t-1} \leq R_m^{up}, \quad \forall m \in \mathcal{G}\cup\mathcal{N}, t \tag{4.9}$$

$$\sum_{tt=t-T_m^{on}+1}^{t} v_{m,t}^u \leq u_{m,t}, \quad \forall m \in \mathcal{G}\cup\mathcal{N}, i, t \tag{4.10}$$

$$\sum_{tt=t-T_m^{off}+1}^{t} v_{m,t}^d \leq 1 - u_{m,t}, \quad \forall m \in \mathcal{G}\cup N, i, t \tag{4.11}$$

$$p_{w,t}^{wind} \leq \overline{P}_{w,t}^{wind}, \quad \forall w \in \mathcal{W}_i, i, t \tag{4.12}$$

$$-\overline{F}_{i,i'} \leq f_{i,i',t} \leq \overline{F}_{i,i'}, \quad \forall i' \in \mathcal{I}'(i), i, t \tag{4.13}$$

$$f_{i,i',t} = \frac{\theta_{i,t} - \theta_{i',t}}{X_{i,i'}}, \quad \forall i' \in \mathcal{I}'(i), i, t \tag{4.14}$$

$$\mu_{g,t} = \phi_g p_{g,t}, \quad \forall g \in \mathcal{G}, t \tag{4.15}$$

$$\begin{aligned} \alpha_{j,t}^{-} + \sum_{\lambda \in \Lambda(j)} p_{\lambda,t}^{ng} + \sum_{\psi \in \Psi(j)} \left(q_{\psi,t}^{out} - q_{\psi,t}^{in}\right) + \sum_{j'' \in \mathcal{J}''(j)} \eta_{j'',j,t} + \sum_{c'' \in \mathcal{C}''(j)} \eta_{c'',j,t} \\ = \chi D_{j,t}^{ng} + \sum_{j' \in \mathcal{J}'(j)} \eta_{j,j',t} + \sum_{c' \in \mathcal{C}'(j)} \eta_{j,c',t} + \sum_{i \in \mathcal{I}} \sum_{g \in \mathcal{G}(i,j)} \mu_{g,t} + \alpha_{j,t}^{+}, \forall j, t : \qquad \kappa_{j,t} \end{aligned} \tag{4.16}$$

$$\underline{L}_{\psi} \leq l_{\psi,t} \leq \overline{L}_{\psi}, \quad \forall \psi, t \tag{4.17}$$

$$-Q_{\psi} \leq \left(q_{\psi,t}^{out} - q_{\psi,t}^{in}\right) \leq Q_{\psi}, \quad \forall \psi, t \tag{4.18}$$

$$l_{\psi,t} = l_{\psi,t-1} - q_{\psi,t}^{out} + q_{\psi,t}^{in}, \quad \forall \psi, t \tag{4.19}$$

$$l_{\psi,t-1} - \overline{L}_{\psi} \leq q_{\psi,t}^{out} - q_{\psi,t}^{in} \leq l_{\psi,t-1} - \underline{L}_{\psi}, \quad \forall \psi, t \tag{4.20}$$

$$\underline{\pi}_j \leq \pi_{j,t} \leq \overline{\pi}_j, \quad \forall j, t \tag{4.21}$$

$$\frac{\pi_{j,t}}{\tau_{j,c'}} \leq \pi_{c',t} \leq \pi_{j,t}\tau_{j,c'}, \quad \forall c' \in \mathcal{C}'(j), t \tag{4.22}$$

$$y_{j,j',t}^{+} + y_{j,j',t}^{-} = 1, \quad \forall j' \in \mathcal{J}'(j), t \tag{4.23a}$$

$$y_{j,j',t}^{+} \in \{0,1\}, y_{j,j',t}^{-} \in \{0,1\}, \quad \forall j' \in \mathcal{J}'(j), t \tag{4.23b}$$

$$(1 - y_{j,j',t}^{+})(\underline{\pi}_j - \overline{\pi}_{j'}) \leq \pi_{j,t} - \pi_{j',t} \leq (1 - y_{j,j',t}^{-})(\overline{\pi}_j - \underline{\pi}_{j'}), \quad \forall j' \in \mathcal{J}'(j), t \tag{4.23c}$$

$$-(1 - y_{j,j',t}^{+})\mathrm{M} \leq \eta_{j,j',t} \leq (1 - y_{j,j',t}^{-})\mathrm{M}, \quad \forall j' \in \mathcal{J}'(j), t \tag{4.23d}$$

$$\tilde{\pi}_{j,j',t} \geq \pi_{j',t} - \pi_{j,t} + (\underline{\pi}_j - \overline{\pi}_{j'})(y_{j,j',t}^{+} - y_{j,j',t}^{-} + 1) \tag{4.23e}$$

$$\tilde{\pi}_{j,j',t} \geq \pi_{j,t} - \pi_{j',t} + (\overline{\pi}_j - \underline{\pi}_{j'})(y_{j,j',t}^{+} - y_{j,j',t}^{-} - 1) \tag{4.23f}$$

$$\tilde{\pi}_{j,j',t} \leq \pi_{j',t} - \pi_{j,t} + (\overline{\pi}_j - \underline{\pi}_{j'})(y_{j,j',t}^{+} - y_{j,j',t}^{-} + 1) \tag{4.23g}$$

$$\tilde{\pi}_{j,j',t} \leq \pi_{j,t} - \pi_{j',t} + (\underline{\pi}_j - \overline{\pi}_{j'})(y_{j,j',t}^{+} - y_{j,j',t}^{-} - 1) \tag{4.23h}$$

$$C^2_{j,j'}\tilde{\pi}_{j,j',t} \geq \eta^2_{j,j',t}, \quad \forall j' \in \mathcal{J}'(j), t \tag{4.23i}$$

The objective (4.1) is to minimize the total cost including the thermal generator start-up and shut-down costs, plus the gas production cost, gas supply cost, electricity production costs, penalties on unserved/excess electricity, penalties on unserved/excess gas and the net cost of gas outflows from storage. Constraints (4.2) are the energy balance at each electricity node for each hour. The UC constraints (4.3)–(4.11) include generator start-up/shut-down, maximum/minimum generation, ramping limits, and minimum on/off time. Constraints (4.12) limit the wind energy output using the available wind energy in each hour. Constraints (4.13)–(4.14) describe the lossless, linearized DC formulation of power flows, and limit the power flows by the transmission line capacities.

The gas and power system are connected through the amount of gas consumed by NGFGs (4.15).

The gas flow constraints (4.16) represent the flow conservation for each hour at each gas node, where the product of non-electric load factor and baseline non-electric load, $\chi D^{ng}_{j,t}$, is the non-electric load for each location. Here the non-electric load factor, $\chi$, is defined to characterize the ratio of the actual and baseline non-electric load for numerical studies. Constraints (4.17)–(4.18) enforce upper and lower bounds on the storage levels and flow rates into and out of each gas storage facility. Constraints (4.19) connect storage levels of consecutive hours with the flow rates. Constraints (4.20) impose limits on the flow rates to maintain storage levels within prescribed bounds. The gas flow through a pipeline depends on the difference of squared pressure levels between the two end nodes, and the gas flow model is expressed as a function of the squared pressure, $\pi_{j,t}$. Constraints (4.21) guarantee the upper and lower limits of the squared pressure, $\pi_{j,t}$. In accordance with a simplified compressor model, constraints (4.22) bounded the squared pressure increase for each active pipeline.

Constraints (4.23) calculate the gas flow through a passive pipeline using the gas squared pressure difference of the two end nodes, which are the mixed-integer second-order cone program (MISOCP) relaxations of the nonlinear non-convex Weymouth equation, expressed as $\eta_{j,j',t} = sgn\left(\pi_{j,t} - \pi_{j',t}\right) C_{j,j'} \sqrt{|\pi_{j,t} - \pi_{j',t}|}, \forall j' \in \mathcal{J}'(j), t$. Here we use binary variables $y^+_{j,j',t}$ and

$y^-_{j,j',t}$ to indicate the gas flow direction in pipelines, which sum to one, as in constraints (4.23a)-(4.23b). Constraints (4.23c) guarantee that the flow direction $y^+_{j,j',t}$ is one ($y^-_{j,j',t}$ is zero) when the gas squared pressure difference is positive and $y^+_{j,j',t}$ is zero ($y^-_{j,j',t}$ is one) otherwise. Constraints (4.23d) decide the flow direction, where M is a big number. We introduce a nonnegative variable $\tilde{\pi}_{j,j',t} = |\pi_{j,t} - \pi_{j',t}|$ to represent the magnitude of the gas squared pressure difference. Then constraints (4.23e)–(4.23h), which are an exact reformulation of $\tilde{\pi}_{j,j',t} = |\pi_{j,t} - \pi_{j',t}|$, assure that $\tilde{\pi}_{j,j',t}$ is the magnitude of the gas squared pressure difference. Lastly, constraints (4.23i) are the MISOCP relaxation of $C^2_{j,j'}\tilde{\pi}_{j,j',t} = \eta^2_{j,j',t}$, which calculates the flow magnitude using the gas squared pressure difference magnitude [9]. The relaxation allows a feasible solution to push less flow than the squared pressure difference would suggest. Totally, the MISOCP co-optimized model (COM) consists of (4.1)–(4.23).

### 4.2.2 Separately Optimized Model (SOM)

Currently, in the U.S., the gas and power systems are each managed by their own operator and some information about the current system status is exchanged between them. The power system is operated by the ISO, while the natural gas system is scheduled by the pipeline company. We construct the separately optimized model (SOM) in accordance with the simplified operating process, as shown in Fig. 4.2. The one-day power system operation is divided into the day-ahead problem, where UC decisions are made, and the real-time problem, where the ED solution is adjusted according to the actual gas availability and real-time gas price. The one-day gas system operation is simplified into the day-ahead scheduling problem and the real-time scheduling problem, where the day-ahead scheduling problem decides the amount of gas available from the interruptible contracts and the real-time gas scheduling problem decides the real-time gas price and availability. These two systems are not co-optimized in parallel. Instead, as illustrated in Fig. 4.2, these two systems are operated by their own operators and there are some interdependencies between them. Models of the day-ahead and the real-time markets of the SOM are presented in Sections 4.2.2.1

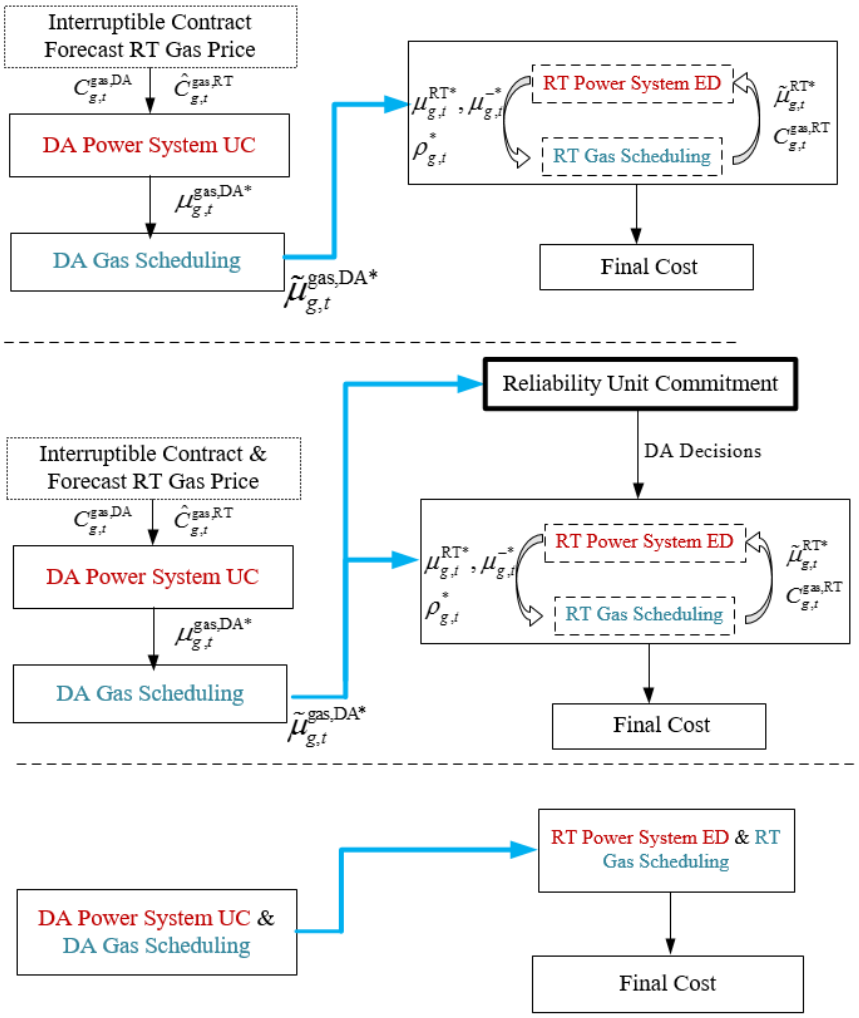


Figure 4.3: Flowcharts for the separately optimized model (top), the separately optimized model with reliability unit commitment (middle) and the co-optimized model (bottom) for the operation of the natural gas and power systems.

and 4.2.2.2, respectively. A corresponding flowchart is shown in Fig. 4.3. To focus on the impact of interruptible contracts, we assume that all the NGFGs hold this type of gas contract.

#### 4.2.2.1 Day-Ahead (DA) Market

The DA market comprises the DA market for power system and the DA market for the natural gas system, where the power system UC problem is solved first and the natural gas system is scheduled afterwards.

*A. Day-Ahead Power System Unit Commitment*

We consider the DA UC problem for the power system with natural gas being the fuel for the NGFGs. Because the NGFGs acquire gas from either the interruptible contracts or the real-time market, the ISO makes DA UC decisions based on the contract gas price, $C_{g,t}^{\text{gas,DA}}$, and the forecast real-time gas price, $\hat{C}_{g,t}^{\text{gas,RT}}$, and obtains the optimal DA UC cost, $\zeta^{\text{Power,DA}}(C_{g,t}^{\text{gas,DA}}\hat{C}_{g,t}^{\text{gas,RT}})$, where $\Theta^{\text{Power,DA}} = \{u_{m,t}, v_{m,t}^{u}, v_{m,t}^{d}, p_{m,t}, \theta_{i,t}, f_{i,i',t}, \mu_{g,t}, \beta_{i,t}^{+}, \beta_{i,t}^{-}\}$. The ISO then reports the optimal DA requested gas amount, $\mu_{g,t}^{\text{DA}}$, to the natural gas system. The difference between the objective (4.24) and (4.1) in the COM model is that in (4.24) the fuel cost of NGFGs is calculated as the sum of gas cost from both the interruptible contract and the real-time market, instead of the gas supply cost from wells and storage facilities plus gas imbalance penalty. For each hour, each NGFG's fuel cost from the interruptible contract is the product of contract gas price, $C_{g,t}^{\text{gas,DA}}$, and the DA requested gas amount, $\mu_{g,t}^{\text{DA}}$. For the real-time gas fuel cost, the NGFGs expect that there will be some gas available from the real-time market, but they do not know the exact real-time gas price and availability. Here, the ISO uses the forecast real-time gas price, $\hat{C}_{g,t}^{\text{gas,RT}}$, to indicate the real-time gas price, and assumes there is no limit on the real-time gas availability due to lack of information. Thus, the fuel cost for the gas from the real-time market is the product of forecast real-time gas price, $\hat{C}_{g,t}^{\text{gas,RT}}$, and the RT requested gas amount, $\mu_{g,t}^{\text{RT}}$, for each hour and each NGFG. Constraints (4.2)–(4.14) are the power system operational constraints. Constraints (4.25a)–(4.25b) enforce that the total requested gas quantity, $(\mu_{g,t}^{\text{DA}} + \mu_{g,t}^{\text{RT}})$, is greater than or equal to the electric gas demand by the NGFGs. The power system DA UC problem is a mixed integer linear program

(MILP):

$$\zeta^{\text{Power,DA}}(C_{g,t}^{\text{gas,DA}}, \hat{C}_{g,t}^{\text{gas,RT}}) = \min_{\Theta^{\text{Power,DA}}} \sum_{t\in\mathcal{T}} \Bigg\{ \sum_{m\in\mathcal{M}} \left( C_m^{su} v_{m,t}^{u} + C_m^{sd} v_{m,t}^{d} \right) + \sum_{n\in\mathcal{N}} C_n^{prod} p_{n,t} + \sum_{i\in\mathcal{I}} \left( \Gamma_{\beta}^{+} \beta_{i,t}^{+} + \Gamma_{\beta}^{-} \beta_{i,t}^{-} \right) + \sum_{g\in\mathcal{G}} \left( C_g^{\text{gas,DA}} \mu_{g,t}^{\text{DA}} + \hat{C}_g^{\text{gas,RT}} \mu_{g,t}^{\text{RT}} \right) \Bigg\} \tag{4.24}$$

$$s.t. \quad \text{Constraints (4.2)} - \text{(4.14)}$$

$$\mu_{g,t}^{\text{RT}} + \mu_{g,t}^{\text{DA}} \geq \phi_g p_{g,t}, \quad \forall g \in \mathcal{G}, t \tag{4.25a}$$

$$\mu_{g,t}^{\text{DA}} \geq 0, \mu_{g,t}^{\text{RT}} \geq 0, \quad \forall g \in \mathcal{G}, t \tag{4.25b}$$

*B. Day-Ahead Natural Gas System Scheduling*

In the DA market, the natural gas system minimizes its net cost while satisfying the non-electric and electric gas demand along with the gas operational constraints. Here, the electric gas demand is the DA requested gas amount, $\mu_{g,t}^{\text{DA}*}$. An asterisk (*) indicates the fixed value coming from the DA UC problem in the previous step. The natural gas system solves the DA gas system scheduling problem given the fixed value of the DA requested gas amount, $\mu_{g,t}^{\text{DA}*}$, and the contract gas price, $C_{g,t}^{\text{gas,DA}}$. The total cost in (4.26) consists of the gas cost from wells and storage facilities, plus the imbalance terms, and minus the revenue for supplying the electric gas demand, where $\Theta^{\text{Gas,DA}} = \{p_{\lambda,t}^{ng}, q_{\psi,t}^{out}, q_{\psi,t}^{in}, l_{\psi,t}, y_{j,j',t}^{+}, y_{j,j',t}^{-}, \pi_{j,t}, \tilde{\pi}_{j,j',t}, \eta_{j,j',t}, \alpha_{j,t}^{+}, \alpha_{j,t}^{-}, \tilde{\mu}_{g,t}^{\text{DA}}\}$. Constraints (4.17)–(4.23) are the natural gas network operating constraints. Constraints (4.27a) are the gas flow balance constraints at each node while trying to satisfy all the demand. Here we introduce a new variable for the electric gas demand actually supplied by the DA gas system, $\tilde{\mu}_{g,t}^{\text{DA}}$, because the electric gas demand is interruptible. Constraints (4.27b) impose limits on $\tilde{\mu}_{g,t}^{\text{DA}}$, and the revenue for supplying the electric gas demand is the product of $\tilde{\mu}_{g,t}^{\text{DA}}$ and $C_{g,t}^{\text{gas,DA}}$ for each hour and each NGFG. Once the optimal solution is obtained, the gas system reports the optimal electric gas demand actually supplied by the DA gas system, $\tilde{\mu}_{g,t}^{\text{DA}*}, \forall j, t$, to the real-time market. The whole DA gas system scheduling

problem is a MISOCP:

$$\zeta^{\text{Gas,DA}}(C^{\text{gas,DA}}_{g,t}, \mu^{\text{DA}*}) = \min_{\Theta^{\text{Gas,DA}}} \sum_{t\in\mathcal{T}} \Bigg\{ \sum_{\lambda\in\Lambda} C^{ng}_{\lambda} p^{ng}_{\lambda,t} + \sum_{\psi\in\Psi} C^{stor}_{\psi} q^{out}_{\psi,t} + \sum_{j\in\mathcal{J}} \left( \Gamma^{+}_{\alpha}\alpha^{+}_{j,t} + \Gamma^{-}_{\alpha}\alpha^{-}_{j,t} \right) - \sum_{g\in\mathcal{G}} C^{\text{gas,DA}}_{g,t} \tilde{\mu}^{\text{DA}}_{g,t} \Bigg\} \tag{4.26}$$

$$s.t. \quad \text{Constraints (4.17)} - \text{(4.23)}$$

$$\alpha^{-}_{j,t} + \sum_{\lambda\in\Lambda(j)} p^{ng}_{\lambda,t} + \sum_{\psi\in\Psi(j)} \left( q^{out}_{\psi,t} - q^{in}_{\psi,t} \right) + \sum_{j''\in\mathcal{J}''(j)} \eta_{j'',j,t} + \sum_{c''\in\mathcal{C}''(j)} \eta_{c'',j,t} = \chi D^{ng}_{j,t} + \sum_{j'\in\mathcal{J}'(j)} \eta_{j,j',t} + \sum_{c'\in\mathcal{C}'(j)} \eta_{j,c',t} + \sum_{i\in\mathcal{I}} \sum_{g\in\mathcal{G}(i,j)} \tilde{\mu}^{\text{DA}}_{g,t} + \alpha^{+}_{j,t}, \forall j,t \tag{4.27a}$$

$$0 \le \tilde{\mu}^{\text{DA}}_{g,t} \le \mu^{\text{DA}*}_{g,t}, \forall g,t \tag{4.27b}$$

#### 4.2.2.2 Real-Time (RT) Market

The optimal UC decisions and the optimal amount of electric gas demand actually supplied by the DA gas system, $\tilde{\mu}^{\text{DA}*}_{g,t}, \forall j,t$, are obtained by solving the DA problem. In other words, the amounts of the just described gas available from the interruptible contracts to the NGFGs, $\tilde{\mu}^{\text{DA}*}_{g,t}, \forall j,t$, are known and fixed. As the NGFGs have an option to acquire gas from the real-time market, this subsection presents methodologies to find the real-time gas price and availability through an equilibrium analysis between the power and natural gas systems, as illustrated in the right part of the top subfigure of Fig. 4.3. This equilibrium is obtained through an iterative process. Within each iteration, the power system solves the ED problem and reports the willingness-to-pay price for gas, $\rho^{*}_{g,t}$, along with the requested real-time gas quantity, $(\mu^{\text{RT}*}_{g,t}, \mu^{-*}_{g,t})$, to the natural gas system. Then, based on this information, the natural gas system solves the real-time scheduling problem and reports the actual available real-time gas quantity, $\tilde{\mu}^{\text{RT}*}_{g,t}$, and willingness-to-sell price, $\nu^{*}_{j,t}$, to the electric system for next iteration. A competitive equilibrium is reached when this process converges to a consistent set of prices and gas quantities. We present the optimization models for

the power system and the natural gas system, respectively, followed and the equilibrium process between them.

*A. Real-Time Economic Dispatch of the Power System*

The RT ED problem fixes all the UC decisions, $(u^*_{m,t}, v^{u*}_{m,t}, v^{d*}_{m,t})$, and the electric gas demand actually supplied by the DA gas system, $\tilde{\mu}^{\mathrm{DA}*}_{g,t}$, and solves for the optimal dispatch solution with hourly steps considering gas price and availability from both contracts and the real-time gas market. In the process to reach equilibrium, for each iteration, two important parameters are introduced: the real-time available gas quantity, $\tilde{\mu}^{\mathrm{RT}*}_{g,t}$, and the real-time gas price, $C^{\mathrm{gas,RT}}_{g,t}$, both of which come from the real-time gas market of the previous iteration. Specifically, $\tilde{\mu}^{\mathrm{RT}*}_{g,t}$ and $C^{\mathrm{gas,RT}}_{g,t}$ characterize the gas availability and price in the previous iteration and are initialized to infinity and the forecast real-time gas price, $\hat{C}^{\mathrm{gas,RT}}_{g,t}$, respectively.

The objective function minimized includes the production cost of non-gas-fired generators, imbalanced penalties, and the payment for gas from the RT gas markets, where $\Theta^{\mathrm{Power,RT}} = \{p_{m,t}, \theta_{m,t}, f_{i,i',t}, \mu^{\mathrm{RT}}_{g,t}, \mu^{-}_{g,t}, \beta^{+}_{i,t}, \beta^{-}_{i,t}\}$. Similar to constraints (4.25a)–(4.25b), constraints (4.29a)–(4.29b) impose limits on the nonnegative RT requested gas quantity. Here we separate the RT requested gas quantity into two parts. The first part is the RT requested gas quantity within the limit, $\mu^{\mathrm{RT}}_{g,t}$, and the second part is the additional RT requested gas quantity, $\mu^{-}_{g,t}$. The reason for this separation is that the value of the parameter $\tilde{\mu}^{\mathrm{RT}*}_{g,t}$ is determined by the iterative process too. We use $\mu^{-}_{g,t}$ to indicate the additional requested gas quantity beyond the current limit, for which the NGFGs are willing to pay a higher price for the gas. For each hour and each NGFG, the fuel cost for gas from the real-time market consists of the RT requested gas cost within the limit, $C^{\mathrm{gas,RT}}_{g,t}\mu^{\mathrm{RT}}_{g,t}$, and the additional RT requested gas cost, $C^{\mathrm{gas},-}_{g,t}\mu^{-}_{g,t}$. The additional RT requested gas price, $C^{\mathrm{gas},-}_{g,t}$, could be viewed as the outflow storage cost for a hypothetical storage facility with unlimited capacity which exists at each NGFG. Constraints (4.29a) limit the total requested gas quantity from DA and RT market to be at least the total electric gas demand by the NGFGs. Constraints (4.29b) impose an upper bound on the RT requested gas quantity within the limit. Note that since usually $C^{\mathrm{gas},-}_{g,t} > C^{\mathrm{gas,RT}}_{g,t}$, only when $\phi_g p_{g,t} > \tilde{\mu}^{\mathrm{DA}*}_{g,t} + \tilde{\mu}^{\mathrm{RT}*}_{g,t}$, we may have $\mu^{-}_{g,t} > 0$.

The total RT requested gas quantity is $\mu_{g,t}^{\mathrm{RT}*} + \mu_{g,t}^{-*}$. To summarize, the ISO solves the ED problem considering the gas price and availability information from the previous iteration and reports the total RT requested gas quantity, $\mu_{g,t}^{\mathrm{RT}*} + \mu_{g,t}^{-*}$ to the RT natural gas scheduling problem. The RT willingness-to-pay price for gas by the NGFGs, $\rho_{g,t}^{*}$, is the optimal dual variable of (4.29a). The RT ED problem is a linear program (LP):

$$\begin{aligned}
&\zeta^{\mathrm{Power,RT}}(u_{m,t}^{*}, v_{m,t}^{u*}, v_{m,t}^{d*}, C_{g,t}^{\mathrm{gas,DA}}, \tilde{\mu}_{g,t}^{\mathrm{DA}*}, \tilde{\mu}_{g,t}^{\mathrm{RT}*}) \\
&= \sum_{t\in\mathcal{T}} \left\{ \sum_{m\in\mathcal{M}} \left( C_{m}^{su*} v_{m,t}^{u*} + C_{m}^{sd*} v_{m,t}^{d*} \right) + \sum_{g\in\mathcal{G}} C_{g,t}^{\mathrm{gas,DA}} \tilde{\mu}_{g,t}^{\mathrm{DA}*} \right\} \\
&+ \min_{\Theta^{\mathrm{Power,RT}}} \sum_{t\in\mathcal{T}} \left\{ \sum_{n\in\mathcal{N}} C_{n}^{prod} p_{n,t} + \sum_{i\in\mathcal{I}} \left( \Gamma_{\beta}^{+} \beta_{i,t}^{+} + \Gamma_{\beta}^{-} \beta_{i,t}^{-} \right) + C_{g,t}^{\mathrm{gas,RT}} \mu_{g,t}^{\mathrm{RT}} + C_{g,t}^{\mathrm{gas},-} \mu_{g,t}^{-} \right) \right\}
\end{aligned} \tag{4.28}$$

$$s.t. \quad \text{Constraints (4.2)} - \text{(4.14)}$$

$$\phi_{g} p_{g,t} \le \tilde{\mu}_{g,t}^{\mathrm{DA}*} + \mu_{g,t}^{\mathrm{RT}} + \mu_{g,t}^{-}, \quad \forall g \in \mathcal{G}, t \tag{4.29a}$$

$$0 \le \mu_{g,t}^{\mathrm{RT}} \le \tilde{\mu}_{g,t}^{\mathrm{RT}*}, \mu_{g,t}^{-} \ge 0, \quad \forall g \in \mathcal{G}, t : \qquad \rho_{g,t} \tag{4.29b}$$

*B. Real-Time Scheduling of the Natural Gas System*

Given the fixed requested gas quantity from DA and RT market, $\tilde{\mu}_{g,t}^{\mathrm{DA}*}$ and $\mu_{g,t}^{\mathrm{RT}*} + \mu_{g,t}^{-*}$, along with the willingness-to-pay for gas $\rho_{g,t}^{*}$, the natural gas system solves for the minimal net cost to satisfy all the demand and assess the RT gas price, $C_{g,t}^{\mathrm{gas,RT}}$, and the real-time available gas quantity $\tilde{\mu}_{g,t}^{\mathrm{RT}*}$, where $\Theta^{\mathrm{gas,RT}} = \{q_{\psi,t}^{out}, q_{\psi,t}^{in}, p_{\lambda,t}^{ng}, \pi_{j,t}, \eta_{j,j',t}, \tilde{\mu}_{g,t}^{\mathrm{RT}}, \alpha_{j,t}^{+}, \alpha_{j,t}^{-}\}$. The net cost minimized includes the gas supply cost from wells and storage facilities and imbalance penalties minus the revenue for supplying electric gas demand in the real-time market. Constraints (4.31a) differ from (4.27a) at the electric gas demand. Constraints (4.27a) represent that, in the day-ahead market, the natural gas system must satisfy only $\tilde{\mu}_{g,t}^{\mathrm{DA}*}$, whereas (4.31a) aims at satisfying $\tilde{\mu}_{g,t}^{\mathrm{DA}*} + \tilde{\mu}_{g,t}^{\mathrm{RT}}$. Here constraints (4.31b) limit the RT available gas quantity to be no more than the requested amount. Denote $\nu_{j,t}$ as the dual variable of (4.31a). Then $\nu_{j,t}$, where NGFG $g$ is located at gas node $j$, is the gas price. The RT scheduling problem of the natural gas system is a MISOCP, and the optimal $\nu_{j,t}^{*}$ and $\tilde{\mu}_{g,t}^{\mathrm{RT}*}$

are reported to the RT power system market.

$$\zeta^{\text{Gas,RT}}(C_{g,t}^{\text{gas,DA}}, \tilde{\mu}_{g,t}^{\text{DA}*}, \mu_{g,t}^{\text{RT}*}, \mu_{g,t}^{-*}) = -\sum_{t\in\mathcal{T}}\sum_{g\in\mathcal{G}} C_{g,t}^{\text{gas,DA}}\tilde{\mu}_{g,t}^{\text{DA}*}$$
$$+ \min_{\Theta^{\text{Gas,RT}}} \sum_{t\in\mathcal{T}}\left\{\sum_{\lambda\in\Lambda} C_{\lambda}^{ng} p_{\lambda,t}^{ng} + \sum_{\psi\in\Psi} C_{\psi}^{stor} q_{\psi,t}^{out} + \sum_{j\in\mathcal{J}}\left(\Gamma_{\alpha}^{+}\alpha_{j,t}^{+} + \Gamma_{\alpha}^{-}\alpha_{j,t}^{-}\right) - \sum_{g\in\mathcal{G}} \rho_{g,t}^{*}\tilde{\mu}_{g,t}^{\text{RT}}\right\} \tag{4.30}$$
$$s.t. \quad \text{Constraints (4.17)} - \text{(4.23)}$$

$$\alpha_{j,t}^{-} + \sum_{\lambda\in\Lambda(j)} p_{\lambda,t}^{ng} + \sum_{\psi\in\Psi(j)}\left(q_{\psi,t}^{out} - q_{\psi,t}^{in}\right) + \sum_{j''\in\mathcal{J}''(j)} \eta_{j'',j,t} + \sum_{c''\in\mathcal{C}''(j)} \eta_{c'',j,t}$$
$$= \chi D_{j,t}^{ng} + \sum_{j'\in\mathcal{J}'(j)} \eta_{j,j',t} + \sum_{c'\in\mathcal{C}'(j)} \eta_{j,c',t} + \sum_{i\in\mathcal{I}}\sum_{g\in\mathcal{G}(i,j)} (\tilde{\mu}_{g,t}^{\text{DA}*} + \tilde{\mu}_{g,t}^{\text{RT}}) + \alpha_{j,t}^{+}, \forall j,t: \quad \nu_{j,t} \tag{4.31a}$$

$$0 \le \tilde{\mu}_{g,t}^{\text{RT}} \le \mu_{g,t}^{\text{RT}*} + \mu_{g,t}^{-*}, \quad \forall g,t \tag{4.31b}$$

*C. Equilibrium of the Real-Time Power and Natural Gas Systems*

The previous two paragraphs describe the details of the real-time market. This subsection outlines the equilibrium between the power and natural gas systems, in which the RT gas price and flow information are exchanged between them. According to [79], if this process converges to a consistent set of prices, a competitive equilibrium is reached. The details of the equilibrium are shown in Algorithm 2.

**Algorithm 2:** Real-time natural gas/electricity system equilibrium.

1: **input:** Stopping criterion $\epsilon$; $\tilde{\mu}_{g,t}^{\text{DA}*}, C_{g,t}^{\text{gas,DA}}, \hat{C}_{g,t}^{\text{gas,RT}}, C_{g,t}^{\text{gas},-}$
2: **output:** $\mu_{g,t}^{\text{RT}}, \mu_{g,t}^{-}, \tilde{\mu}_{g,t}^{\text{RT}}, C_{g,t}^{\text{gas,RT}}$
3: **Initialize:** iter $\leftarrow 0$, $\tilde{\mu}_{g,t}^{\text{RT}*} \leftarrow \infty$, $C_{g,t}^{\text{gas,RT}} \leftarrow \hat{C}_{g,t}^{\text{gas,RT}}$
4: **repeat**
5: min (4.28) s.t. (4.2)-(4.14), (4.29a)-(4.29b)
6: $p_{g,t}^{(\text{iter})} \leftarrow p_{g,t}$, $\rho_{g,t}^{*} \leftarrow \rho_{g,t}$, $\mu_{g,t}^{\text{RT}*} \leftarrow \mu_{g,t}^{\text{RT}}$, $\mu_{g,t}^{\text{RT(iter)}} \leftarrow \mu_{g,t}^{\text{RT}}$, $\mu_{g,t}^{-(\text{iter})} \leftarrow \mu_{g,t}^{-}$, $\mu_{g,t}^{-*} \leftarrow \mu_{g,t}^{-}$
7: min (4.30) s.t. (4.17)-(4.23), (4.31a)-(4.31b)
8: $C_{g,t}^{\text{gas,RT}} \leftarrow \nu_{j,t}$, $\tilde{\mu}_{g,t}^{\text{RT}*} \leftarrow \tilde{\mu}_{g,t}^{\text{RT}}$
9: iter $\leftarrow$ iter $+ 1$
10: **until** $\frac{||p_{g,t}^{(\text{iter-1})} - p_{g,t}^{(\text{iter-2})}||}{||p_{g,t}^{(\text{iter-1})} + p_{g,t}^{(\text{iter-2})}||} \le \epsilon$, $\frac{||\mu_{g,t}^{-(\text{iter-1})} - \mu_{g,t}^{-(\text{iter-2})}||}{||\mu_{g,t}^{-(\text{iter-1})} + \mu_{g,t}^{-(\text{iter-2})}||} \le \epsilon$ and $\frac{||\mu_{g,t}^{\text{RT(iter-1)}} - \mu_{g,t}^{\text{RT(iter-2)}}||}{||\mu_{g,t}^{\text{RT(iter-1)}} + \mu_{g,t}^{RT(\text{iter-2})}||} \le \epsilon$

The proposed algorithm is implemented by iteratively solving the RT ED of the power system, which minimizes (4.28) subject to (4.2)-(4.14), (4.29a)-(4.29b), and the real-time scheduling of the natural gas system, which minimizes (4.30) subject to (4.17)-(4.23), (4.31a)-(4.31b).

Before we discuss the details of the algorithm, note that we have $\rho_{g,t}$ defined as the Lagrange multiplier that is associated with the natural gas-quantity constraint (4.29a) for NGFG $g$ in time step $t$. We also define $\nu_{j,t}$ as the dual variable that is associated with constraint (4.31a) for electricity bus $j$ and time step $t$. These dual variables are obtained by re-solving the linear ED problem and the linear relaxation of the MISOCP real-time gas scheduling problem in which the binary variables are fixed to be their optimal values. Then the dual variable $\rho_{g,t}$ represents the price the NGFGs are willing to pay for the gas, and the dual variable $\nu_{j,t}$ is the RT gas price the gas system charges, where NGFG $g$ is located at node $j$.

The two models also exchange the gas quantity, which represents the amount of gas for electricity generation demanded by the NGFGs and supplied by the gas supplier. Specifically, after obtaining a solution to the RT ED problem, we update the requested gas quantity within the current gas availability from real-time gas market $\mu_{g,t}^{\mathrm{RT}^*}$, where $\mu_{g,t}^{\mathrm{RT}^*} \leq \tilde{\mu}_{g,t}^{\mathrm{RT}^*}$, and the additional requested RT gas quantity $\mu_{g,t}^{-*}$. These two parameters and the updated willingness-to-pay for gas $\rho_{g,t}^*$ are the input parameters to the real-time gas system. Then we solve for the optimal solution to the real-time gas system, update the available gas quantity $\tilde{\mu}_{g,t}^{\mathrm{RT}^*}$ along with the RT gas price $\hat{C}_{g,t}^{\mathrm{gas,RT}}$, which indicates the willing-to-sell gas price in the real time, and pass this information to the real-time power system.

Algorithm 2 gives pseudocode for the equilibrium system. It takes input parameters including the convergence tolerance, $\epsilon$, the optimal gas quantity from the interruptible contracts calculated from the day-ahead market, $\tilde{\mu}_{g,t}^{\mathrm{DA}^*}$, the contract gas price, $C_{g,t}^{\mathrm{gas,DA}}$, the forecast RT gas price, $\hat{C}_{g,t}^{\mathrm{gas,RT}}$ and the additional requested RT gas price, $C_{g,t}^{\mathrm{gas},-}$. Outputs from Algorithm 2 are the optimal values of variables consisting of real-time gas quantity from the natural gas system to the power system, including the requested amount of gas within the current gas availability from real-time gas market

$\mu_{g,t}^{\mathrm{RT}*}$, the additional real-time requested gas quantity $\mu_{g,t}^{-*}$ and the available gas from the real-time gas system, $\tilde{\mu}_{g,t}^{\mathrm{RT}*}$, as well as the actual RT gas price, $C_{g,t}^{\mathrm{gas,RT}}$.

Line 3 initializes some parameters such as the iteration number, the RT available gas quantity, $\tilde{\mu}_{g,t}^{\mathrm{RT}*}$, and the RT gas price, $C_{g,t}^{\mathrm{gas,RT}}$. Line 5 solves the RT ED problem of the power system, saves the dispatch level of each generator to $p_{g,t}^{(\mathrm{iter})}$, the RT requested gas cost within the limit to $\mu_{g,t}^{\mathrm{RT(iter)}}$, and the additional requested RT gas quantity to $\mu_{g,t}^{-(\mathrm{iter})}$, where *iter* is the iteration number, and updates $\rho_{g,t}^{*}, \mu_{g,t}^{\mathrm{RT}*}$ and $\mu_{g,t}^{-*}$. Line 7 then solves the real-time scheduling problem of the gas system, and updates $C_{g,t}^{\mathrm{gas,RT}}$ and $\tilde{\mu}_{g,t}^{\mathrm{RT}*}$. This process is repeated until the convergence criterion in line 10 is achieved. This convergence criterion requires that the electricity-production levels of all the generators and the real-time electric gas demand of two successive iterations are close enough.

### 4.2.3 Separately Optimized Model with Reliability Unit Commitment (SOMRUC)

Section 4.2.2 discusses the current SOM model for the power and natural gas system, consisting of the day-ahead and real-time markets. It is worth noting that Fig. 4.2 and the top subfigure of Fig. 4.3 show that the DA UC decisions are made without any gas availability information. This can also be seen in the fact that constraints (4.25b) do not have any upper limit for the gas quantity from either contracts (day-ahead) or real-time market. This timing difference between natural gas and power systems can result in severe risks. Specifically, the actual available gas quantity could be less than the requested amount (i.e. $\tilde{\mu}^{\mathrm{DA}*} < \mu^{\mathrm{DA}*}$), which is highly possible and occurs only for $g, t$ once (4.27b) is not binding. Considering that the other source of gas is the real-time market, in the case of less gas from the contract than requested, the NGFGs can acquire gas from the real-time market. However, the supplying ability of the real-time gas system is also limited. If the requested real-time gas amount is very high, the real-time gas system might not able to supply enough gas to the power system. Under the extreme case, such as high non-electric gas load and high real-time electric gas demand, it is even possible that there is not enough gas fuel to support the unit commitment status. This can cause high risks of high RT gas price, electricity price and operational cost.

One possible way to reduce this risk is to run a reliability unit commitment (RUC) step while assuming gas quantity from the real-time market is zero. This idea can also be extended to the case of limiting the gas quantity from the real-time market. In this paper, we consider the case of RUC problem with no available gas from the real-time market. The middle subfigure of Fig. 4.3 illustrates the flow chart of this SOMRUC model. We add a RUC step between the DA natural gas scheduling and the RT power system ED problem. In this way, we re-optimize the UC decisions. The RUC step adjusts the UC decisions while minimizing total cost (4.32) and limiting the gas consumption, as shown in (4.33), where $\Theta^{\text{RUC}} = \{u_{m,t}, v^u_{m,t}, v^d_{m,t}, p_{m,t}, \theta_{i,t}, f_{i,i',t}, \beta^+_{i,t}, \beta^-_{i,t}\}$. The objective function (4.32) consists of rmal generator start-up and shut-down costs, plus the non-gas-fired generator production cost and penalty cost. Constraints (4.33) limit the fuel consumption by the NGFGs. This RUC step is a MILP. Then the fixed UC decisions and $\tilde{\mu}^{\text{DA}*}$ are passed to the real-time iterative process for equilibrium, which is the same as the SOM model, as shown in Fig. 4.3.

$$\begin{aligned}\zeta^{\text{RUC}}(C^{\text{gas,DA}}_{g,t}, \tilde{\mu}^{\text{DA}*}_{g,t}) &= \sum_{t\in\mathcal{T}}\sum_{g\in\mathcal{G}} C^{\text{gas,DA}}_{g,t}\tilde{\mu}^{\text{DA}*}_{g,t} \\ &+ \min_{\Theta^{\text{RUC}}} \sum_{t\in\mathcal{T}} \Bigg\{ \sum_{m\in\mathcal{M}} \left(C^{su}_m v^u_{m,t} + C^{sd}_m v^d_{m,t}\right) + \sum_{n\in\mathcal{N}} C^{prod}_n p_{n,t} + \sum_{i\in\mathcal{I}} \left(\Gamma^+_\beta \beta^+_{i,t} + \Gamma^-_\beta \beta^-_{i,t}\right)\Bigg\} \\ &\qquad s.t. \quad \text{Constraints (4.2)} - \text{(4.14)}\end{aligned} \tag{4.32}$$

$$\phi_g p_{g,t} \le \tilde{\mu}^{\text{DA}*}_{g,t}, \qquad \forall g, t \tag{4.33}$$

## 4.3 Numerical Studies

In this section, we conduct a series of numerical studies and analyze the results. In Section 4.3.1, a small case study of a six-bus power system with a seven-node gas system [43] is used to demonstrate and compare these three models with respect to the economic performance, such as the allocation of costs between the owner and natural gas systems, the RT gas price, and some other operational level decisions including UC decisions. Considering that the interruptible contract gas price and the non-electric gas load are two important parameters, Section 4.3.2 uses a larger

system, composed of the IEEE 24-bus system with a 20-node gas system [18], to compare the cost breakdown of these three models given different parameter values for the interruptible gas contract price and non-electric gas load.

As shown in the extensive review of the natural gas system data [60], similar to power system markets, the natural gas markets are located at different geographic hubs. Although each region has its own gas market, the Henry Hub in Louisiana is the most widely-referenced hub for ISOs because of its high quantity traded and relatively stable prices. According to the historic record of the Henry Hub natural gas daily spot price [71], the maximum price is no more than \$20/kcf from January 1997 until now. Hence we set the additional requested RT gas price, $C_{g,t}^{\text{gas}-}$, to be \$20/kcf. The unserved and excess energy cost are respectively set to be \$3500/MWh and \$350/MWh, as recommended by MISO [47], while the unserved gas and excess gas penalties are set to be \$3500/kcf and \$350/kcf, respectively. We assume that 1 kcf of natural gas generates 1 MBtu of energy. All models are programmed in GAMS by calling the MISOCP solver ILOG CPLEX 12.6 and MILP solver OSIGUROBI. All simulations are implemented on a personal computer, which has Intel Core i7 processors with a CPU at 3.40 GHz and a RAM space of 16 GB.

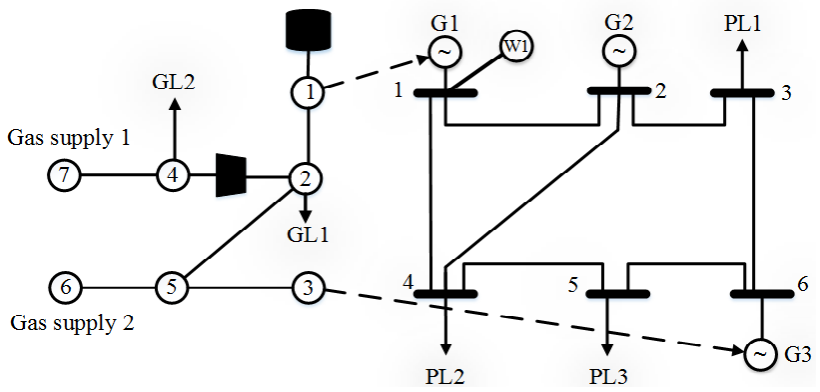


Figure 4.4: Six-bus power system with seven-node gas system. The natural gas system with gas loads (GL) shown on the left-hand side and the power system with power loads (PL), NGFGs(G) and wind generators (W) is shown on the right-hand side. Dashed lines show connections between the two systems.

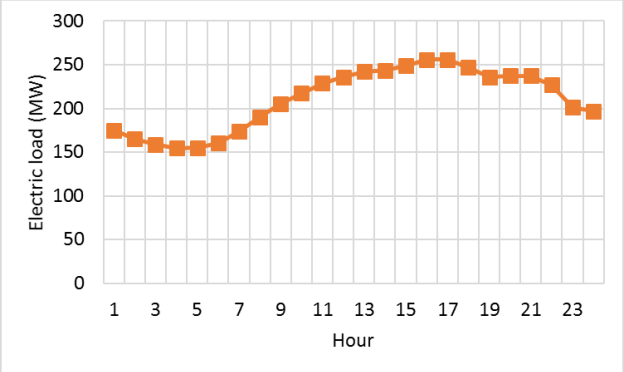


Figure 4.5: The total electric load of the six-bus power system with seven-node gas system.

### 4.3.1 An Illustrative Example: A Six-Bus System with Seven-Node Gas System

We use a six-bus power system with a seven-node gas system, as shown in Fig. 4.4, to illustrate the proposed models. This test system consists of two NGFGs, one coal-fired generator, one wind generator (farm), three power loads, seven transmission lines, one storage facility, one active pipeline, five passive pipelines, two non-electric gas loads and two gas suppliers [43]. The production cost of generator 2 is \$56.56/MWh, and the efficiency of NGFG 1 and 3 is 17.73 and 19.73 kcf/MWh, respectively. The well gas costs are \$1.68/kcf and \$2.28/kcf, respectively, and the stored gas cost is \$3/kcf. According to the data source [31], the start-up /shut-down costs of thermal generators are zero. Hourly gross non-electric gas demand is 9600 kcf/h, divided between gas nodes 2 and 4 with the ratio of 2 to 1. The total hourly electric load is shown in Fig. 4.5 and is allocated to power nodes 1, 2 and 3 with the ratio of 1:2:2. The wind generation capacity is 30% of the total thermal capacity. The contract gas price is a crucial parameter for analysis. For simplicity, we assume all the NGFGs hold the same contract gas price. Here the two well costs are \$1.68/kcf and \$2.28/kcf, respectively, whereas the storage cost is \$3/kcf. Considering that the gas price should be greater than the well cost and that the gas from storage facility usually is responsible for the real-time adjustment, we set the interruptible contract gas price and the forecast RT gas price to be \$2.5/kcf and \$3/kcf, respectively. More sensitivity analysis of the interruptible contract gas price is conducted in a large case study in Section 4.3.2.

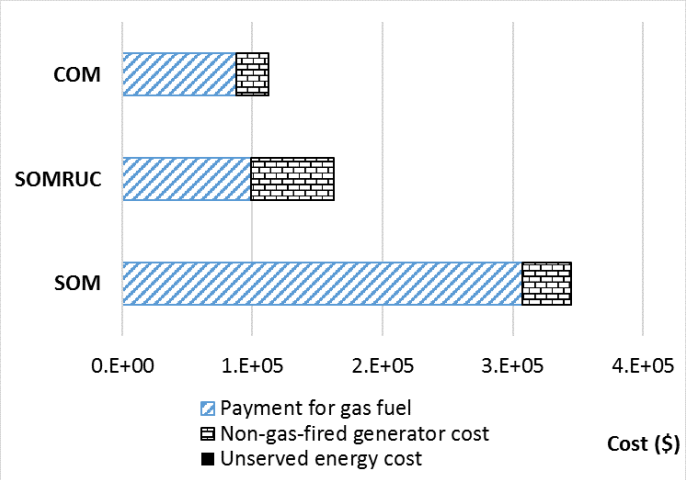


Figure 4.6: The comparison of power system cost decomposed as payments to gas system, non-gas fired generator cost, and unserved energy cost among the three models.

Fig. 4.6 compares the power system cost breakdown in the payment for gas fuel, non-gas-fired generator cost and the unserved energy cost. None of the three models has unserved energy cost. The non-gas-fired generator cost in the SOMRUC model is approximately twice that in the SOM model. However, the gas fuel cost of the SOM model is about three times that of the SOMRUC model. The payments for gas fuel of the COM model and the SOMRUC model are very close. But the non-gas-fired generator cost of the SOMRUC model is about three times that of the COM model. Generally, the COM model, as the cost benchmark, has the lowest cost, whereas the SOM model has the greatest cost.

To compare these three models at the operational level, the comparison of the hourly optimal unit commitment status and the hourly optimal dispatch of each generator among the three models are shown in Table 4.1 and Fig. 4.7, respectively. Note that generators 1 and 3 are NGFGs, whereas generator 2 is the coal-fired generator. Once a generator is committed, the maximum (minimum) dispatch of generator 1, 2, and 3 are 220 (100), 100 (10), and 20 (10), respectively. Specifically, in Fig. 4.7, for each generator, the upper limit of the y-axis is the maximum capacity. The only wind farm is always dispatched to its available value (i.e. $P_{w,t}^{\text{wind}} = \overline{P}_{w,t}^{\text{wind}}$). The COM model assumes that there is a centralized system operator who has full information about both systems and operates them simultaneously. The production cost of generator 2 is \$56.56/MWh, and the

Table 4.1: Unit commitment status comparison among the three models for generator 1, 2 and 3.

| Model | Unit | Hour | | | | | | | | | | | | | | | | | | | | | | | |
|---|---|---|---|---|---|---|---|---|---|---|---|---|---|---|---|---|---|---|---|---|---|---|---|---|---|
| | | 1 | 2 | 3 | 4 | 5 | 6 | 7 | 8 | 9 | 10 | 11 | 12 | 13 | 14 | 15 | 16 | 17 | 18 | 19 | 20 | 21 | 22 | 23 | 24 |
| SOM | 1 | 1 | 0 | 0 | 0 | 0 | 0 | 1 | 1 | 1 | 1 | 1 | 1 | 1 | 1 | 1 | 1 | 1 | 1 | 1 | 1 | 1 | 1 | 1 | 1 |
| SOMRUC | 1 | 1 | 0 | 0 | 0 | 0 | 0 | 0 | 0 | 0 | 1 | 1 | 1 | 1 | 1 | 1 | 1 | 1 | 1 | 1 | 1 | 1 | 1 | 1 | 1 |
| COM | 1 | 1 | 0 | 0 | 0 | 0 | 1 | 1 | 1 | 1 | 1 | 1 | 1 | 1 | 1 | 1 | 1 | 1 | 1 | 1 | 1 | 1 | 1 | 1 | 1 |
| SOM | 2 | 1 | 0 | 0 | 0 | 0 | 1 | 1 | 1 | 1 | 1 | 1 | 1 | 1 | 1 | 1 | 1 | 1 | 1 | 1 | 1 | 1 | 1 | 1 | 1 |
| SOMRUC | 2 | 1 | 1 | 1 | 1 | 1 | 1 | 1 | 1 | 1 | 1 | 1 | 1 | 1 | 1 | 1 | 1 | 1 | 1 | 1 | 1 | 1 | 1 | 1 | 1 |
| COM | 2 | 1 | 1 | 1 | 1 | 1 | 0 | 0 | 0 | 0 | 0 | 1 | 1 | 1 | 1 | 1 | 1 | 1 | 1 | 1 | 1 | 1 | 0 | 0 | 0 |
| SOM | 3 | 0 | 0 | 1 | 1 | 1 | 1 | 1 | 0 | 0 | 1 | 1 | 1 | 1 | 1 | 1 | 1 | 1 | 1 | 1 | 1 | 1 | 1 | 0 | 0 |
| SOMRUC | 3 | 0 | 0 | 1 | 1 | 1 | 1 | 0 | 1 | 1 | 0 | 1 | 1 | 1 | 1 | 1 | 1 | 1 | 1 | 1 | 1 | 1 | 1 | 0 | 0 |
| COM | 3 | 0 | 0 | 1 | 1 | 1 | 1 | 0 | 1 | 1 | 1 | 1 | 1 | 1 | 1 | 1 | 1 | 1 | 1 | 1 | 1 | 1 | 1 | 1 | 1 |

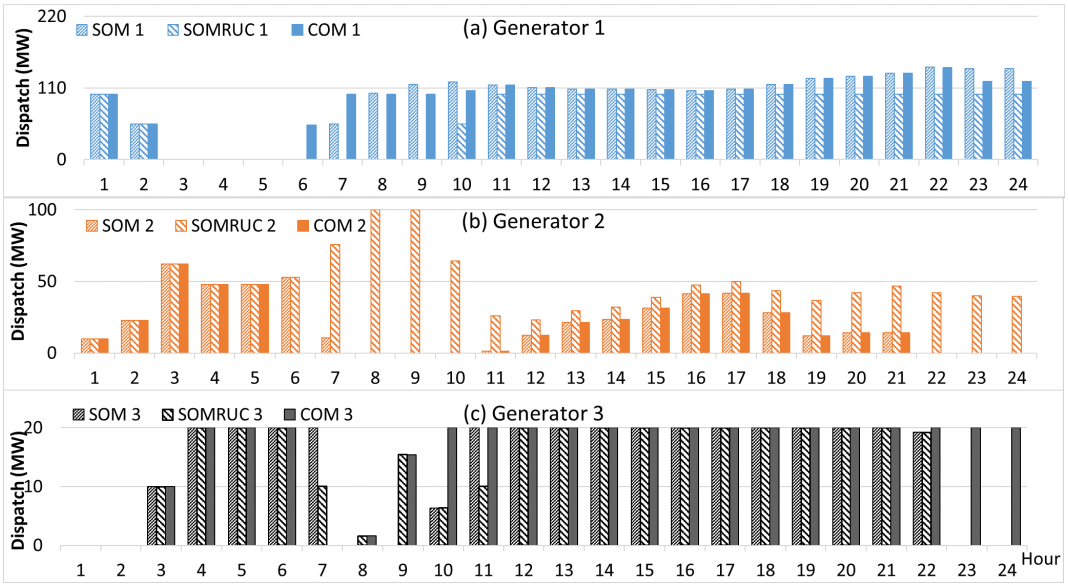


Figure 4.7: Hourly dispatch comparison for (a) generator 1, (b) generator 2 and (c) generator 3.

efficiency of NGFG 1 and 3 is 17.73 and 19.73 kcf/MWh, respectively. The well gas costs are \$1.68/kcf and \$2.28/kcf, respectively, while the storage gas cost is \$3/kcf. Since the COM has the full information, the marginal cost of generator 1 is equal to the product of the efficiency, 17.73 kcf/MWh, and the gas cost, possibly being \$1.68/kcf, \$2.28/kcf or \$3/kcf. Then the marginal cost per MWh of generator 1 may be \$23.07, \$31.30 or \$53.19, which are all lower than the cost of generator 2. Since the only storage facility is quite far away from generator 3, and generator 3 is supplied by gas well 2, the marginal cost of generator 3 is \$44.98/MWh, which is also less than that of generator 2. Since the NGFGs (generators 1 and 3) are cheaper than the coal-fired generator (generator 2), the COM model tends to commit more NGFGs (generators 1 and 3), but commits generator 2 less often, as shown in hour 6 to 10 and hour 22 to 24 in Table. 4.1. Table 4.1 also shows that the SOMRUC model commits more non-gas fired generators (generator 2), but fewer NGFGs (generators 1 and 3), as shown in hours 2 to 10 and hours 23 and 24.

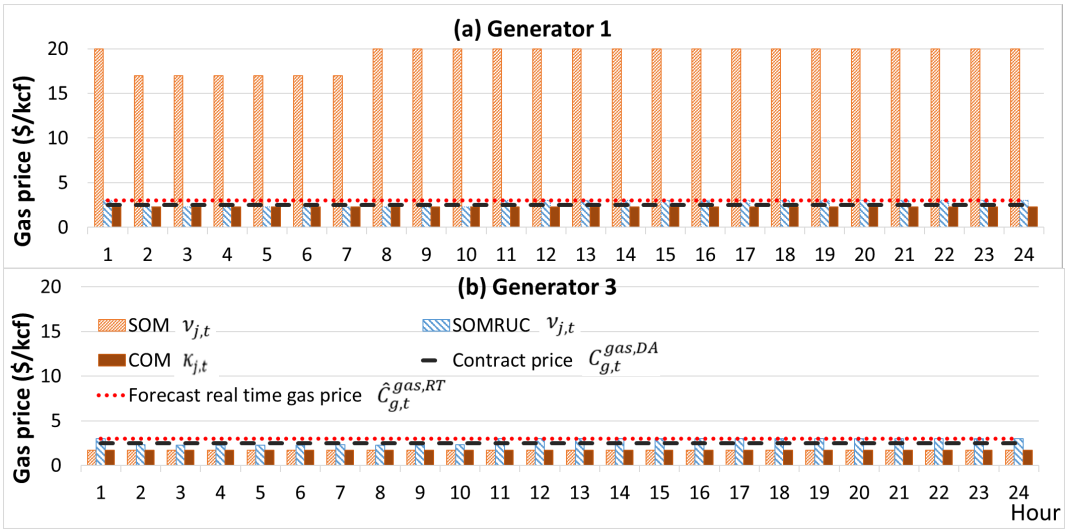


Figure 4.8: The comparison of gas prices including contract gas price, $C_{g,t}^{\text{gas,DA}}$ (dashed black line), forecast real-time gas price, $\hat{C}_{g,t}^{\text{gas,RT}}$ (dotted red line), and real-time gas price, $\nu_{j,t}$, for the SOM model and the SOMRUC model, and the marginal gas price of the COM model for the gas nodes connected to NGFG (a) 1 and (b) 3.

Fig. 4.8 illustrates the comparison among the real-time gas price of the SOM model and the SOMRUC model, and the marginal gas price of the COM model. For comparison, Fig. 4.8 also plots the contract gas price, $C_{g,t}^{\text{gas,DA}}$ (dashed black line) and the forecast RT gas price, $\hat{C}_{g,t}^{\text{gas,RT}}$

(dotted red line). Here both $C_{g,t}^{\text{gas,DA}}$ and $\hat{C}_{g,t}^{\text{gas,RT}}$ are identical for each generator in each hour and each model, and we have $C_{g,t}^{\text{gas,DA}} = \$2.5/\text{kcf}, \forall g, t$ and $\hat{C}_{g,t}^{\text{gas,RT}} = \$3/\text{kcf}, \forall g, t$. As Fig. 4.8 shows, the real-time gas price of the SOMRUC model is always less than or equal to \$3/kcf for each generator, whereas that of the SOM model is around \$20/kcf for generator 1. In other words, the SOMRUC model is able to maintain the real-time gas price at moderate level, while the SOM model might result in a high real-time gas price.

Fig. 4.9 compares the gas quantities from multiple sources including the contract, $\tilde{\mu}_{g,t}^{\text{DA}}$, real-time market, $\mu_{g,t}^{\text{RT}}$, and additional requested real-time gas quantity, $\mu_{g,t}^{-}$, for NGFGs 1 and 3 between the SOM model and the SOMRUC model. The gas quantity from contract, $\tilde{\mu}_{g,t}^{\text{DA}}$, is the same for the SOM model and the SOMRUC model since it is fixed in the day-ahead gas scheduling problem. Afterwards, the RUC is solved and the unit commitment decisions are re-optimized based on $\tilde{\mu}_{g,t}^{\text{DA}}$, while assuming there is no gas flow from the RT market. This RUC step in the SOMRUC model commits more non-gas-fired generators, as discussed before and shown in Table 4.1, and requests less gas quantity from the real-time market, as can been seen from hours 8 to 10 and hours 22 to 24 for generator 1 in Fig. 4.9. For the SOM model, the large amount of natural gas that generator 1 requests in the real-time market cannot be fully supplied by the two gas wells and the storage facility, so there is some value for the additional required real-time gas volume.

To summarize, the SOMRUC model adjusts the unit commitment decisions according to the gas availability from the gas market such that, like the COM model, the SOMRUC model relies more on non-gas-fired generators, compared with the SOM model. Besides, due to this change of the unit commitment decisions, the SOMRUC maintains a low real-time gas price, low gas flow from the real-time market and low power system cost.

### 4.3.2 IEEE 24-Bus System with Modified Belgian 20-Node Gas System

A modified IEEE 24-bus system and modified Belgian 20-node natural gas system are used according to [18], as shown in Fig. 4.10, with the ramp up and down rates and production cost revised in accordance with [66]. The system has 3 NGFGs, 4 coal-fired units, 3 hydro units, 2

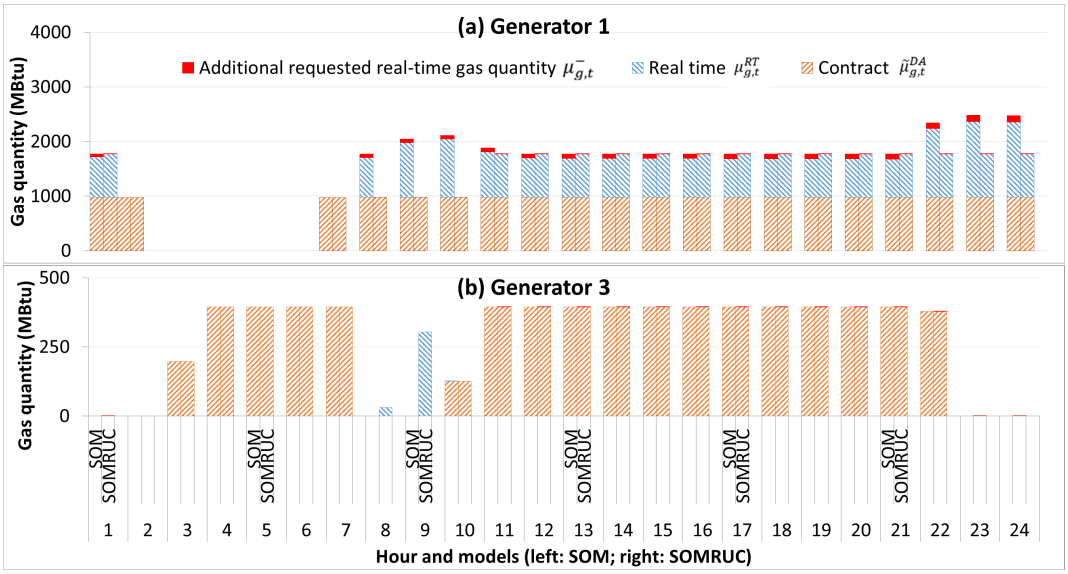


Figure 4.9: The comparison between the SOM model and the SOMRUC model of gas quantities from multiple sources including the contract, $\tilde{\mu}^{\mathrm{DA}}_{g,t}$, real-time market, $\mu^{\mathrm{RT}}_{g,t}$, and additional requested real-time gas quantity, $\mu^{-}_{g,t}$, for NGFG (a) 1 and (b) 3.

wind generators, 38 transmission lines, 9 power loads, 2 gas suppliers (wells), 4 storage facilities, 21 passive pipelines, 3 active pipelines, and 17 non-electric gas demands. The total thermal generating capacity is 3453 MW, which is the sum of the capacities of all 10 thermal generators. Two wind generators with identical capacity are added at nodes 7 and 15, while the wind generation capacity is 5% of the total thermal capacity. All the data are available at [31]. As a crucial parameter, the contract gas price, $C^{\mathrm{gas,DA}}_{g,t}$, depends on the location and the specific contract between the NGFGs and the gas pipeline company. Considering that the gas well costs per kcf are \$1.0080 and \$1.2096, respectively, and the storage costs per kcf are \$1.5576, \$1.5576, \$1.6886, and \$1.7491, respectively, we test three cases of contract gas price per kcf, $C^{\mathrm{gas,DA}}_{g,t}$, equaling to \$1.25, \$1.5, and \$1.75, respectively. In addition, the non-electric gas load varies, and thus we also consider five levels of the gas load factor, as the baseline value plus or minus 5 or 10 percent. For each case, the non-electric load equals the product of the gas load factor, $\chi$, and the gas load of the baseline case, $D^{ng}_{j,t}$. Altogether, we consider each combination of the contract gas price and the gas load factor for a total of 15 case studies. Section 4.3.2.1 fixes the contract gas price to be \$1.5/kcf,

(i.e. $C_{g,t}^{\text{gas,DA}} = 1.5$), and presents the impact of the gas load factor, $\chi$, on the cost. Section 4.3.2.2 presents the results varying both the gas load factor, $\chi$, and the contract gas price, $C_{g,t}^{\text{gas,DA}}$.

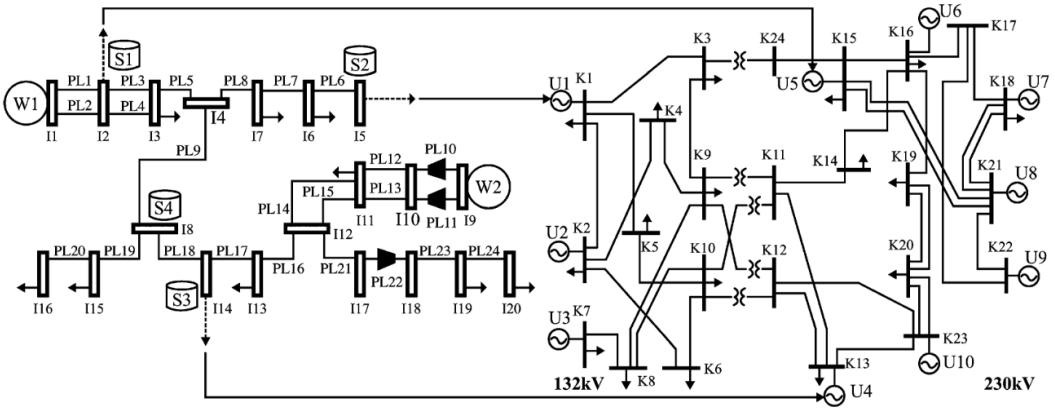


Figure 4.10: Modified IEEE 24-bus system and modified Belgian 20-node natural gas system [18].

#### 4.3.2.1 The Effect of Non-Electric Gas Load

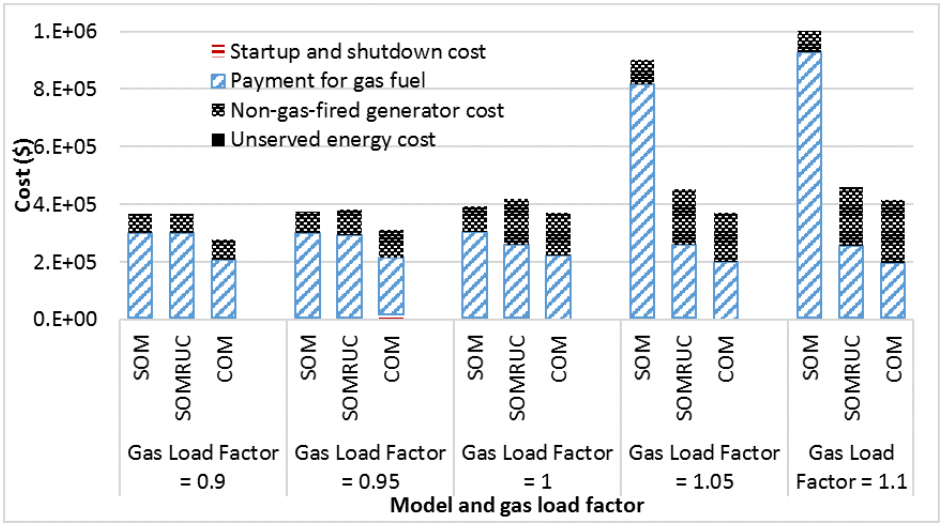


Figure 4.11: Cost comparison for different gas load factors including 0.9, 0.95, 1.0, 1.05, and 1 among three models for the large system.

The non-electric gas load affects the simulation results strongly because of the high priority of the non-electric gas load. The NGFGs can use only the remaining part of gas after the non-electric gas demand is satisfied. We investigate the effect of the non-electric gas load on the power system

operational cost and the cost comparison among the COM, SOMRUC and SOM models. With an interruptible contract gas price of \$1.5/kcf, (i.e. $C_{g,t}^{\text{gas,DA}} = 1.5$), we consider five cases of gas load factor, $\chi$, being 0.9, 0.95, 1, 1.05 and 1.1. This parameter affects the final solution via constraints (4.16) in the COM model but via constraints (4.27a) and (4.31a) in both the SOM model and the SOMRUC model.

Fig. 4.11 compares the power system cost given different gas load factors. The power system cost consists of the start-up and shut-down costs, gas fuel payment, non-gas-fired generator cost, and unserved energy cost. Given a low gas load factor, $\chi = 0.9$ or 0.95, as shown in the left two parts of Fig. 4.11, the costs and the cost breakdowns of the SOM model and the SOMRUC model are quite close. Both the SOM model and the SOMRUC model have a greater payment for gas fuel than the COM model. When $\chi \leq 1$, the cost of the SOMRUC model is greater than that of the SOM model. When the non-electric load factor is high (i.e. $\chi = 1.05$ or 1.1), the payment for the gas fuel of the SOM model increases dramatically and results in the largest total cost among these three models. As the non-electric gas load is higher, less gas is available for the NGFGs and there is a greater difference between $\mu_{g,t}^{\text{DA}*}$ and $\tilde{\mu}_{g,t}^{\text{DA}*}$ because of the low priority of the interruptible contracts. As a result, more gas is requested in the real-time market which gives high real-time gas prices and high payment for the gas fuel in the SOM model. Thus, when the non-electric gas load is high, the RUC step commits more non-gas fired generators and the SOMRUC is able to reduce total power system operational cost.

#### 4.3.2.2 The Effect of Interruptible Contract Gas Price

Fig. 4.12 compares the power system cost given different contract gas prices per kcf, $C_{g,t}^{\text{gas,DA}}$, and non-electric gas load factors, $\chi$, among these three models. The power system cost comprises the start-up and shut-down costs, payment for gas fuel, non-gas generator cost, and unserved energy cost. Given a low non-electric gas load factor, $\chi \leq 1$, as shown in Fig. 4.12(a)–(c), the effect of contract gas price, $C_{g,t}^{\text{gas,DA}}$, is not obvious. Specifically, a higher contract gas price results in a higher total cost for both the SOM model and the SOMRUC model. But given a large non-electric

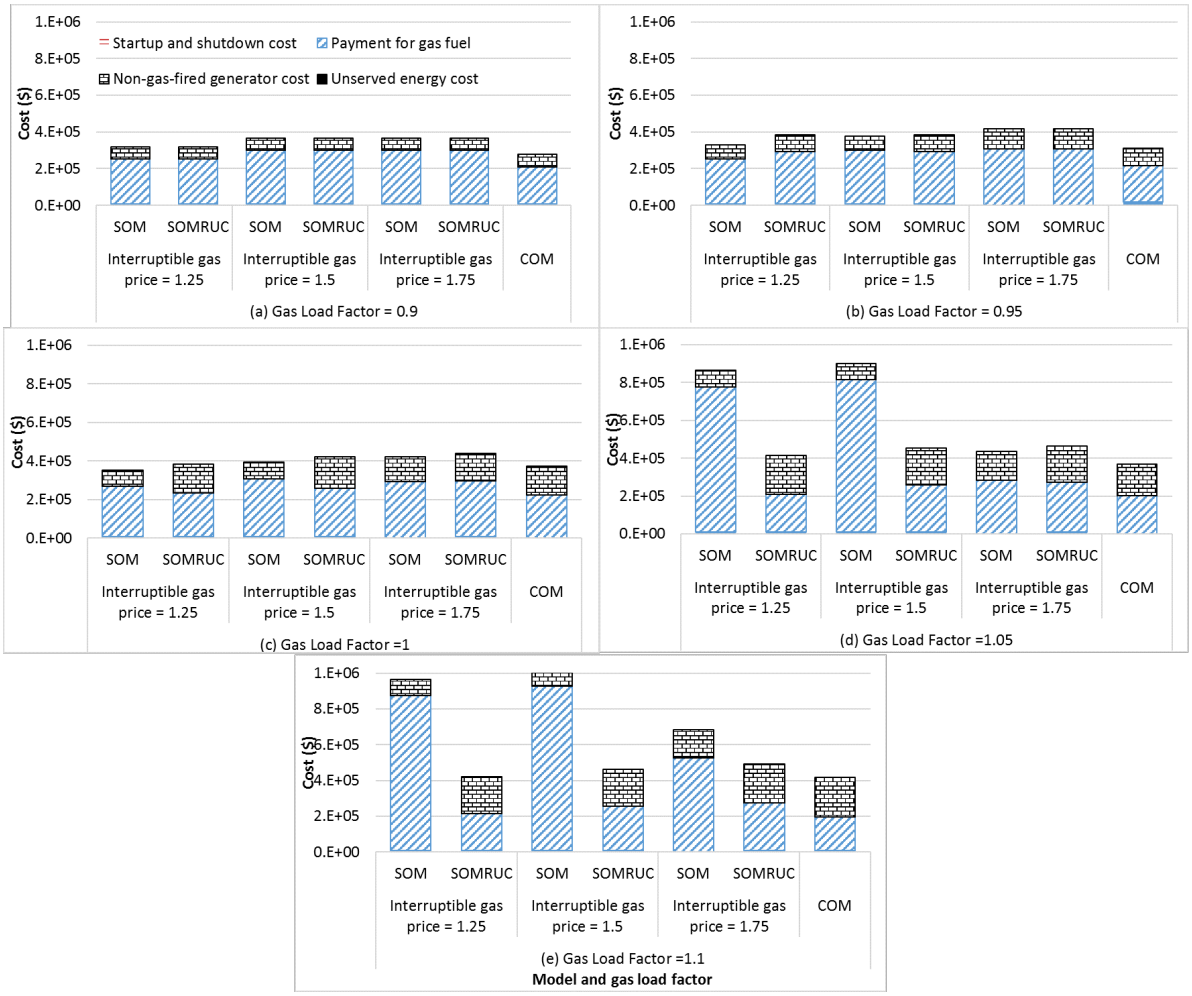


Figure 4.12: Cost comparison given different interruptible contract gas prices, $C_{g,t}^{\text{gas,DA}}$, for (a) gas load factor = 0.9, (b) gas load factor = 0.95, (c) gas load factor = 1, (d) gas load factor = 1.05 and (e) gas load factor = 1.1 among the three models for the large system.

gas load factor, $\chi = 1.05$ or 1.1, as shown in Fig. 4.12(d)–(e), the contract gas price, $C_{g,t}^{\text{gas,DA}}$, is very important. For each of the Fig. 4.12(d)–(e), with a high non-electric gas load, the gas available to the NGFGs is limited, and there is a big difference in the cost between the SOM model and the SOMRUC model. Additionally, a high contract gas price pushes the power system to commit more non-gas-fired generators and request less gas in the day-ahead market, which results in a smaller difference between $\mu_{g,t}^{\text{DA}*}$ and $\tilde{\mu}_{g,t}^{\text{DA}*}$ and less gas requested in real-time market. Then with a higher contract gas price, $C_{g,t}^{\text{gas,DA}}$, the SOM model tends to have low real-time gas price and less gas deficiency and maintains a cost closer to the SOMRUC model. From Fig. 4.12(d) to

Fig. 4.12(e), as the non-electric gas load increases, the gas quantity available to the NGFGs is less, with the same contract gas price, the difference between $\mu_{g,t}^{\mathrm{DA}*}$ and $\tilde{\mu}_{g,t}^{\mathrm{DA}*}$ is greater, and the SOM model is more likely to result in high real-time gas price and gas deficiency. Thus, the effect of the RUC in the SOM model is more significant, as the difference in the power system cost between the SOM model and the SOMRUC model in Fig. 4.12(e) is greater, compared with Fig. 4.12(d). In summary, the SOMRUC dominates the SOM model at reducing total power system operational cost given high non-electric load factor and low contract gas price.

## 4.4 Conclusions

In this paper, we modeled the current operating process as a daily separately optimized model for the operations of the natural gas and power systems, which consists of the day-ahead and real-time market. In the day-ahead market, due to the low priority of the interruptible gas contracts, NGFGs can use only the gas remaining after the non-electric gas demand is satisfied. The NGFGs can also acquire gas from the real-time market where the availability and price of the gas are determined by an iterative process between the natural gas and power systems. Due to the unawareness of the gas availability in the day-ahead unit commitment problem, the NGFGs experience risks of high price and limited gas availability in the real-time market. To address this issue, we proposed a separately optimized model with reliability unit commitment, which adds a reliability unit commitment step between the day-ahead gas scheduling problem and the real-time electricity market. Different from the RA focusing on load uncertainty, this RUC step focuses on the gas fuel and enables the power system to adjust their unit commitment decisions in accordance with the gas availability information from the day-ahead gas system. For comparison, a co-optimized model, which assumes a centralized system operator has perfect information and can operate both the natural gas and power systems simultaneously, was also formulated and taken as a benchmark.

We compared the cost of the power system among these three models and investigated the role of RUC in limiting the risk from gas system. A small case study was used to compare the solutions to these three models at the detailed operational level such as unit commitment decisions,

dispatches, and the real-time gas price. It demonstrated that the SOMRUC model is able to reduce cost while avoiding the real-time gas deficiency and the high gas price. The main difference is that the RUC step adjusts the unit commitment decisions according to the most updated gas availability information from the day-ahead gas market and commit the non-gas-fired generators more often. This also results in a limited amount of gas requested from the real-time gas market by the SOMRUC model. It is important to note that the interruptible contract gas price, $C_{g,t}^{\text{gas,DA}}$, is a critical parameter. Besides, the non-electric gas load is also crucial due to its high priority. We compare these three models given different values for $C_{g,t}^{\text{gas,DA}}$ and non-electric gas load factor, $\chi$, in a large case study. The simulation results show that the SOMRUC model reduces the operational cost for the power system given high non-electric load and low interruptible contract gas price, compared with the SOM model.

# CHAPTER 5. GENERAL CONCLUSION

In this dissertation, we aimed to investigate the short-term operation of the power system and natural gas system under uncertainty from various viewpoints. We focused on the unit commitment problem and the economic dispatch problem for the power system and the daily scheduling problem for the natural gas system from the viewpoint of either a centralized system operator or a power system operator. Our research plan was to propose a practical separately optimized model where each of the power system and the natural gas system is operated by its own operator. This separately optimized model can be taken as a benchmark which can be compared with the recent or future models for the power system and natural gas system with respect to the total operational cost and corresponding gas and power price.

In the first paper, from a viewpoint of an assumed centralized system operator who can operate the power system and natural gas system simultaneously, we proposed a stochastic programming model for the daily short-term operations for the combined system under wind energy uncertainties. Due to the intractability of the nonlinear non-convex pipeline gas flow constraints, linearization experiments were done for both the small and large case studies to choose a number of segments that balances accuracy and computational efficiency. Results from a small case study of a six-bus power system and a seven-node natural gas system indicated that the stochastic programming model yields a much lower standard deviation and mean cost, suggesting that probabilistic-scenario-based scheduling of the combined system is better able to maintain a stable cost, according to a year's worth of days to capture the variability of the daily wind energy forecast and the resulting wind energy scenarios. A larger case study of a 24-bus power system and 20-node natural gas system in four days, that differ according to discrepancy between the wind energy scenarios and

forecast, with three wind energy capacity penetration factors of 5%, 15% and 30%, illustrates the deterministic model with reserves maintains no expected unserved energy and has less expected cost than the stochastic programming model.

In the second paper, from the viewpoint of the power system operator, we proposed a daily economic dispatch model with natural gas from the spot market and contracts while considering the natural gas availability constraints and gas fuel cost. Data are clustered based on weather information and, within each cluster, a bivariate normal joint distribution of daily electric load and gas spot market price is estimated by transforming the data, using maximum likelihood estimation to identify a parameter for the transformation. By simulation, we obtained two cost probability distributions where the first one fixes the gas spot price at its point estimate, and the second one incorporates the estimated gas spot price probability distributions. The results for different days, clustered according to weather information in winter, show that the effect of gas spot price uncertainty is weakened as the contracted gas availability increases. Based on the investment cost and risk reduction comparison, this quantification method can be applied to help choose the most effective risk-mitigation strategy for a given investment cost. Our case study suggested that adding a gas storage facility could be preferred over dual fuel conversion. However, since the results are based on an artificial test case, this conclusion is not universal. A system operator could conduct its own case study based on its available data in order to select a better strategy according to the risk metrics.

The final paper presented the current operating process of the natural gas and power systems as a separately optimized model, where either the power system operator or the natural gas system operator minimizes their own net cost considering the gas from contracts and the real-time market. A reliability unit commitment step was added between the day-ahead market and the real-time market of the separately optimized model. A co-optimized model, which assumes all the decisions are made by a centralized system operator simultaneously, was used as the benchmark for the cost comparison. This reliability unit commitment step adjusts the unit commitment decisions, mostly committing the non-gas-fired generators more often but committing the gas-fired generators less

often, such that less gas is requested in the real-time market. In this way, the simulation results demonstrated that the reliability unit commitment is able to avoid high real-time gas price and real-time gas deficiency along with maintaining a low power system cost, which consists of the startup and shutdown cost, payment for gas fuel, non-gas-fired generator cost, and the unserved energy cost. Specifically, the effect of the reliability unit commitment is significant when we have a low interruptible gas price or high non-electric gas load.

We claim the following three contributions of this dissertation. Firstly, we compared the deterministic model with reserves with the stochastic programming model given various wind energy uncertainty to see the benefits of reducing the cost and risks of the latter model. Secondly, we quantified the effects of the uncertain gas availability and the uncertain gas price on the power system economic dispatch cost and provided suggestions to the operator about how to select a better risk-mitigation strategy. Lastly, we modeled the realistic process of the daily operation of the power system and natural gas system as a separately optimized model. We demonstrated that a reliability unit commitment step can achieve many of the benefits of co-optimizing operators in the two systems to manage the natural gas cost in the power system operations.

For future research, there exist several interesting directions. In terms of the formulation and the tractability of the non-linear non-convex natural gas short-term operation model, more algorithms and more reformulations need to be developed to obtain feasible quasi-optimal and optimal solutions quickly. Recently, there are some real data published for the combined natural gas and power system, based on which more numerical studies can be added. In addition, in the second paper, we use simulation to obtain the CVaR value. The linearized formulation of the dispatch cost CVaR can also be included in the objective function to represent risk aversion in the optimization.

# BIBLIOGRAPHY


[1] J. M. Adder. ISO-New England dual fuel capabilities to limit natural gas and electricity interdependencies, 2016. URL https://www.eenews.net/assets/2017/11/21/document_gw_11.pdf.

[2] A. Alabdulwahab, A. Abusorrah, X. Zhang, and M. Shahidehpour. Coordination of interdependent natural gas and electricity infrastructures for firming the variability of wind energy in stochastic day-ahead scheduling. *IEEE Transactions on Sustainable Energy*, 6(2):606–615, 2015.

[3] A. Azzalini and A. Capitanio. Statistical applications of the multivariate skew normal distribution. *Journal of the Royal Statistical Society: Series B*, 61(3):579–602, 1999.

[4] L. Bai, F. Li, T. Jiang, and H. Jia. Robust scheduling for wind integrated energy systems considering gas pipeline and power transmission N-1 contingencies. *IEEE Transactions on Power Systems*, 32(2):1582–1584, Mar. 2017.

[5] P. N. Biskas, N. G. Kanelakis, A. Papamatthaiou, and I. Alexandridis. Coupled optimization of electricity and natural gas systems using augmented Lagrangian and an alternating minimization method. *International Journal of Electrical Power & Energy Systems*, 80:202–218, Sep. 2016.

[6] Bonneville Power Administration. Wind power forecasting data, Mar. 2015. URL http://www.bpa.gov/Projects/Initiatives/Wind/Pages/Wind-Power-Forecasting-Data.asp.

[7] Bonneville Power Administration. Wind operational data, Mar. 2015. URL http://transmission.bpa.gov/Business/Operations/Wind/default.aspx.

[8] Bonneville Power Administration. Wind installed capacity, Mar. 2015. URL http://transmission.bpa.gov/Business/Operations/Wind/WIND.InstalledCapacity_DATA.pdf.

[9] C. Borraz-Sánchez, R. Bent, S. Backhaus, H. Hijazi, and P. V. Hentenryck. Convex relaxations for gas expansion planning. *INFORMS Journal on Computing*, 28(4):645–656, 2016.

[10] G. E. P. Box and D. R. Cox. An analysis of transformations. *Journal of the Royal Statistical Society. Series B (Methodological)*, pages 211–252, 1964.

[11] G. Byeon and P. V. Hentenryck. Unit commitment with gas network awareness. *arXiv preprint arXiv:1902.03236*, 2019.

[12] M. Chaczykowski. Transient flow in natural gas pipeline–The effect of pipeline thermal model. *Applied Mathematical Modelling*, 34(4):1051–1067, 2010.

[13] S. Chen, Z. Wei, G. Sun, K. W. Cheung, and Y. Sun. Multi-linear probabilistic energy flow analysis of integrated electrical and natural-gas systems. *IEEE Transactions on Power Systems*, 32(3):1970–1979, 2017.

[14] S. Chen, Z. Wei, G. Sun, D. Wang, and H. Zang. Steady state and transient simulation for electricity-gas integrated energy systems by using convex optimisation. *IET Generation, Transmission & Distribution*, 12(9):2199–2206, May 2018.

[15] C. M. Correa-Posada and P. Sánchez-Martin. Stochastic contingency analysis for the unit commitment with natural gas constraints. In *2013 IEEE Grenoble Power Tech Conference*, pages 1–6, Grenoble, France, Jun. 2013. IEEE.

[16] C. M. Correa-Posada and P. Sánchez-Martin. Gas network optimization: A comparison of piecewise linear models. *Optimization Online*, 2014. URL http://www.optimization-online.org/DB_FILE/2014/10/4580.pdf.

[17] C. M. Correa-Posada and P. Sánchez-Martin. Security-constrained optimal power and natural-gas flow. *IEEE Transactions on Power Systems*, 29(4):1780–1787, Jul. 2014.

[18] C. M. Correa-Posada and P. Sánchez-Martin. Integrated power and natural gas model for energy adequacy in short-term operation. *IEEE Transactions on Power Systems*, 30(6):3347–3355, 2015.

[19] C. M. Correa-Posada, P. Sánchez-Martín, and S. Lumbreras. Security-constrained model for integrated power and natural-gas system. *Journal of Modern Power Systems and Clean Energy*, 5(3):326–336, 2017.

[20] J. Dupačová, N. Gröwe-Kuska, and W. Römisch. Scenario reduction in stochastic programming. *Mathematical Programming*, 95(3):493–511, 2003.

[21] H. Fang, A. Ciatto, and F. Brock. U.S. natural gas storage capacity and utilization outlook, 2016. URL https://www.energy.gov/sites/prod/files/2017/01/f34/U.S.NaturalGasStorageCapacityandUtilizationOutlook_0.pdf.

[22] Federal Energy Regulatory Commission. FERC Order No. 809: Coordination of the scheduling processes of interstate natural gas pipelines and public utilities, 2015. URL https://www.ferc.gov/whats-new/comm-meet/2015/041615/M-1.pdf.

[23] Y. Feng and S. M. Ryan. Day-ahead hourly electricity load modeling by functional regression. *Applied Energy*, 170:455–465, 2016.

[24] Y. Feng, I. Rios, S. M. Ryan, K. Spurkel, J.-P. Watson, R. J.-B. Wets, and D. L. Woodruff. Toward scalable stochastic unit commitment - part 1: load scenario generation. *Energy Systems*, 6(3):309–329, 2015.

[25] P. Filzmoser, R. G. Garrett, and C. Reimann. Multivariate outlier detection in exploration geochemistry. *Computers & Geosciences*, 31(5):579–587, 2005.

[26] S. Ge, X. Liu, H. Liu, C. Gu, and L. Ge. Research on unit commitment optimization of high permeability wind power generation and P2G. *Journal of Renewable and Sustainable Energy*, 10(3):34702, 2018.

[27] C. He, L. Wu, T. Liu, and M. Shahidehpour. Robust co-optimization scheduling of electricity and natural gas systems via ADMM. *IEEE Transactions on Sustainable Energy*, 8(2):658–670, 2017.

[28] H. Heitsch and W. Römisch. A note on scenario reduction for two-stage stochastic programs. *Operations Research Letters*, 35(6):731–738, 2007.

[29] D. Hu and S. M. Ryan. Quantifying the effect of natural gas price uncertainty on economic dispatch cost uncertainty. In *Proc. IEEE Power Energy Society General Meeting*, pages 1–5, July 2017.

[30] D. Hu and S. M. Ryan. Quantifying the effect of uncertainty in the gas spot price on power system dispatch costs with estimated correlated uncertainties. 2018. URL https://works.bepress.com/sarah_m_ryan/99/.

[31] D. Hu and S. M. Ryan. Datasets for reliability unit commitment to manage natural gas cost in power system operations, 2019. URL http://dx.doi.org/10.17632/ynb88g67xy.1.

[32] D. Hu and S. M. Ryan. Stochastic vs. deterministic scheduling of a combined natural gas and power system with uncertain wind energy. *International Journal of Electrical Power & Energy Systems*, 108:303–313, 2019.

[33] ISO-New England. ISO-New England energy, load and demand reports zonal information, 2016. URL https://www.iso-ne.com/isoexpress/web/reports/load-and-demand/-/tree/zone-info.

[34] J. Jin and J. Kim. Forecasting natural gas prices using wavelets, time series, and artificial neural networks. *PloS One*, 10(11):e0142064, 2015.

[35] X. Jin, Y. Mu, H. Jia, J. Wu, X. Xu, and X. Yu. Optimal day-ahead scheduling of integrated urban energy systems. *Applied Energy*, 180:1–13, Oct. 2016.

[36] N. Kazemzadeh, S. M. Ryan, and M. Hamzeei. Robust optimization vs. stochastic programming incorporating risk measures for unit commitment with uncertain variable renewable generation. *Energy Systems*, pages 1–25, 2017. doi: 10.1007/s12667-017-0265-5.

[37] H. Khani, N. El-Taweel, and H. E. Farag. Real-time optimal management of reverse power flow in integrated power and gas distribution grids under large renewable power penetration. *IET Generation, Transmission & Distribution*, 12(10):2325–2331, May 2018.

[38] J. B. Klein. The use of heat rates in production cost modeling and market modeling, 1998. URL http://www.energy.ca.gov/papers/98-04-07_HEATRATE.PDF.

[39] S. Korkmaz, D. Goksuluk, and G. Zararsiz. MVN: An R package for assessing multivariate normalit. *The R Journal*, 6/2, 2014. URL https://cran.r-project.org/web/packages/MVN/vignettes/MVN.pdf.

[40] G. Li, R. Zhang, T. Jiang, H. Chen, L. Bai, and X. Li. Security-constrained bi-level economic dispatch model for integrated natural gas and electricity systems considering wind power and power-to-gas process. *Applied Energy*, 194:696–704, 2017.

[41] T. Li, M. Eremia, and M. Shahidehpour. Interdependency of natural gas network and power system security. *IEEE Transactions on Power Systems*, 23(4):1817–1824, Nov. 2008.

[42] Y. Li, Y. Zou, Y. Tan, Y. Cao, X. Liu, M. Shahidehpour, S. Tian, and F. Bu. Optimal stochastic operation of integrated low-carbon electric power, natural gas, and heat delivery system. *IEEE Transactions on Sustainable Energy*, 9(1):273–283, Jan. 2018.

[43] C. Liu, M. Shahidehpour, Y. Fu, and Z. Li. Security-constrained unit commitment with natural gas transmission constraints. *IEEE Transactions on Power Systems*, 24(3):1523–1536, 2009.

[44] C. Liu, M. Shahidehpour, and J. Wang. Coordinated scheduling of electricity and natural gas infrastructures with a transient model for natural gas flow. *Chaos: An Interdisciplinary Journal of Nonlinear Science*, 21(2):25102, 2011.

[45] H. M. Markowitz and A. S. Manne. On the solution of discrete programming problems. *Econometrica.*, pages 84–110, 1957.

[46] Midcontinent Independent System Operator. Business practices manual: energy and operating reserve markets, 2012. URL https://www.misoenergy.org/legal/business-practice-manuals/.

[47] Midwest Independent System Operator. Business Practices Manual: Energy and Operating Reserve Markets, 2012.

[48] Morales-Espana, J. M. Latorre, and A. Ramos. Tight and compact MILP formulation for the thermal unit commitment problem. *IEEE Transactions on Power Systems*, 28(4):4897–4908, nov 2013.

[49] North American Energy Standards Board. North American Energy Standards Board version 3.0: April 1, 2016, 2016. URL http://fgttransfer.energytransfer.com/fginfopost/postedDocs/NAESBVer3Changes.pdf.

[50] Northern Natural Gas Company. Capacity release frequently asked questions, 2017. URL http://www.northernnaturalgas.com/Document%20Postings/Capacity_Release_FAQs_09-05-17.pdf.

[51] C. Ordoudis, S. Delikaraoglou, P. Pinson, and J. Kazempour. Exploiting flexibility in coupled electricity and natural gas markets: A price-based approach. In *PowerTech 2017*, pages 1–6. IEEE, Jun. 2017.

[52] A. Osiadacz. *Simulation and analysis of gas networks*. Gulf Publishing Company, Houston, TX, 1987.

[53] A. Papavasiliou, S. S. Oren, and R. P. O'Neill. Reserve requirements for wind power integration: A scenario-based stochastic programming framework. *IEEE Transactions on Power Systems*, 26(4):2197–2206, 2011.

[54] Power Systems Control and Automation Laboratory, Georgia Tech Unversity. Three-phase, breaker-oriented IEEE 24-substation reliability test system, 2018. URL http://pscal.ece.gatech.edu/archive/testsys/generators.html.

[55] M. Qadrdan, J. Wu, N. Jenkins, and E. Janake. Operating strategies for a GB integrated gas and electricity network considering the uncertainty in wind power forecasts. *IEEE Transactions on Sustainable Energy*, 5:128–138, 2015.

[56] S. T. Rachev and L. Rüschendorf. *Mass Transportation Problems. Volume I: Theory*. Springer Science & Business Media, 1998.

[57] I. Rios, R. J. B. Wets, and D. L. Woodruff. Multi-period forecasting and scenario generation with limited data. *Computational Management Science*, 12(2):267–295, 2015.

[58] R. T. Rockafellar and S. Uryasev. Conditional value-at-risk for general loss distributions. *Journal of Banking & Finance*, 26(7):1443–1471, 2002.

[59] A. Rudkevich. Gas-electric co-optimization, 2017. URL https://www.energy.gov/sites/prod/files/2017/06/f34/3_Gas%20Electric%20Integration%20Panel%20-%20Alex%20Rudkevich%2C%20ARPA-E.pdf.

[60] S. M. Ryan, G. Gross, D. Hu, and A. L. Abrantes. Analysis of power system operational risks from gas system dependence, 2018. URL https://pserc.wisc.edu/publications/reports/2018_reports/M-36_Final_Report.pdf.

[61] D. Sari, Y. Lee, S. Ryan, and D. Woodruff. Statistical metrics for assessing the quality of wind power scenarios for stochastic unit commitment. *Wind Energy*, 19(5):873–893, 2009.

[62] M. Shahidehpour, Y. Fu, and T. Wiedman. Impact of natural gas infrastructure on electric power systems. *Proceedings of the IEEE*, 93(5):1042–1056, May 2005.

[63] C. A. Sugar and G. M. James. Finding the number of clusters in a dataset: an information-theoretic approach. *Journal of the American Statistical Association*, 98(463):750–763, 2003.

[64] The North American Electric Reliability Corporation. Assessment of previous severe winter weather reports 1983-2011, 2013. URL https://www.nerc.com/pa/rrm/ea/February%202011%20Southwest%20Cold%20Weather%20Event/Final_Draft_Assessment_of_Previous_Severe_Winter_Weather_Report.pdf.

[65] The North American Electric Reliability Corporation. 2015 Long-term reliability assessment, 2015. URL http://www.nerc.com/pa/RAPA/ra/ReliabilityAssessmentsDL/2015LTRA-FinalReport.pdf.

[66] The Renewable Energy Lab, The University of Washington. Unit commitment data for modernized IEEE RTS-96. URL http://www.ee.washington.edu/research/real/library.html.

[67] A. R. D. Thorley and C. H. Tiley. Unsteady and transient flow of compressible fluids in pipelines - a review of theoretical and some experimental studies. *International Journal of Heat and Fluid Flow*, 8(1):3–15, 1987.

[68] C. Unsihuay, J. W. Marangon-Lima, and A. C. Z. de Souza. Short-term operation planning of integrated hydrothermal and natural gas systems. In *Proc. IEEE Lausanne Power Tech*, pages 1410–1416, 2007.

[69] U.S. Department of Energy Information Administration. Annual energy outlook 2015 with projections to 2040. *U.S. Department of Energy, Washington*, 2015. URL https://www.eia.gov/outlooks/aeo/pdf/0383(2015).pdf.

[70] U.S. Energy Information Administration. Annual energy outlook 2018: With projections to 2050, 2018. URL https://www.eia.gov/outlooks/aeo/pdf/AEO2018.pdf.

[71] U.S. Energy Information Administration. Daily Henry Hub natural gas spot price, 2019. URL http://www.eia.gov/dnav/ng/hist/rngwhhdD.htm.

[72] C. Wang, W. Wei, J. Wang, L. Bai, and Y. Liang. Distributed optimal gas-power flow using convex optimization and ADMM. *arXiv preprint arXiv:1610.04681*, 2016.

[73] Y. Wen, X. Qu, W. Li, X. Liu, and X. Ye. Synergistic operation of electricity and natural gas networks via ADMM. *IEEE Transactions on Smart Grid*, 9(5):4555–4565, Sep. 2018.

[74] L. Wu, C. He, C. Dai, and T. Liu. Robust network hardening strategy for enhancing resilience of integrated electricity and natural gas distribution systems against natural disasters. *IEEE Transactions on Power Systems*, pages 1–1, 2018.

[75] X. Xiao, Y. Shui, H. Gao, J. Liu, Q. Chen, T. Li, Y. Liu, and X. Ouyang. A two-stage distributionally robust coordinated dispatch for integrated electricity and natural-gas energy systems considering uncertainty of wind power. *IOP Conference Series: Materials Science and Engineering*, 366:012016, Jun. 2018.

[76] J. Yu, L. Guo, M. Ma, S. Kamel, W. Li, and X. Song. Risk assessment of integrated electrical, natural gas and district heating systems considering solar thermal CHP plants and electric boilers. *International Journal of Electrical Power & Energy Systems*, 103:277–287, Dec. 2018.

[77] X. Zhang, M. Shahidehpour, A. Alabdulwahab, and A. Abusorrah. Hourly electricity demand response in the stochastic day-ahead scheduling of coordinated electricity and natural gas networks. *IEEE Transactions on Power Systems*, 31(1):592–601, 2016.

[78] B. Zhao, A. J. Conejo, and R. Sioshansi. Unit commitment under gas-supply uncertainty and gas-price variability. *IEEE Transactions on Power Systems*, 32(3):2394–2405, 2017.

[79] B. Zhao, A. J. Conejo, and R. Sioshansi. Shadow price-based co-ordination of natural gas and electric power systems. *IEEE Transactions on Power Systems*, 33(3):3064–3075, 2018.

[80] A. Zlotnik, L. Roald, S. Backhaus, M. Chertkov, and G. Andersson. Coordinated scheduling for interdependent electric power and natural gas infrastructures. *IEEE Transactions on Power Systems*, 32(1):600–610, Jan. 2017.